國 立 交 通 大 學
機械工程學系

博士論文

同心旋轉圓柱間

調制Couette流及Taylor渦旋流之不穩定

Instabilities of Modulated Couette Flow and Taylor Vortex Flow Between Concentric Rotating Cylinders

研 究 生:林豪傑

指導教授:楊文美 博士

中華民國九十八年十一月

同心旋轉圓柱間調制Couette流及Taylor渦旋流之不穩定

Instabilities of Modulated Couette Flow and Taylor Vortex Flow Between Concentric Rotating Cylinders

研 究 生：林豪傑　　Student：Hau-Chieh Lin

指導教授：楊文美　　Advisor：Wen-Mei Yang

國 立 交 通 大 學

機 械 工 程 學 系

博 士 論 文

A Thesis

Submitted to Department of Mechanical Engineering

College of Engineering

National Chiao Tung University

In partial Fulfillment of the Requirements

for the Degree of

Doctor of Philosophy

in

Mechanical Engineering

Nov. 2009

Hsinchu, Taiwan, Republic of China

中華民國九十八年十一月

同心旋轉圓柱間

調制Couette流及Taylor渦旋流之不穩定

學生:林豪傑　　指導教授:楊文美 博士

國立交通大學機械工程學系博士班

摘要

同心圓柱間的旋轉流場在流體動力學之研究上處於極為重要之一環，其有趣且複雜之現象，至今仍是眾多學者及研究人員相當關注的研究課題。本論文主要目的為利用數值方法建構及分析不同半徑比之同心圓柱間旋轉流場的型態，對於同心圓柱間多變之流況，以雷諾數做為描繪流況之參數，探討此旋轉流場在調制與非調制轉速下之流動特性。

本研究主題包括(1)不同調制效應的Couette流轉換為Taylor渦旋流(2)調制與非調制Taylor渦旋流流場分析(3)非調制Taylor渦旋流轉換為波動Taylor渦旋流。首先，針對在不同的調制振幅及頻率下的Couette流進行穩定性分析研究，發生此不穩定將形成調制Taylor渦旋流。根據Floquet理論可將擾動量分成時間與空間兩部份，其中時間函數與調制具相同的頻率。數值方法採用Galerkin和Collocation法將擾動方程式轉換為代數的特徵方程式，最後以QZ法求解特徵值，此複數型態特徵值

的實數部將為流場穩定與否的判斷指標。其次，探討調制與非調制Taylor渦旋流場，在運算上直接求解二維、時變並以圓柱座標系統表示的Navier-Stokes方程式以及連續方程式，其中數值方法是以Adam-Bashforth法和Crank-Nicolson法分別處理方程式中的非線性及線性項，再將擾動方程式轉換為矩陣方程式並進行求解原始的壓力及速度分量。最後，針對超臨界、軸對稱的非調制Taylor渦旋流進行穩定性分析，求取在不同波數與半徑比下Taylor渦旋流轉換為波動渦旋流的最低穩定曲線，在此階段主要以線性理論來簡化三維擾動的Navier-Stokes方程式以及連續方程式，再利用Galerkin和Collocation等數值方法，將擾動方程式轉換為代數的特徵方程式，如同第一階段Couette流場分析準則，根據複數型態特徵值的實數部作為判斷Taylor渦旋流發生不穩定之依據。

Instabilities of Modulated Couette Flow and Taylor Vortex Flow Between Concentric Rotating Cylinders

Student：Hau-Chieh Lin　　Advisor：Dr. Wen-Mei Yang

Department of Mechanical Engineering
National Chiao Tung University

ABSTRACT

Fluid flow between two concentric rotating cylinders has remained an important topic in fluid dynamics, attracting scholars and researchers to date. In this study, numerical methods are used to analyze and simulate flows and stabilities, which are characterized by a Reynolds number, under different radius ratios and modulated effects.

This study focuses on (1) the transition of Couette flow to Taylor vortex flow under different modulated amplitudes and frequencies, (2) the non-modulated and modulated Taylor vortex flows, and (3) the transition of the non-modulated Taylor vortex flow to wavy vortex flow.

First, the instability of modulated Couette flow before it transitions to modulated Taylor vortex flow, as well as the effects of modulated amplitude and frequency are studied. By using the Floquet theorem, perturbations are expanded into two series with time periodical coefficients which has the same period as that of the modulation. By following the work of Galerkin and using collocation methods, the equation is transformed into an algebraic eigenvalue problem. The QZ algorithm is employed to solve for the eigenvalues that determine the flow stability.

Second, the primitive variables of modulated and non-modulated Taylor vortex flows are solved numerically using the Crank-Nicolson and Adam-Bashforth methods to discretize the linear and nonlinear terms, respectively, of the Navier-Stokes equations.

Finally, the stabilities of supercritical Taylor vortex flows are studied by perturbing the nonlinear Taylor vortex flows. Using the same techniques as in part I, the marginal curves of transition to wavy vortex flows are obtained for different radius ratios and axial wave numbers. The resulting stability boundary curve for transition of supercritical Taylor vortex flow is different from that obtained in previous studies, in which the Reynolds number of the inner cylinder is assumed to increase quasi-statically.

致謝

取得學位的這條路這麼的漫長，無法置信的是我終於已經走到這個臨界點了。內心有許多的感謝滿滿的一股腦想吶喊出來；謝謝文美老師您近幾年來的教誨，在這領域的研究上之所以能夠紮穩根基，全然因為您的細心指導，雖然您平日較不苟言笑，但我想這個表現還不算太差的學生畢業了，您應該可以放下心中大石，微笑一下吧！我知道日後研究的路還很長，我不會令您失望的。

感謝武雄老師、雄略老師、慶耀老師及筱明老師蒞臨指導我的學位考試，經由您的意見使我在這領域中更加豁然開朗，也學習到更多如何解決問題、表達結果的技巧，謝謝各位老師的指導；也感謝曾經與我一同在實驗室共同打拼的學弟們，讓我在實驗室中擁有溫暖的回憶。

當初斷然選擇退伍進而求取學位，主要為的就是想給家人一個不一樣的生活，然而在這研修的道路上，並非全然平坦無阻，現實的生活曾給予我莫大的打擊與壓力的負荷，然而一路走來，我的妻子-宜棻，始終如一的陪伴著我，她曾說過他不是一個堅強的人，但我想對他說：若不堅強如妳，就不會有雙堅毅的推手使我向前行，感謝妳的真心與無怨無悔的付出，今日與往後的所有榮耀完全歸功於妳，謝謝妳！

謹將本論文的研究成果獻給所有愛我及我所愛的父親、宜棻及最可愛的楚小咪。

Table of Content

摘要 ..... **i**

ABSTRACT ..... **iii**

致謝 ..... **v**

Table of Content ..... **vi**

List of Tables ..... **viii**

List of Figures ..... **ix**

Nomenclature ..... **xii**

Chapter 1 Introduction **1**

1.1 Motive of the Present Study 1

1.2 Literatures Review 1

1.3 Objective of This Study 6

Chapter 2 Instability of Non-modulated and Modulated Circular Couette Flow **7**

2.1 General Features 7

2.2 Numerical Procedures 7

2.3 The Result of Non-modulated Effect on Couette Flow 13

2.4 The Result of Modulated Effect on Couette Flow 14

Chapter 3 Taylor Vortex Flow **36**

3.1 General Description of the TVF 36

3.2 Numerical Method 37

3.2.1 Model description 37

3.2.2 Governing Equations 37

3.2.3 Model Validation 41

3.3 The Onset of Taylor Vortices under Modulated Effect 42
3.4 Conclusion 44

Chapter 4 Transition to Wavy Vortex Flow 57
4.1 The Second Transition of Taylor-Couette Flow 57
4.2 Numerical Method 58
4.2.1 Model Description 58
4.2.2 Governing Equations 58
4.2.3 Solution Method and Definition of Instability 63
4.3 Lowest Instability of the Wavy Vortices under Inner Cylinder Rotation which is Re_1 64
4.4 The Lowest Instability Curve of the Transition from TVF to WVF under the Condition of Concerntric Rotating Cylinders 65
4.4 Results Summary 66

Chapter 5 Concluding Remarks 85

References 87

List of Tables

Table 1 Comparison list of results from this study and other scholars under the condition of a non-modulated Couette flow 18

Table 2 Radial velocity at the point of observation ($\xi = 0$, z = 0) for $\eta = 0.5$ as the outer cylinder is fixed and the inner cylinder rotates at a constant velocity. The definition of T_a is represented by $T_a = 2(1-\eta)\mathrm{Re}^2/(1+\eta)$ 45

Table 3 Comparison of experimental and theoretical data of Re values for $\eta = 0.782$ 68

List of Figures

Figure 1 Physics mode graph 19

Figure 2 Coordinate graph 20

Figure 3 (a) The relationship of relative variable Δ vs modulated frequency is showing under modulated effect $\varepsilon = 1$ (b) A chart showing the variation of Re_1 on different modulated amplitudes vs frequencies. ($\eta = 0.4833$) 21

Figure 4 Relationship between relative variable Δ of the Re_1 and amplitude under different modulated effects..... 23

Figure 5 Different inner and outer radius ratios, and the relationship between critical Re and frequency. 27

Figure 6 Influence of aspect ratio (h) on variable Δ of the critical Re (see Huang[45]). 28

Figure 7 Influence of different upper and lower boundaries on variable Δ of the critical Re (see Huang[45]). 29

Figure 8 Relationship between wave number of the modulated Couette flow under a stable critical number and modulated frequency; upper and lower fixed boundaries are $\varepsilon = 0.5$ and $\eta = 0.4833$, respectively. 30

Figure 9 Relationship between critical wave number and frequency at different modulated amplitudes. 31

Figure 10 Relationship between the relative variable of the critical Re and frequency under different radius ratios. 34

Figure 11 The relationship between offset of the critical Reynolds number Δ and modulated frequency when the outer cylinder is fixed and modulated amplitude of the inner cylinder is $\varepsilon = 1$ 46

Figure 12 The flow instability of the relationship between the rotating outer and inner cylinder. ($\eta = 0.937$) 47

Figure 13 The inner cylinder rotates with $\Omega_1 = \bar{\Omega}_1$, the outer cylinder $\Omega_2 = \varepsilon\bar{\Omega}_1 \cos\omega' t$ rotates with a non-zero mean modulated rotation. The relationship between the Reynolds number of the inner cylinder and frequency. ($\eta = 0.937$) 48

Figure 14 The outer cylinder is fixed and the inner cylinder rotates at different modulated frequencies. The axial speed $\bar{V}_z$ changes with time τ at the point of observation ($\xi = 0.5$, $Z = \lambda/4$). ($\eta = 0.4833$, $\varepsilon = 1$) 49

Figure 15 The outer cylinder is fixed and the inner cylinder rotates at different modulated frequencies. The axial speed $\bar{V}_z$ changes with time τ at the point of observation ($\xi = 0.5$, $Z = \lambda/4$). ($\eta = 0.4833$, $\varepsilon = 2$) 53

Figure 16 Combines both numerical and experimental results for the onset of WVF for $\eta = 0.893$ 69

Figure 17 Neutral stability curves of the transition of Taylor vortex flow to wavy vortex flow for various η. 70

Figure 18 The wave number of the lowest stability boundary for various η. The numbers denote k_1. 79

Figure 19 The lowest stability boundary for the bifurcation from Taylor vortices. 80

Figure 20 The lowest stability boundary for the bifurcation from Taylor vortices (with the simulated result obtained by Jones[34]). 81

Figure 21 Different regimes in the flow between two rotating cylinders. $\eta = 0.88$, $\Gamma = 14.4$. The fluid is silicone oil of 0.11 cm^2/sec viscosity. Below the Taylor boundary there is circular Couette flow. Above the Taylor boundary there is axisymmetric Taylor vortex flow. Above the second boundary marked by the full circles there is

wavy (doubly periodic) Taylor vortex flow. After Coles [8] 82

Figure 22 Lowest stability boundary for different azimuthal wavenumbers k_1 corresponding to nonaxisymmetric TVF that is transformed to a WVF. 83

Nomenclature

Alphabetic

d	gap of cylinders
h	aspect ratio
k_1	azimuthal wave number (wavy mode)
k_2	axial wave number (wavy mode)
k_c	critical axial wave number (for first transition)
p	pressure
P	pressure, dimensionless
r,θ,z	cylindrical coordinates, dimensionless
R	radius of cylinder
Re	Reynolds number
t	time
v_r, v_θ, v_z	velocity component
V_r, V_θ, V_z	velocity component, dimensionless

Greek

α	wave number
Δ	variation of critical Reynolds number $((\mathrm{Re}_c - \mathrm{Re}_0)/\mathrm{Re}_0)$
ε	modulated amplitude
η	radius ratio ($\eta = R_1 / R_2$)

λ	wavelength ($\lambda = 2\pi / \alpha$)
ν	dynamic viscosity coefficiency
ξ	collocation coordinate
ρ	density
σ	growth rate of instability
τ	time, dimensionless
ω	modulated frequency, dimensionless
ω'	modulated frequency
Ω	angular velocity of cylinder

Subscript

0	critical value, non-modulated
1	inner cylinder
2	outer cylinder
c	critical value, modulated

Superscript

'	dimensional

Chapter 1 Introduction

1.1 Motive of the Present Study

Fluid flow between concentric rotating cylinders, generally known as circular Couette or Taylor-Couette flow (Couette[1]; Taylor[2]), is a classic problem in hydrodynamic stability and has provided an important paradigm for the dynamics of shear flows. This problem has been the focus of numerous theoretical and experimental studies.

Taylor[2] went one step further and studied the instability when both cylinders rotate. However, it is my opinion that the current problems concerning this instability (in particular the nonlinear problems) are outlined more clearly in the simpler case in which the outer cylinder is at rest. This strategy also is in line with the scientific paradigm of proceeding from the simple to the complex. Each additional variable makes the theoretical explanation of a nonlinear problem significantly more difficult.

The present study focuses on the centerpiece of the Taylor vortex problem, which is the instability of an infinitely long fluid column between concentric rotating cylinders. This instability is manifested in four ways: linear and nonlinear axisymmetric Taylor vortex flow (TVF), wavy vortex flow (WVF), irregular or chaotic Taylor vortex flow, and turbulent Taylor vortex flow. In this study, we only focus on the instability of the Couette flow, Taylor vortex flow, and wavy vortex flow and pursue the lowest instability boundary curves between these different types of flow.

1.2 Literatures Review

In this study, the behavior of flow motion for the following cases is investigated: (1) rotation of an inner cylinder, which remains static in an outer cylinder, (2) the inner and outer cylinders rotate at different speeds, and (3) the rotation of the inner cylinder is

periodic and modulated.

Donnelly[3] and Simon and Donnelly[4] utilized the torque produced in a cylinder during viscous flow motion to measure the circular Couette flow at the critical point between stable and unstable flow. As the rotational speed of the inner cylinder increases, the torque suddenly changes when the fluid status changes from stable to unstable. From this, the Reynolds number of the critical point can be acquired. The critical point marks the transition from one-dimensional stable Couette flow to two-dimensional Taylor vortex flow. Koschmieder[5], Burkhalter and Koschmieder[6], and Swinney and Gollub[7] obtained the same result by observing flows. For inner and outer cylinders with the same rotational speed and direction, Taylor[2] experimentally demonstrated that when the rotational speed increases gradually to a speed exceeding the critical speed, the flow still retains its one-dimensional flow status. In other words, the rotating outer cylinder has inhibition to stable status. Coles[8], Schwarz *et al.*[9], and Nissan *et al*.[10] obtained the same experimental result as Taylor. Moreover, Walsh and Donnelly[11] demonstrated that when the rotational speed of the inner cylinder is fixed and the outer cylinder undergoes periodic motion, the flow is stabilized. Gollub and Swinney[12] and Walden and Donnelly[13] used the Laser Doppler Anemometer (LDA) to investigate circular Taylor-Couette flow by measuring the radial temperature of flow measurement points.

Through power-spectrum analysis, the time domain is transformed into a frequency domain. The advantage of power spectrum analysis is that different characteristics of a spectrum represent different flow states. When flow is periodic, peaks of a certain size appear in the spectrum at relative and harmonic frequencies. When flow transitions into quasi-periodic flow, a new frequency appears that is not associated with the original frequency. The power spectrum analysis is an efficient approach for studying the

transformation between quasi-periodic and chaotic flows. Cole[14] experimentally investigated the effect of cylinder height on flow stability and demonstrated that cylinder height does not influence the critical point for transformation from a Couette flow to a Taylor vortex flow, unless the aspect ratio between cylinder height and interval is <8. Additionally, according to the study by Hall and Blennerhasset[15], when the aspect ratio $L/d \geq 12$ 12, the numerical and experimental results are not significantly different, indicating that the effect of cylinder height on flow stability is negligible. Barenghi and Jones[16] and Murray *et al.*[17] obtained the same result numerically. Walowit *et al*.[18] applied linear theory to derive the critical value for different radius ratios and the ratio between inner and outer rotational speeds. To examine the stability of a Couette flow between cylinders with different radial temperatures, Snyder and Karlsson[19] experimentally determined the critical Taylor number ($Ta = 2d^3 R_1 (\Omega/\nu)^2$) under different temperatures with $\eta = 0.958$. They found that the result is stable over a small temperature range. Outside of this range, the positive and negative values of the critical Taylor number become unbalanced, and the flow typically becomes unstable.

The present study focuses primarily on the influence of modulated amplitude and frequency on flow stability between the cylinders. The rotational speed of the cylinder is modulated by the factor $\bar{\Omega}(1+\varepsilon\cos\omega' t)$ to investigate the effects of flow stabilization and destabilization. Donnelly[20] experimentally analyzed modulated flow stability and found that when the outer cylinder remains static and the inner cylinder rotates periodically, parameters such as interval, rotational frequency, and modulation amplitude of the two cylinders can be modified to determine how the circular Couette flow is affected by modulated rotation. Hall[21] utilized linear theory to determine low and high frequencies and used non-linear theory to analyze the flow for high frequency

modulations. Hall demonstrated that flow is slightly destabilized regardless of amplitude for low frequency modulations. Within a certain frequency range, the flow becomes increasingly stable. When the rotation is modulated at high frequency, the stability approaches the critical value of the non-modulated situation. Riley and Laurence[22] utilized Galerkin expansion and Floquet theory for stability analysis and investigated flow stability under modulated conditions with a narrow inter-cylinder gap. The numerical result obtained by Riley and Laurence is the same as that acquired by Hall[21]. Davis[23] developed the notion of the quasi-steady limit by showing that a modulated inner cylinder destabilizes flow. Under extremely low frequency, the critical stability value of a flow declines to $1/(1+\varepsilon)$ of the non-modulated situation. Carmi and Tustaniwskyj[24] examined modulated flow stability under small-gap conditions and the influence of axis symmetry on modulated flow. In their study, the unstable offset of the critical Reynolds number increases at low frequencies. At medium-to-high frequencies, no stable critical value appears. Walsh and Donnelly[11] analyzed the flow between inner and outer cylinders with different radii using the photo voltage of observation particles. They determined that the critical Reynolds number has a relatively large offset at low frequency. In conclusion, a critical Reynolds number lower than the theoretical value indicates that the flow is temporarily unstable, but not permanently unstable. Therefore, the stable critical value is lower than the theoretical value at low frequency.

Walsh *et al*.[25] measured the critical Reynolds number for concentric cylinders with different radius ratios and, multiplying the result by a factor, obtained roughly the same value as that calculated by Carmi and Tustaniwskyj[24]. Kuhlmann *et al*.[26] utilized a low-dimensional model to examine the stability of circular Couette flow and Taylor vortex flow under instability. They found that a large modulated amplitude

causes subharmonic perturbation. Ganske *et al*.[27] used a static outer cylinder and a modulated vortex flow in the inner cylinder to investigate the influence on stability of different amplitudes. They demonstrated that the modulated effect causes the flow to become increasingly unstable, and that the effect of amplitude on flow stability is significantly more important than the effect of frequency. When the amplitude is large, the unstable effect increases and the critical stability value declines further. Meksyn[28] used numerical methods to predict the occurrence of instability when the inner and outer cylinders rotated in either the same or opposite directions. Sparrow *et al*.[29] also applied numerical methods to investigate the same and opposite flows around inner and outer cylinders for a radius ratio of 0.95–0.1. Youd *et al*.[30], who analyzed zero-equivalent modulated flow around concentric cylinders with a radius ratio of $\eta = 0.75$, identified the axis symmetry of the Taylor vortex.

After the Taylor vortex problem had approached nonlinearity for many years, Coles[31] brought it decisively into nonlinearity in reporting the non-uniqueness of the wavy flow in the Taylor-Couette flow. The entire pattern of wavy vortices moves with uniform velocity in the azimuthal direction. Because the term "wavy" is typically associated with a motion that has periodic vertical oscillation, this study emphasizes that wavy Taylor vortices move in the azimuthal direction as rings that have an integer number k_1 of fixed sinusoidal upward and downward deformations (k_1 is the integer number of azimuthal waves). An example of a wavy Taylor vortex flow, as observed by Taylor[2], Lewis[32], Coles[31], and Schultz-Grunow and Hein[33], was not recognized as a characteristic new feature of the flow. After Coles' preliminary results were published, wavy vortices were also observed by Nissan *et al*.[10]. Schwarz *et al*.[9] reported experiments in which they observed an asymmetrical mode with $k_1 = 1$.

Burkhalter and Koschmieder[6] concluded that the wavelength of axisymmetrical

vortices with large radius ratios is independent of the Reynolds number in fluid columns of infinite length when the Reynolds number increases quasi-steadily. However, the wavelength of Taylor vortices is constant only as long as the flow is quasi-static. Jones[34] reported the stability boundary for wave number $\alpha = 3.13$, the critical value of a quasi-static transition, for a wide range of η.

Although Taylor analyzed the flow under supercritical conditions, Stuart[35] concluded that the vortex size remains unchanged above the critical Reynolds number. However, numerous studies (see Ahlers *et al*.[36], Andereck *et al*.[37], Park *et al*.[38], Burkhalter and Koschmieder [6, 39], and Antonijoan[40]) have demonstrated the importance of acceleration/deceleration in determining the final state of the flow. These vortices have axial wavelengths that are shorter or longer than those obtained after a quasi-static transition. This study demonstrates that the lowest stability boundary occurs at the critical wavelength of a quasi-static transition and also in another. These solutions are connected with standard Taylor vortices and can be obtained quasi-statically for certain radius ratios when using a mechanism to modify the axial wavelength (see Ref. [41]).

1.3 Objective of This Study

The literatures reviewed above describes the transition between Couette flow and supercritical Taylor vortex flow through experimental and theoretical work. However, the lowest-stability boundary between supercritical axisymmetric Taylor vortex flow to wavy vortex flow for different wave numbers and for various radius ratios is not clear. In this study, therefore, we will pursue the objective of the lowest stability curve for Taylor-Couette flow. This results will be compared with previous experimental and theoretical research.

Chapter 2 Instability of Non-modulated and Modulated Circular Couette Flow

2.1 General Features

This study analyzes both fluid flow of rotating cylinders and the stability of modulated Couette flow by using numerical methods, under different modulated amplitudes and frequencies, the unstable behaviour caused by fluid flow and the influence to become a Taylor vortex flow is also studied. To investigate the change in stability of a modulated Couette flow, Floquet theorem is used with numerical methods. The amount of perturbation motion is divided into two progressions of time and space. Galerkin and Collocation techniques are then utilized to transform the perturbation motion formula into an algebraic Eigenvalue problem. Then QZ method is applied to solve the Eigenvalue problem. The factors of instability are determined by these Eigenvalues.

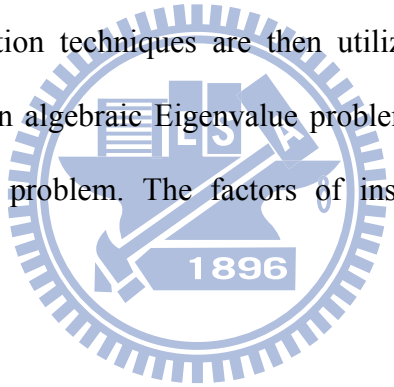

2.2 Numerical Procedures

Figure 1 presents the physics model examined in this study. The two unlimited long vertical and concentric cylinders are full of viscid fluids. The outer cylinder remains static and the inner cylinder rotates at $\Omega_1(1+\varepsilon\cos\omega' t)$. When the inner cylinder rotates at a fixed speed ($\varepsilon = 0$) that is very low, the flow between cylinders is one-dimensional and stable. The fluid particles wind around the centre in a circular motion and is called a circular Couette flow. When rotational speed is increased to a critical value, the flow becomes unstable and forms a two-dimensional stable flow. At that time, the particles wind around the centre in toroidal motion; this is called a Taylor vortex flow (TVF). When the inner cylinder rotates in a modulated manner ($\varepsilon \neq 0$) and average rotational

speed is very low, the flow remains one-dimensional; this is called a modulated circular Couette flow. When average rotational speed is increased to the critical value, the flow becomes unstable and is transformed into a two-dimensional flow. This critical rotational speed is affected by modulated amplitude ε and modulated frequency ω'.

For the convenience of problem analysis, we assume the working fluid is Newtonian fluid. Except for density, all other physical properties are fixed. The change in fluid density satisfies the Boussinesq approximation for gravity and centrifugal force; other items are ignored. The loss of fluid viscidly is also ignored. The governing equations are as follows:

Continuity equation :

$$\frac{1}{r}\frac{\partial}{\partial r}(rv_r)+\frac{1}{r}\frac{\partial v_\theta}{\partial \theta}+\frac{\partial v_z}{\partial z}=0 \tag{2.1}$$

Momentum equations :

$$\frac{\partial v_r}{\partial t}+v_r\frac{\partial v_r}{\partial r}+\frac{v_\theta}{r}\frac{\partial v_r}{\partial \theta}+v_z\frac{\partial v_r}{\partial z}=-\frac{1}{\rho}\frac{\partial p}{\partial r}+\nu\left[\left(\nabla-\frac{1}{r^2}\right)v_r-\frac{2}{r^2}\frac{\partial v_r}{\partial \theta}\right] \tag{2.2}$$

$$\frac{\partial v_\theta}{\partial t}+v_r\frac{\partial v_\theta}{\partial r}+\frac{v_\theta}{r}\frac{\partial v_\theta}{\partial \theta}+v_z\frac{\partial v_\theta}{\partial z}+\frac{v_r v_\theta}{r}=-\frac{1}{\rho\cdot r}\frac{\partial p}{\partial \theta}+\nu\left[\left(\nabla-\frac{1}{r^2}\right)v_\theta-\frac{2}{r^2}\frac{\partial v_r}{\partial \theta}\right] \tag{2.3}$$

$$\frac{\partial v_z}{\partial t}+v_r\frac{\partial v_z}{\partial r}+\frac{v_\theta}{r}\frac{\partial v_z}{\partial \theta}+v_z\frac{\partial v_z}{\partial z}=-\frac{1}{\rho}\frac{\partial p}{\partial z}+\nu\nabla v_z \tag{2.4}$$

Boundary condition :

$$r=R_1\ :\ v_r=v_z=0,\ \ v_\theta=R_1\Omega_1\left(1+\varepsilon\cos\omega' t\right) \tag{2.5}$$

$$r=R_2\ :\ v_r=v_\theta=v_z=0$$

$$\nabla=\frac{\partial^2}{\partial r^2}+\frac{1}{r}\frac{\partial}{\partial r}+\frac{1}{r^2}\frac{\partial^2}{\partial \theta^2}+\frac{\partial^2}{\partial z^2} \tag{2.6}$$

where, ρ is density and ν is the dynamic viscosity coefficient. Figure 2 presents

the definitions of coordinates. the following parameters to make governing equation dimensionless:

$$r=\frac{R}{d},\ z=\frac{Z}{d},\ \tau=\frac{\nu t}{d^2},\ \omega=\frac{d^2\omega'}{\nu},\ \mathrm{Re}_1=\frac{R_1\Omega_1 d}{\nu} \tag{2.7}$$

$$\bar{V}_r=\frac{v_r d}{\nu},\ \bar{V}_\theta=\frac{v_\theta d}{\nu},\ \bar{V}_z=\frac{v_z d}{\nu},\ \bar{P}=\frac{p d^2}{\rho\nu^2}$$

where $d=R_2-R_1$.

When inner cylinder rotates in fixed speed and the rotational speed is very low, the flow of cylinders is one-dimensional stable status and is called circular Couette flow. At that moment

$$\bar{V}_r=0,\ \bar{V}_\theta=\bar{V}_\theta(r,\tau),\ \bar{V}_z=0 \tag{2.8}$$

It is then substituted into dimensionless equation. After the simplification, the following is obtained:

$$\frac{d\bar{V}_\theta}{d\tau}=\left(\frac{d^2}{dr^2}+\frac{1}{r}\frac{d}{dr}-\frac{1}{r^2}\right)\bar{V}_\theta \tag{2.9}$$

Boundary condition:

$$r=\frac{\eta}{1-\eta}\ :\ \bar{V}_r=\bar{V}_z=0\ ,\ \bar{V}_\theta=\mathrm{Re}_1(1+\varepsilon\cos\omega\tau) \tag{2.10}$$

$$r=\frac{1}{1-\eta}\ :\ \bar{V}_r=\bar{V}_\theta=\bar{V}_z=0$$

from the equation above, we can solve and get:

$$\bar{V}_\theta(r,\tau)=-\frac{\eta(1-\eta)}{1-\eta^2}r+\frac{\eta}{(1-\eta^2)(1-\eta)}r^{-1}+$$

$$\mathrm{Re}\,al\left\{\varepsilon\frac{K_1(sr_2)I_1(sr)-I_1(sr_2)K_1(sr)}{I_1(sr_1)K_1(sr_2)-I_1(sr_2)K_1(sr_1)}e^{i\omega\tau}\right\} \tag{2.11}$$

where $s=\sqrt{i\omega}$, $r_1=\frac{\eta}{1-\eta}$ and $r_2=\frac{1}{1-\eta}$ are the position of inner and outer

cylinders respectively. I_1 and K_1 are respectively the first and second kind first order modulated Bessel functions.

According to the study by Carmi and Tustaniwskyj[24], axial symmetrical status is easily become unstable than axial asymmetrical status. Therefore, this study only considers disturbance as a symmetrical status. When the average rotational speed of a one-dimensional modulated circular Couette flow exceeds the critical value, the flow is transformed into a symmetrical two-dimensional flow. This flow can be considered a one-dimensional flow $\left(0,\bar{V}_\theta,0,\bar{P}\right)$ plus a disturbance $\left(V_r',V_\theta',V_z',P'\right)$. At that moment, $\partial/\partial\theta = 0$. After substituting into the equation, simplification and ignoring the nonlinear items, the following disturbance equation is obtained:

Continuity equation:

$$\frac{1}{r}\frac{\partial}{\partial r}\left(rV_r'\right)+V_z' = 0 \tag{2.12}$$

Momentum equations:

$$\frac{\partial V_r'}{\partial \tau}+\mathrm{Re}_1\left(\bar{V}_z\frac{\partial V_r'}{\partial z}+-\frac{2\bar{V}_\theta V_\theta'}{r}\right)=-\frac{\partial P'}{\partial r}+\left[\left(\nabla-\frac{1}{r^2}\right)V_r'\right] \tag{2.13}$$

$$\frac{\partial V_\theta'}{\partial \tau}+\mathrm{Re}_1\left(\left(\frac{\partial \bar{V}_\theta}{\partial r}+\frac{\bar{V}_\theta}{r}\right)V_r'+\bar{V}_z\frac{\partial V_\theta'}{\partial z}\right)=\left[\left(\nabla-\frac{1}{r^2}\right)V_\theta'\right] \tag{2.14}$$

$$\frac{\partial V_z'}{\partial \tau}+\mathrm{Re}_1\left(V_r'\frac{\partial \bar{V}_z}{\partial r}+\bar{V}_z\frac{\partial V_z'}{\partial z}\right)=-\frac{\partial P'}{\partial z}+\nabla V_z' \tag{2.15}$$

Boundary condition:

$$r=\frac{\eta}{1-\eta}\ :\ V_r'=V_\theta'=V_z'=0,\quad r=\frac{1}{1-\eta}\ :\ V_r'=V_\theta'=V_z'=0 \tag{2.16}$$

The variables P' and V_z' in Eqs. (2.12) - (2.15) can be cancelled out from algebraic

operation, and we can obtain

$$\left\{\frac{\partial}{\partial z}\left(\frac{\partial^2}{\partial\tau\cdot\partial z}\right)+\left(\frac{\partial^2}{\partial\tau\cdot\partial r}-\frac{\partial}{\partial r}\nabla\right)\left(\frac{\partial}{\partial r}+\frac{1}{r}\right)\right\}V_r^{'}-\frac{\partial}{\partial z}\left(\mathrm{Re}_1\frac{2\bar{\bar{V}}_\theta}{r}\right)\cdot\frac{\partial V_\theta^{'}}{\partial z}=\left(\nabla-\frac{1}{r^2}\right)\frac{\partial^2 V_r^{'}}{\partial z^2} \tag{2.17}$$

$$\frac{\partial V_\theta^{'}}{\partial\tau}+\mathrm{Re}_1\left\{\left(\frac{\partial\bar{\bar{V}}_\theta}{\partial r}+\frac{\bar{\bar{V}}_\theta}{r}\right)V_r^{'}\right\}=\left[\left(\nabla-\frac{1}{r^2}\right)V_\theta^{'}\right] \tag{2.18}$$

$V_r^{'}$ is the fourth order differential equation of r, and the boundary conditions are:

$$r=\frac{\eta}{1-\eta}\ :\ V_r^{'}=\frac{dV_r^{'}}{dr}=V_\theta^{'}=0 \tag{2.19}$$

$$r=\frac{1}{1-\eta}\ :\ V_r^{'}=\frac{dV_r^{'}}{dr}=V_\theta^{'}=0$$

The disturbance equation is the differential equation of time and space. Furthermore, time and periodic coefficients are included in the equation. According to Floquet theory (Coddington and Levinson[42]]), the time item for disturbance can be divided into time and an index function, which increases over time. If the disturbance equation is described in normal mode, disturbance $\left(V_r^{'},V_\theta^{'}\right)$ in the equation can be assumed in the axis direction and periodically distributed. Additionally, the index function increases over time, and the disturbance amplitude uses time and space as its function. The disturbance terms can be represented as

$$\begin{bmatrix}V_r^{'}\\V_\theta^{'}\end{bmatrix}=\begin{bmatrix}f(r,\tau)\\g(r,\tau)\end{bmatrix}e^{\sigma\tau+i\alpha z} \tag{2.20}$$

where α is the axial wave number, and σ is the growth rate of a complex disturbance. The stability of basic flow can be determined by the real number of the growth rate of a complex disturbance. When $\sigma_r<0$, the entire flow is stable. The disturbance declines as time increases. When $\sigma_r>0$, the disturbance increases over

time and the flow becomes unstable. When $\sigma_r = 0$, the flow has neutral stability. The characteristic value of flow stability can be determined using the disturbance growth rate σ in the characteristic equation.

This study utilizes the spectral method (Canuto *et al.*[43]) to transform the characteristic equation into an algebraic characteristic equation. The QZ numeric method is then applied to solve the characteristic value of this equation group. According to the Floquet theory, $[f(r,\tau), g(r,\tau)]$ represents the disturbance value. The second orders of time and space are expanded. Time is expanded via a complex Fourier series of period $2\pi/\omega$. Space is expanded by the first type n orders of Chebyshev polynomial (Fox and Parker[44]). The definition of Chebyshev polynomial is

$$T_n(\xi) = \cos\left(n \cdot \cos^{-1}\xi\right) \tag{2.21}$$

The defined domain of r in the original equation is transformed from $\eta/(1-\eta) \le r \le 1/(1-\eta)$ to $-1 \le \xi \le 1$ through the relational equation $\xi = 2r - (1+\eta)/(1-\eta)$. The amplitude in normal mode can be expressed as

$$f(\xi,\tau) = \sum_{m=-\infty}^{\infty}\sum_{n=4}^{\infty} a_{mn}\Psi_n(\xi)e^{-im\omega\tau} \tag{2.22}$$

$$g(\xi,\tau) = \sum_{m=-\infty}^{\infty}\sum_{n=2}^{\infty} b_{mn}\phi_n(\xi)e^{-im\omega\tau} \tag{2.23}$$

where a_{mn} and b_{mn} are unknown coefficients, and Ψ_n and ϕ_n are basis functions. The definition of the basis functions are as follows:

$$\Psi_n = \begin{cases} T_n - \dfrac{n^2}{4}T_2 + \left(\dfrac{n^2}{4} - 1\right)T_0 & \text{for even n} \\ T_n - \dfrac{n^2-1}{8}T_3 + \left(\dfrac{n^2-1}{8} - 1\right)T_1 & \text{for odd n} \end{cases} \quad n \ge 4 \tag{2.24}$$

$$\phi_n = \begin{cases} T_n - T_0 & \text{for even n} \\ T_n - T_1 & \text{for odd n} \end{cases} \quad n \ge 2 \tag{2.25}$$

The Galerkin and collocation methods are applied to make the characteristic equation discrete, and can be represented by a matrix such as

$$\tilde{A}\tilde{Y} = \sigma \tilde{B}\tilde{Y} \tag{2.26}$$

where σ is the characteristic value used to determine flow stability in this study.

$$\tilde{A} = \begin{bmatrix} A^{11} & A^{12} \\ A^{21} & A^{22} \end{bmatrix}, \quad \tilde{B} = \begin{bmatrix} B^{11} & B^{12} \\ B^{21} & B^{22} \end{bmatrix}, \quad \tilde{Y} = \begin{bmatrix} \tilde{a} \\ \tilde{b} \end{bmatrix} \tag{2.27}$$

2.3 The Result of Non-modulated Effect on Couette Flow

Table 1 shows experimental results. The flow generates an unstable critical value and average experimental value of $\mathrm{Re}_0 = 68.75$. Compared with experimental results obtained by other studies, the error rate is < 1.18%. If error deviation is added, then the critical value is $\mathrm{Re}_0 = 68.75 \pm 1.1$. The experimental results acquired by other studies are within the error range in this experiment. The experimental result is the experimental foundation of the modulated Couette flow. For measurement of wave number α, only the total length of 10 cells in the middle of the flow (equivalent to the total length of five wavelengths) were examined to avoid influence from upper and lower boundaries in the experiment. The vortex size is averaged and then its wavelength λ is calculated. The precision of this measurement is within 0.1mm. Then, the wavelength is calculated by $\lambda = 2\pi / \alpha$.

Table 1 shows the average wave number, which is $\alpha = 3.19$. The theoretical value calculated for unlimited length is $\alpha = 3.17$. The error between the experimental result and theoretical value is < 0.6%. Additionally, this experiment also examined different aspect ratios, including $h = 24$, 20 and 16. The experimental result does not change obviously and the critical Re is within 68.75 ± 1.1. Therefore, the aspect ratio does not have a significant effect on the aspect ratio; this is the same experimental result obtained

by Cole[14].

2.4 The Result of Modulated Effect on Couette Flow

Under a modulated effect, the inner cylinder rotates with the $\Omega_1(1+\varepsilon\cos\omega' t)$ period. The stability of the modulated Couette flow is primarily affected by modulated amplitude and modulated frequency. This study analyzed different aspect ratios, upper and lower boundaries to determine how they affect the modulated Couette flow. To compare modulated effect with the non-modulated effect, the change rate of the critical Re_1 is defined here; $\Delta = (\mathrm{Re}_c - \mathrm{Re}_0)/\mathrm{Re}_0$, $\Delta > 0$ represents the modulation has stabilized.

The experimental value was obtained using the optical measurement method and flow observation method. The solid line on Fig. 3(a) is the theoretical result. At a low frequency, when $\Delta < 0$, the critical Re is lower than that for a non-modulated effect. The result demonstrates that the modulated effect has an unstable effect on flow. Additionally, when the frequency continues to decrease, Δ approached the quasi-static limit $-\varepsilon/(1+\varepsilon)$. At a medium-to-high frequency, Δ increases as frequency increases. Generally, in this frequency range, the modulated effect destabilizes the flow. As frequency decreases, destabilization increases.

The error of result in this experiment and theoretical value are relatively large at a medium frequency (Fig. 3(a)). At a high frequency, Δ approaches but remains slightly lower than 0. At that moment, modulated frequency has slightly destabilized the flow. Figure 3(b) presents the curve of medium stable critical Re at different modulated amplitudes. When the flow is unstable, the disturbance has three statuses. For any amplitude, disturbance $\sigma_i = 0$ at a low frequency is synchronous. After the flow becomes unstable, the frequency of the flow and base status are the same. As frequency

increases, disturbance changes to a quasi-periodic state. At that moment, $\sigma_i \neq 0$ and the ratio of the flow frequency to base status frequency is not a rational number. When the frequency increases to an ultra-high frequency, σ_i is multiple times the base status frequency. At that moment, disturbance returns to synchronous.

Figure 4 shows the relationship between relative variable Δ of the Re and amplitude under different frequencies. The solid line in the graph is the experimental result derived using the numerical method. The dotted line in Fig. 4(a) is the quasi-steady limit $-\varepsilon/(1+\varepsilon)$ when $\omega \to 0$. At an extra low frequency, if the amplitude is high, destabilization is also high. If the critical Re approaches $\mathrm{Re}_0/(1+\varepsilon)$ when frequency is $\omega = 0.063$, amplitude increases from 0 to 1.0, and the variable Δ of the Re_1 gradually decreases to around -0.5. Additionally, based on the graph, the experimental result and quasi-static limit $-\varepsilon/(1+\varepsilon)$ are extremely close. When the modulated frequency is $\omega = 0.628$ and $\omega = 6.28$ (Figs. 4(b) and 4(c), respectively), the relative variable Δ of the Re_1 will decrease as modulated amplitude increases. When the modulated amplitude is high, the relative variable Δ of the Re decreases and the flow becomes increasingly unstable. However, the degree of instability is lower than that at a low frequency.

At a high frequency (Fig. 4(d)), when modulated frequency is $\omega = 62.8$, the different modulated amplitude does not have a significant effect on relative variable Δ of the Re. The modulated amplitude does not significantly influence flow stability.

For different radius ratios η, Fig. 5 presents the experimental result obtained by this study and Walsh *et al.*[25]. The graph includes different radius ratios η, which include η = 0.4833, 0.719, 0.88, and a modulated amplitude of 0.5. Regardless of the radius ratio, the stable critical value increases as frequency increases, and approaches a

stable critical value Re_0 under the non-modulated effect. At a low frequency, the stable critical value approaches $\mathrm{Re}_0/(1+\varepsilon)$.

This study investigated the influence of several aspect ratios h on the stable critical value. Figure 6 presents numerical results. When aspect ratio h decreases, Δ also decreases and flow destabilization increases. When frequency is high, the rate reduction is obvious.

This experiment chose three different cylinder boundary conditions: fixed on sides, top free bottom fix, and top rotate bottom fix. The aspect ratio is $h=24$. Figure 7 presents the numerical result. The measured results for the three conditions are similar. The flow is not affected by the upper and lower boundaries. The possible reasons are that measurement points for the optical measurement method are at the middle of the cylinder and the aspect ratio is sufficiently large. Therefore, the effect caused by boundaries near measurement points is extremely small.

For the non-modulated effect, the experimental result for wave number of the stable critical value is $\alpha=3.19$. When the flow is modulated, the flow observation method is used to measure the wave number when flow exceeds a stable state, and determine whether the wave number changes under a modulated effect. Figure 8 shows numerical results. The wave number first decreases as the modulated frequency increases. The wave number is not a fixed value and changes for different modulated frequencies. The degree of change to experimental data is not as large as the theoretical value; however, the tendencies are the same.

Figure 9 presents the relationship between critical wave number k_c and frequency for different radius ratios and modulated amplitudes. When the flow transforms disturbance from synchronous to quasi-periodic, a discontinuous point exists at amplitude. The axial wave number increases as modulated frequency increases. When

the frequency exceeds the first discontinuous point, axial wave number suddenly decreases and then increases again. When the axial wave number reaches a maximum value, the critical Re also reaches a maximum value, the decrease as modulated frequency increases. Finally, the axial wave number approaches the value of non-modulated rotation at an extra high frequency.

Figure 10 presents the relationship between the Re_1 and frequency when amplitude is (a) $\varepsilon = 1$ and (b) $\varepsilon = 2$ under different radius ratios η. When radius ratio η is small, the change to the critical Re under medium-to-high frequency becomes steep; at a stable status, the offset is large.

Table 1 Comparison list of results from this study and other scholars under the condition of a non-modulated Couette flow

	Study method	Aspect ratio h	Radius ratio η	Critical value Re_0	Wave number α
Huang[45]	Flow visualization and Optical method	24	0.4833	68.75	3.19
Donnelly[3]	Torsion measurement method	4	0.5	68.28	
Donnelly[46]	Flow visualization	5	0.5	68.57	3.10
Simon and Donnelly[4]	Torsion measurement method	5	0.5	68.23	
Sparrow et al.[29]	Numerical method	Infinite	0.5	68.19	3.16
Present	Numerical method	Infinite	0.4833	67.94	3.17
Present	Numerical method	Infinite	0.5	68.186	3.16

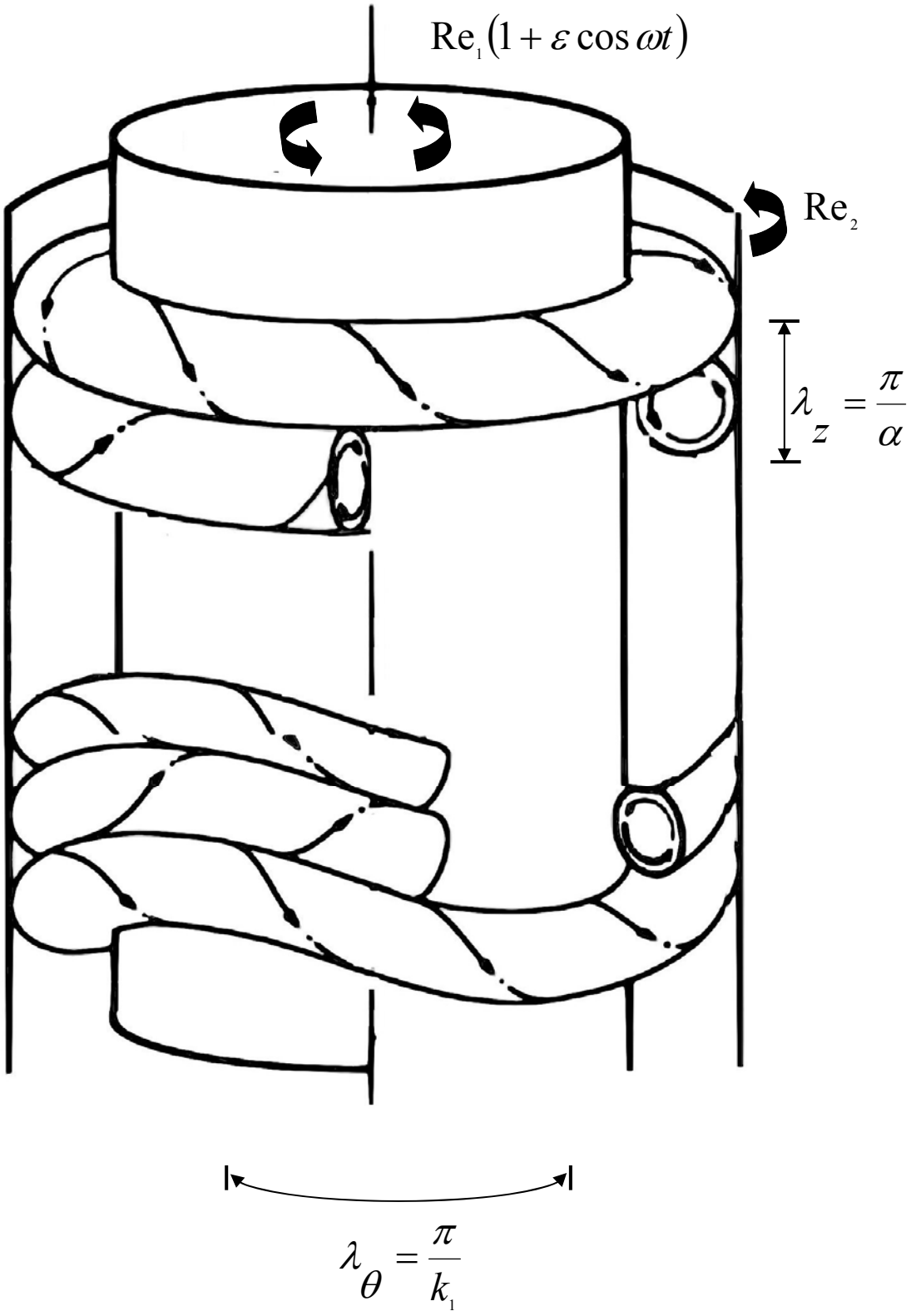

Figure 1 Physics mode graph

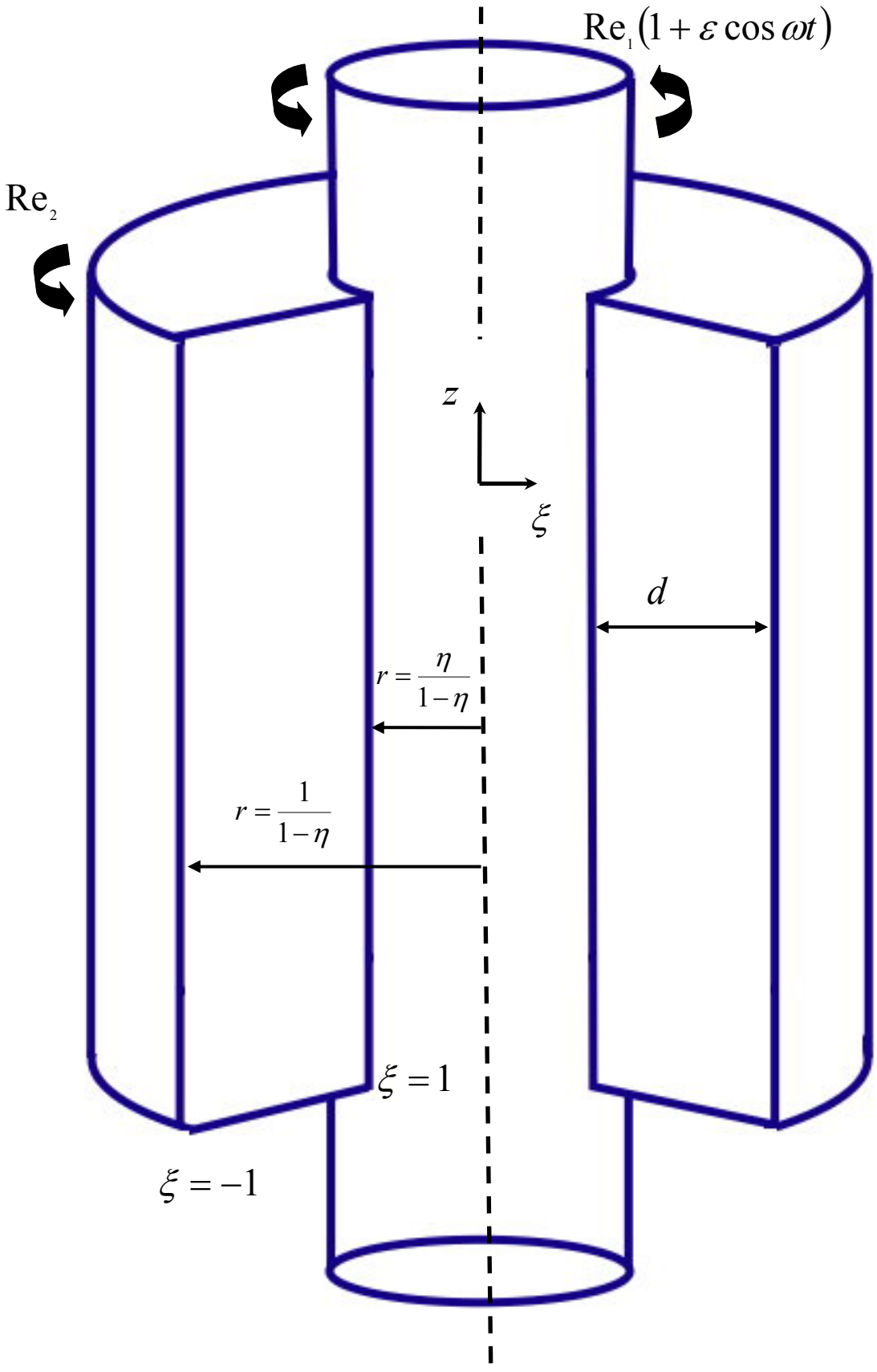

Figure 2 Coordinate graph

(a)

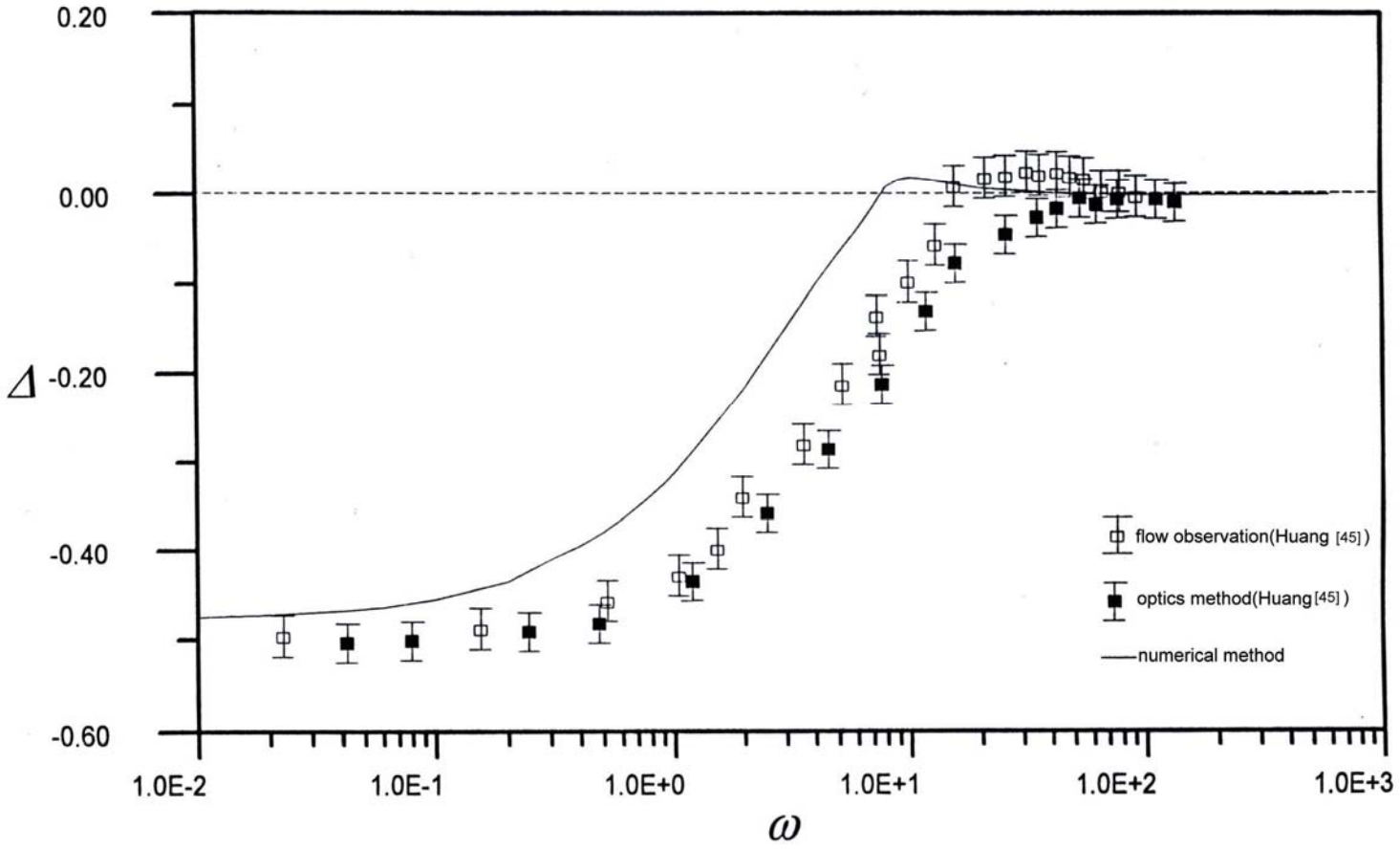

Figure 3 (a) The relationship of relative variable Δ vs modulated frequency is showing under modulated effect $\varepsilon = 1$
(b) A chart showing the variation of Re_1 on different modulated amplitudes vs frequencies. ($\eta = 0.4833$)

(b)

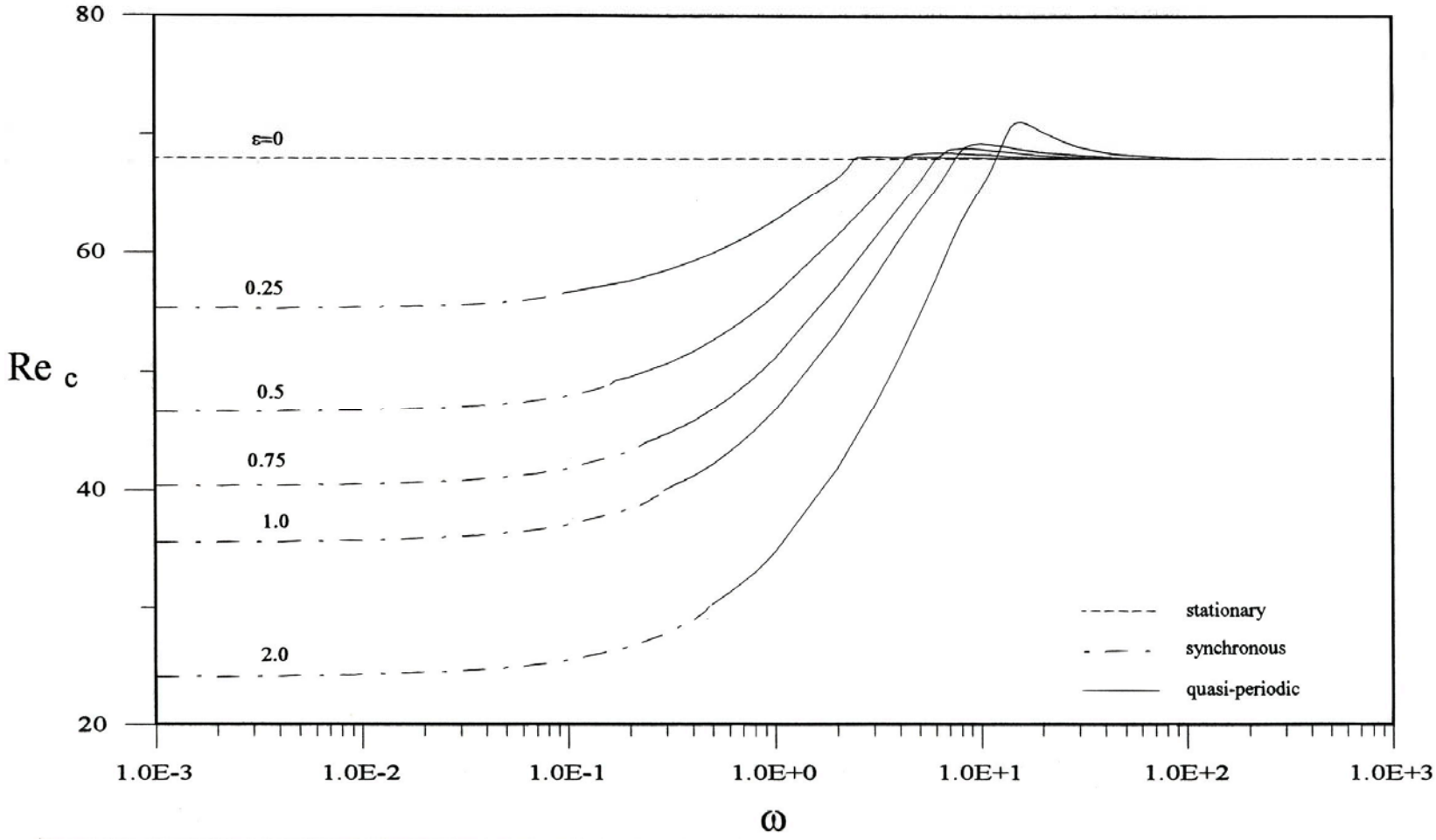
80
60
40
20
Re c
ε=0
0.25
0.5
0.75
1.0
2.0
stationary
synchronous
quasi-periodic
1.0E-3
1.0E-2
1.0E-1
1.0E+0
1.0E+1
1.0E+2
1.0E+3
ω

Continued.

(a)

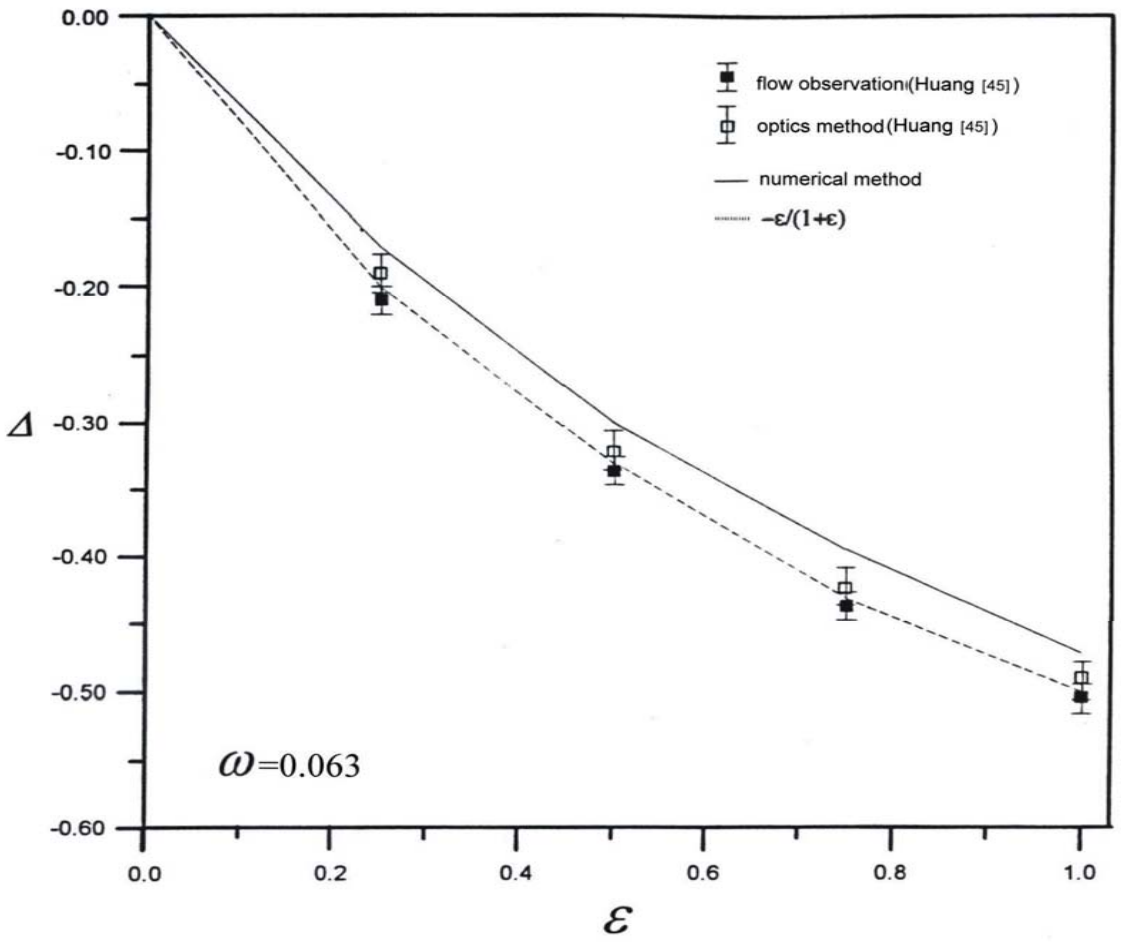

Figure 4 Relationship between relative variable Δ of the Re_1 and amplitude under different modulated effects. (a) $\omega = 0.063$ (b) $\omega = 0.628$ (c) $\omega = 6.28$ (d) $\omega = 62.8$

(b)

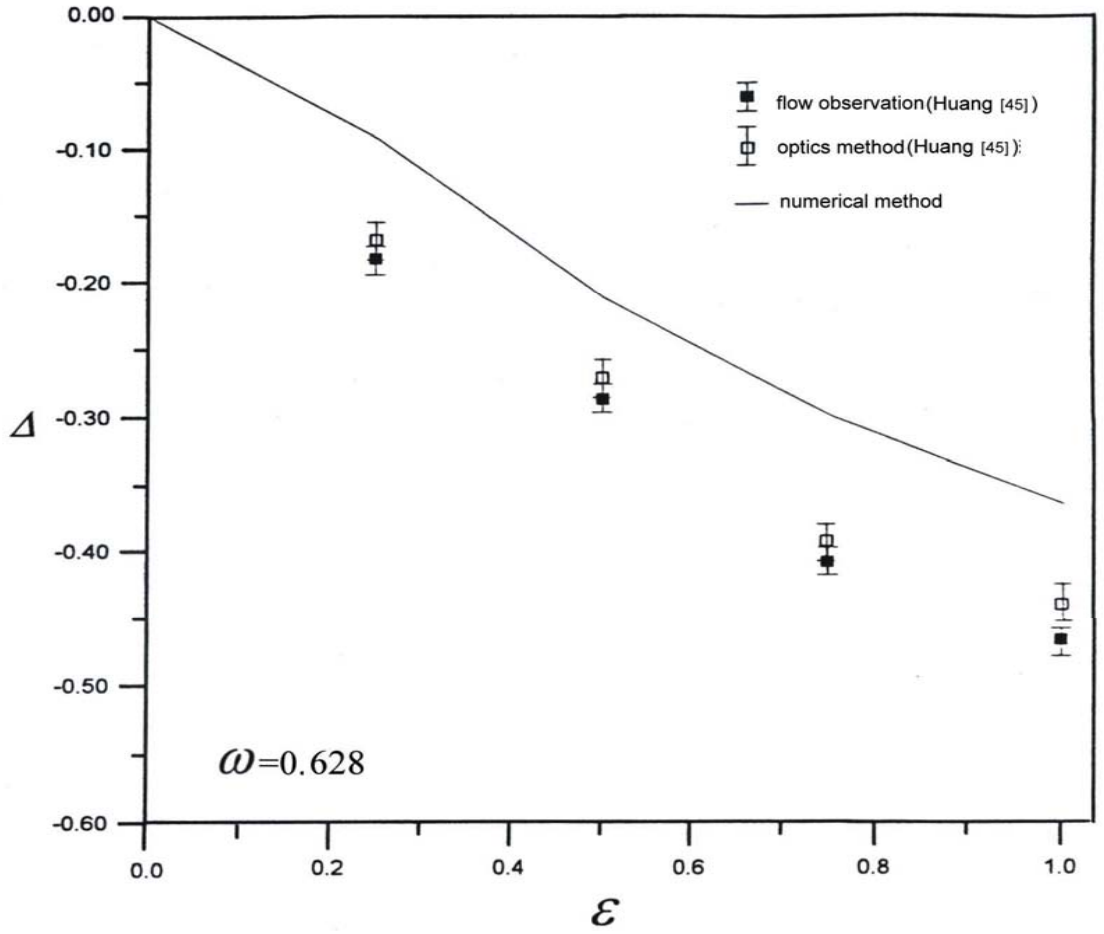
0.00
-0.10
-0.20
-0.30
-0.40
-0.50
-0.60
Δ
0.0
0.2
0.4
0.6
0.8
1.0
ε
flow observation(Huang [45])
optics method(Huang [45])
numerical method
ω=0.628

Continued.

(c)

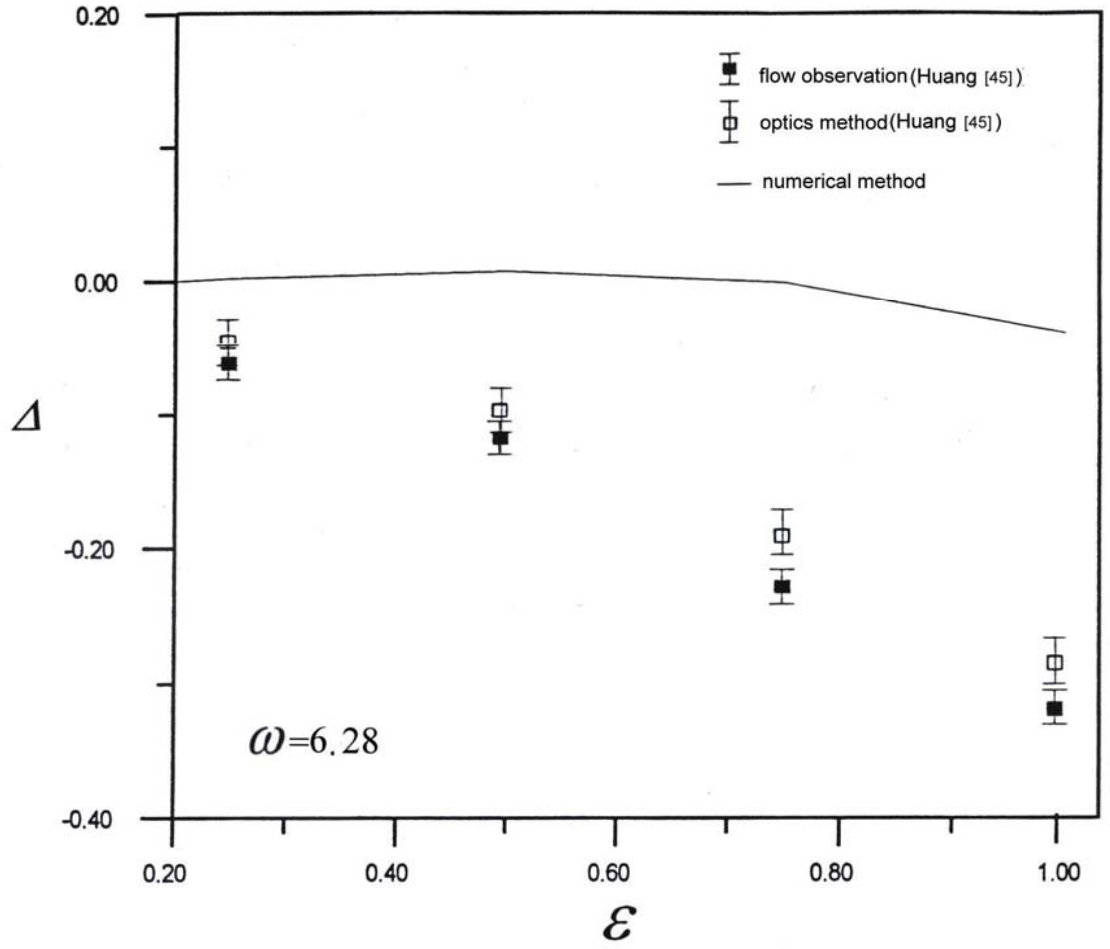
0.20
0.00
-0.20
-0.40
Δ
flow observation(Huang [45])
optics method(Huang [45])
numerical method
ω=6.28
0.20
0.40
0.60
0.80
1.00
ε

Continued.

(d)

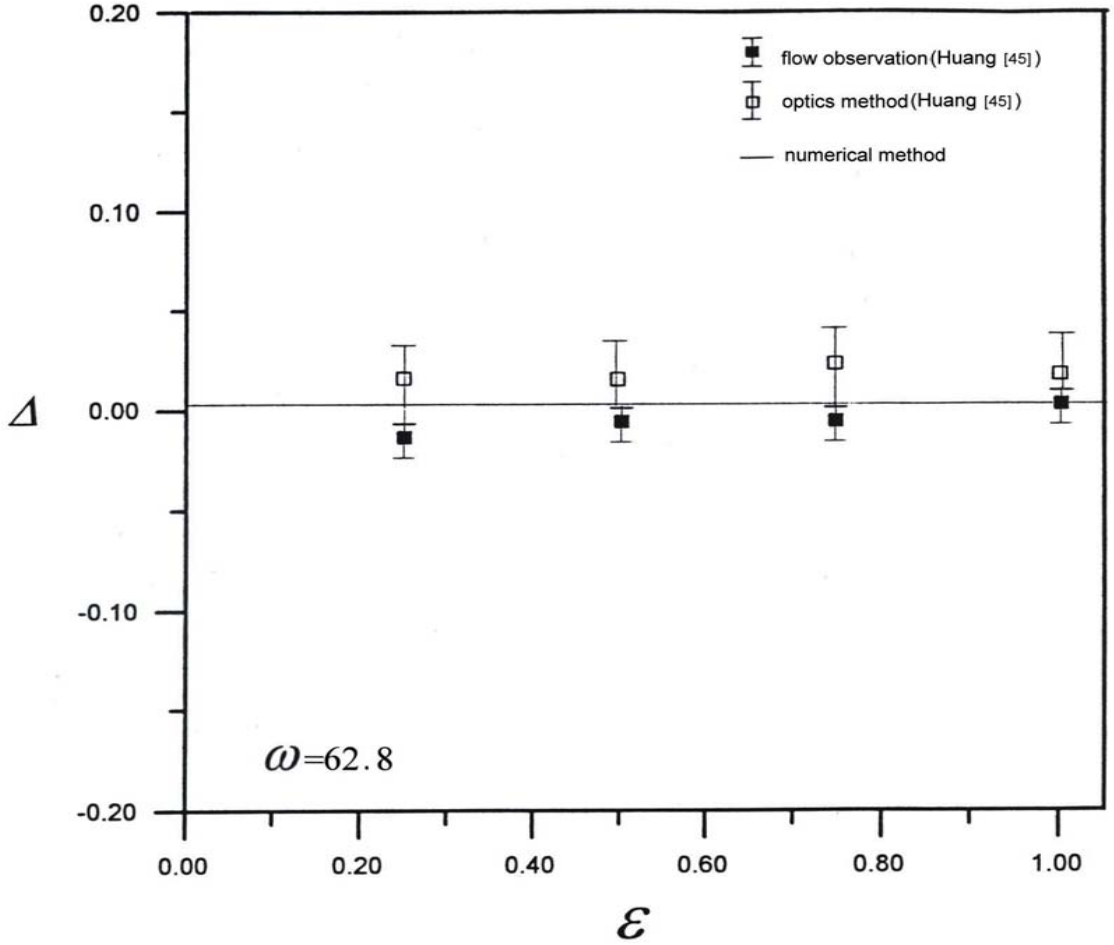
0.20
0.10
0.00
-0.10
-0.20
Δ
flow observation(Huang [45])
optics method(Huang [45])
numerical method
ω=62.8
0.00
0.20
0.40
0.60
0.80
1.00
ε

Continued.

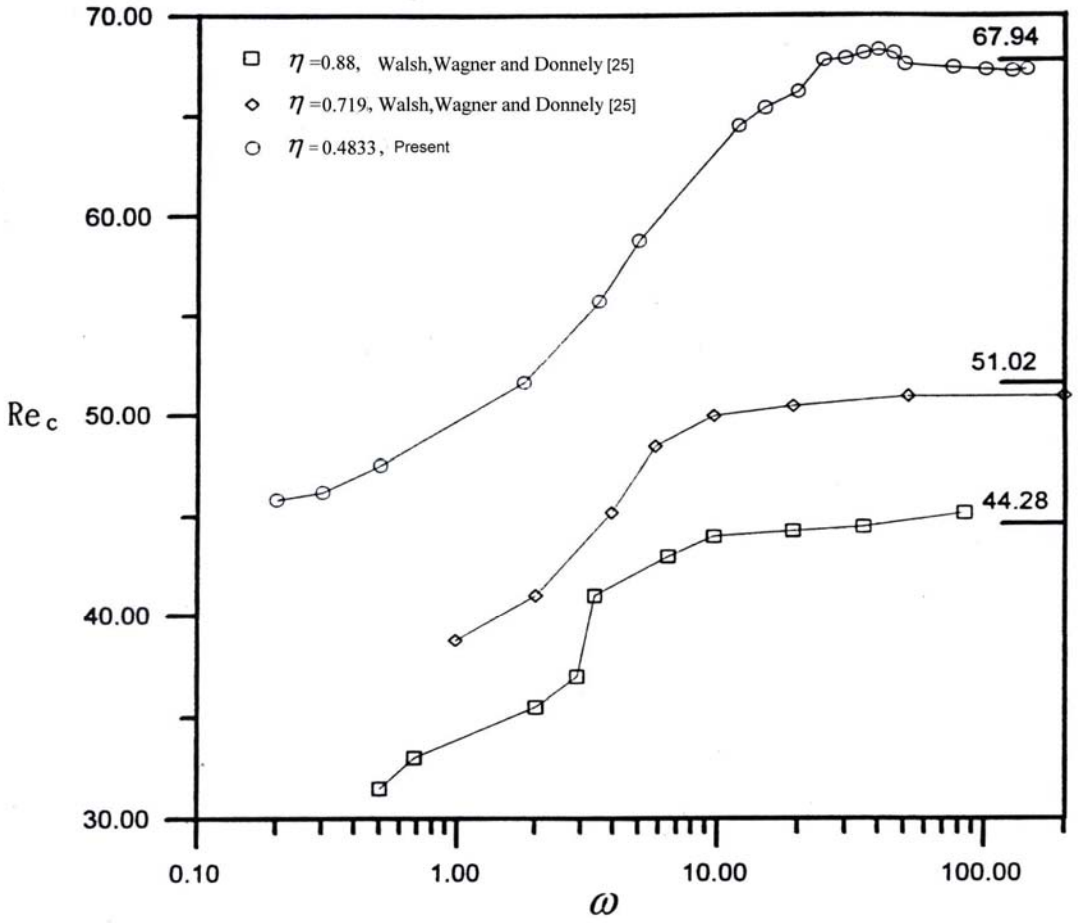

Figure 5 Different inner and outer radius ratios, and the relationship between critical Re and frequency.

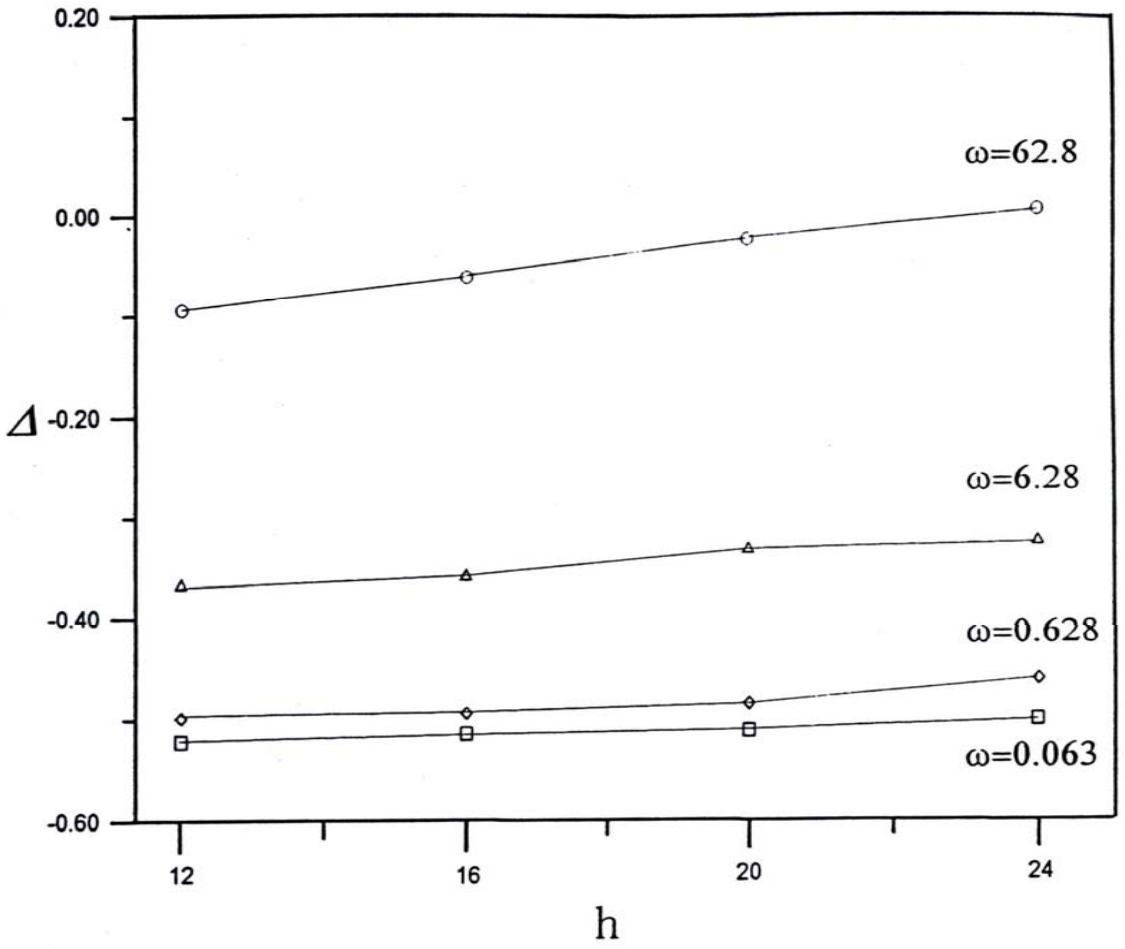

Figure 6 Influence of aspect ratio (h) on variable Δ of the critical Re (see Huang[45]).

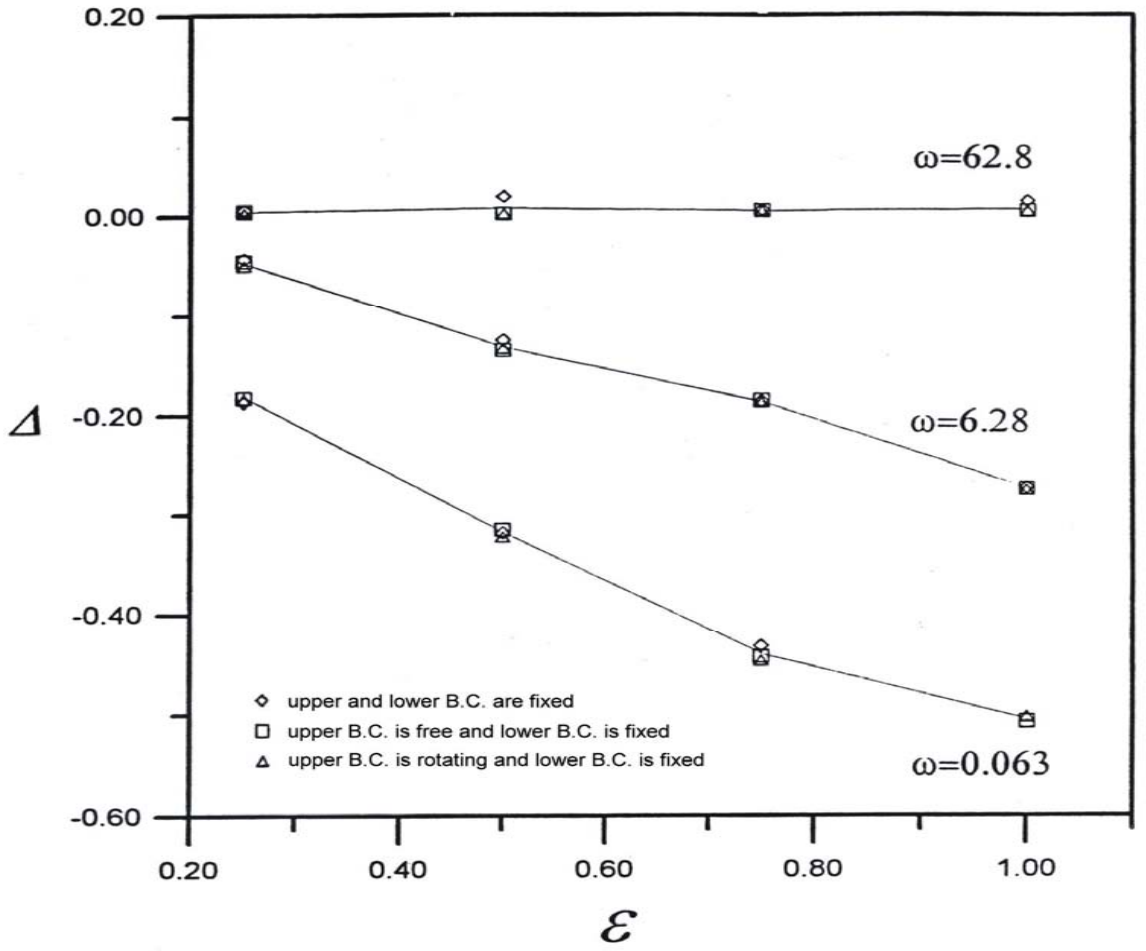

Figure 7 Influence of different upper and lower boundaries on variable Δ of the critical Re (see Huang[45]).

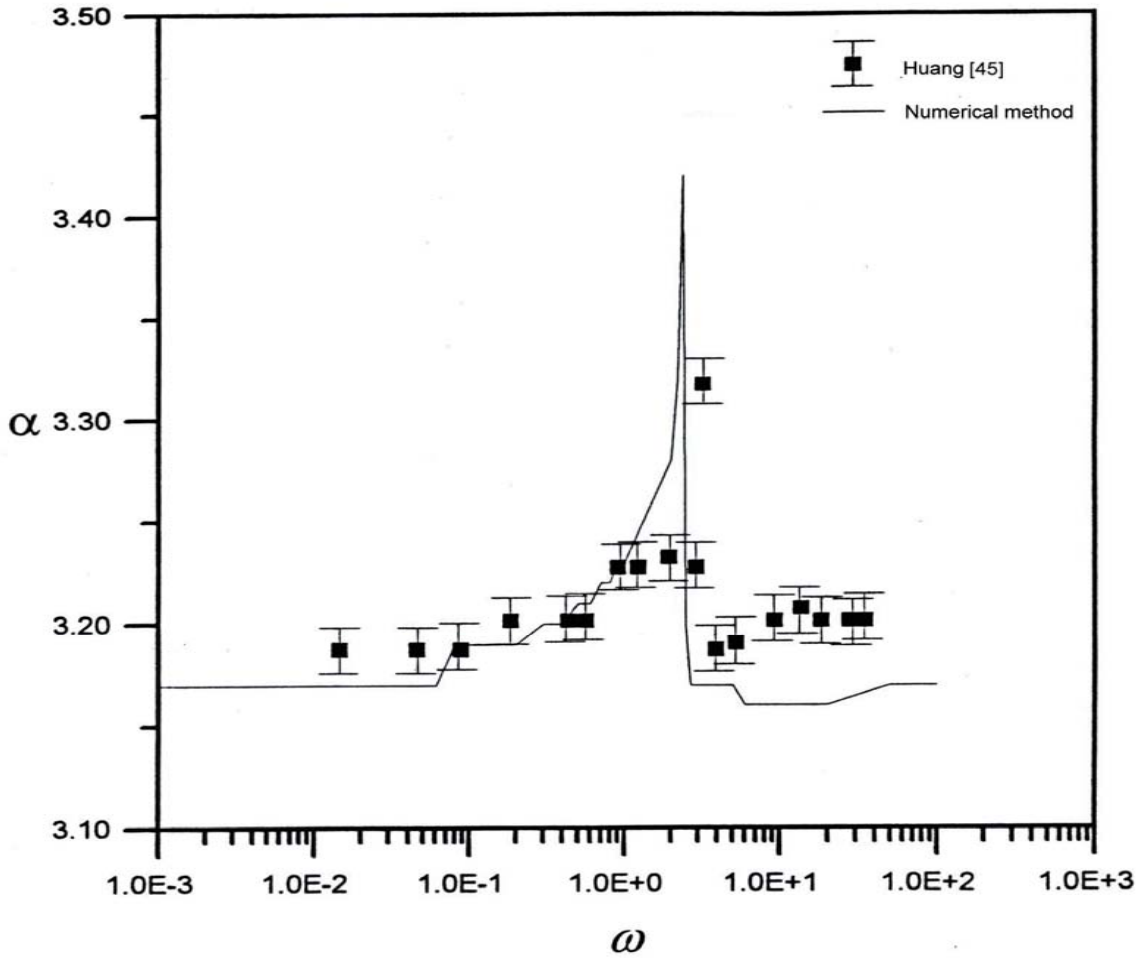

Figure 8 Relationship between wave number of the modulated Couette flow under a stable critical number and modulated frequency; upper and lower fixed boundaries are $\varepsilon = 0.5$ and $\eta = 0.4833$, respectively.

(a) $\eta = 0.9$

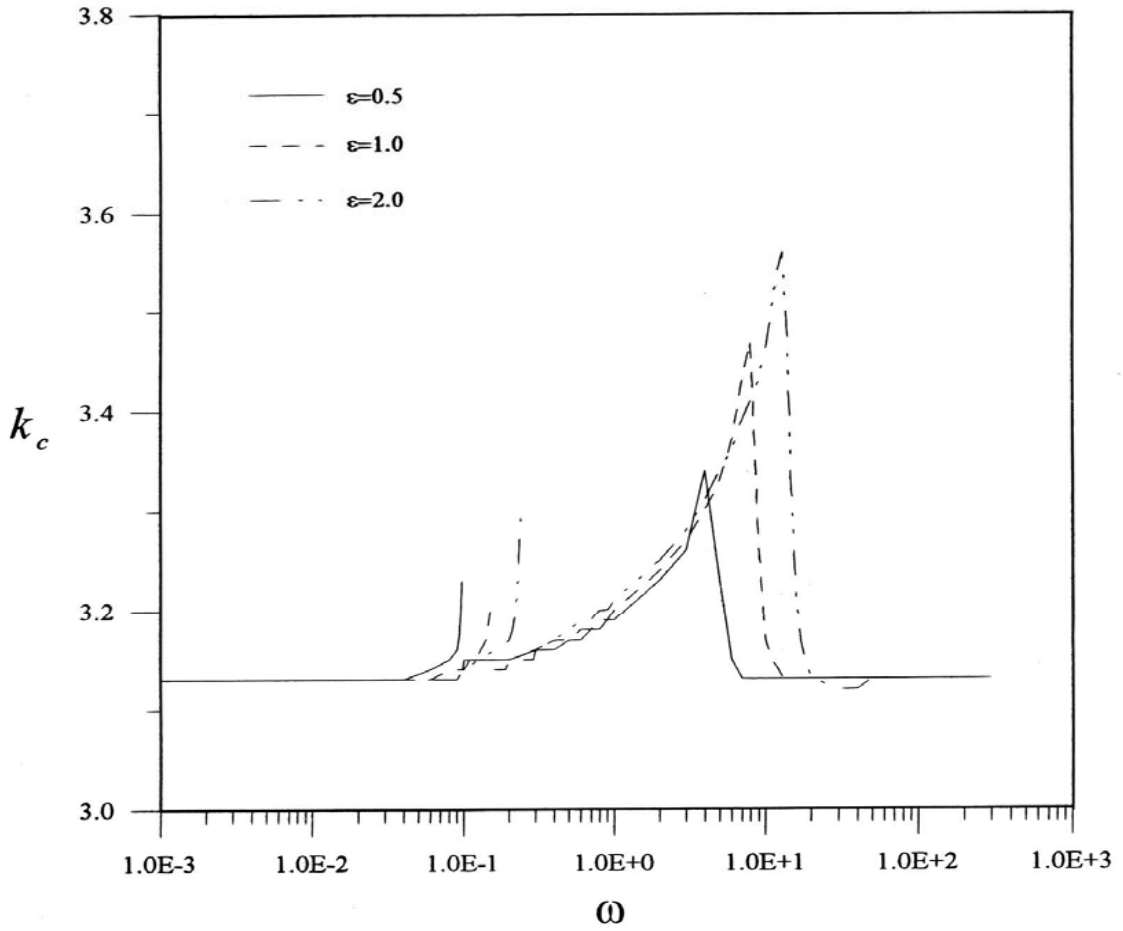

Figure 9 Relationship between critical wave number and frequency at different modulated amplitudes.
(a) $\eta = 0.9$ (b) $\eta = 0.4833$ (c) $\eta = 0.2$

(b) $\eta = 0.4833$

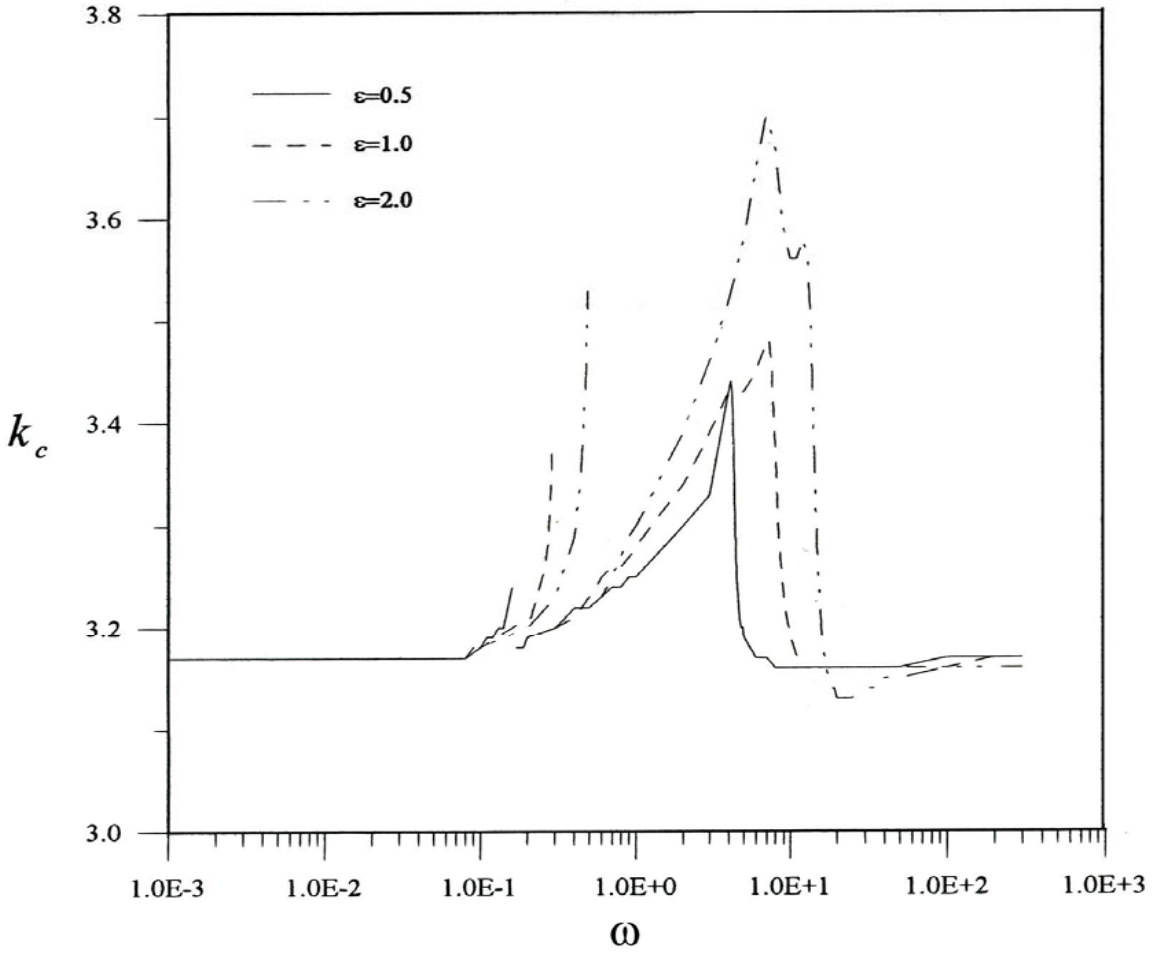

Continued.

(c) $\eta = 0.20$

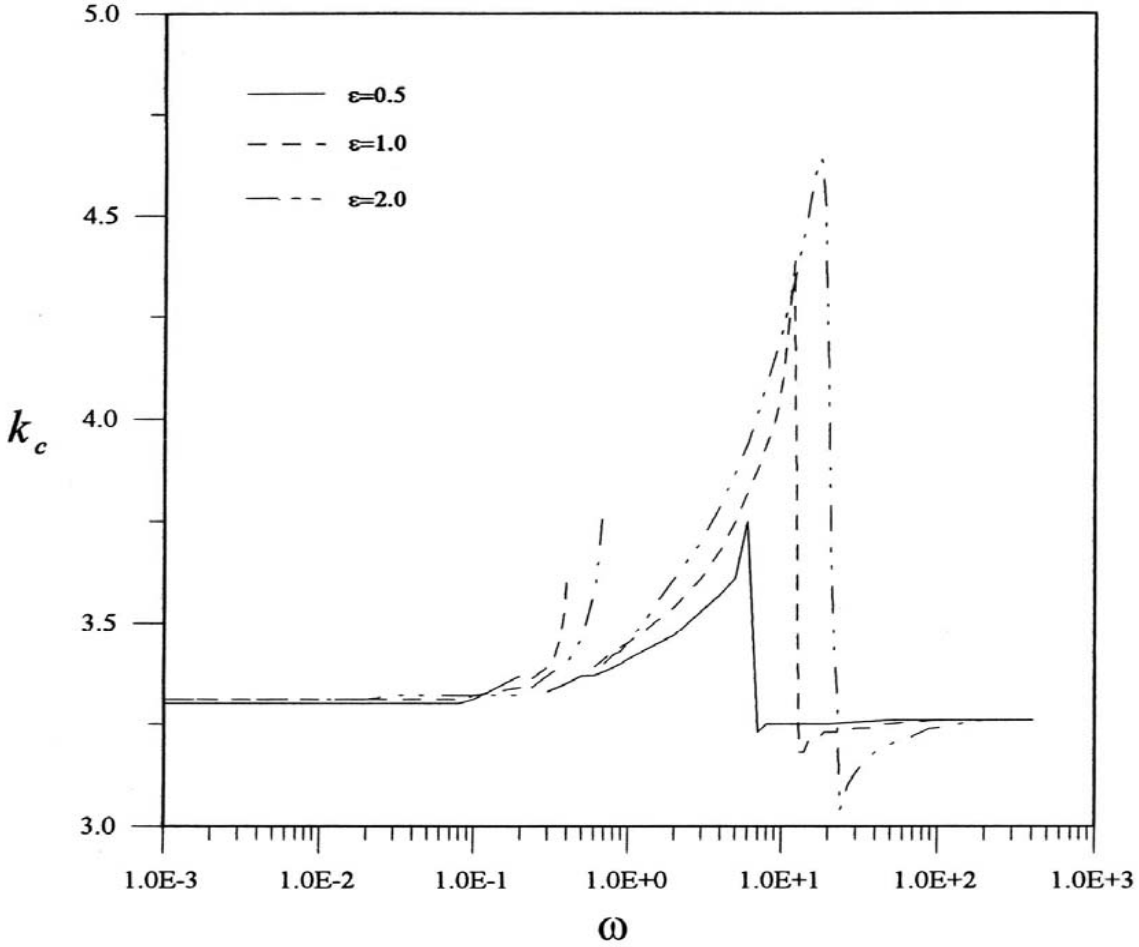

Continued.

(a) $\varepsilon = 1$

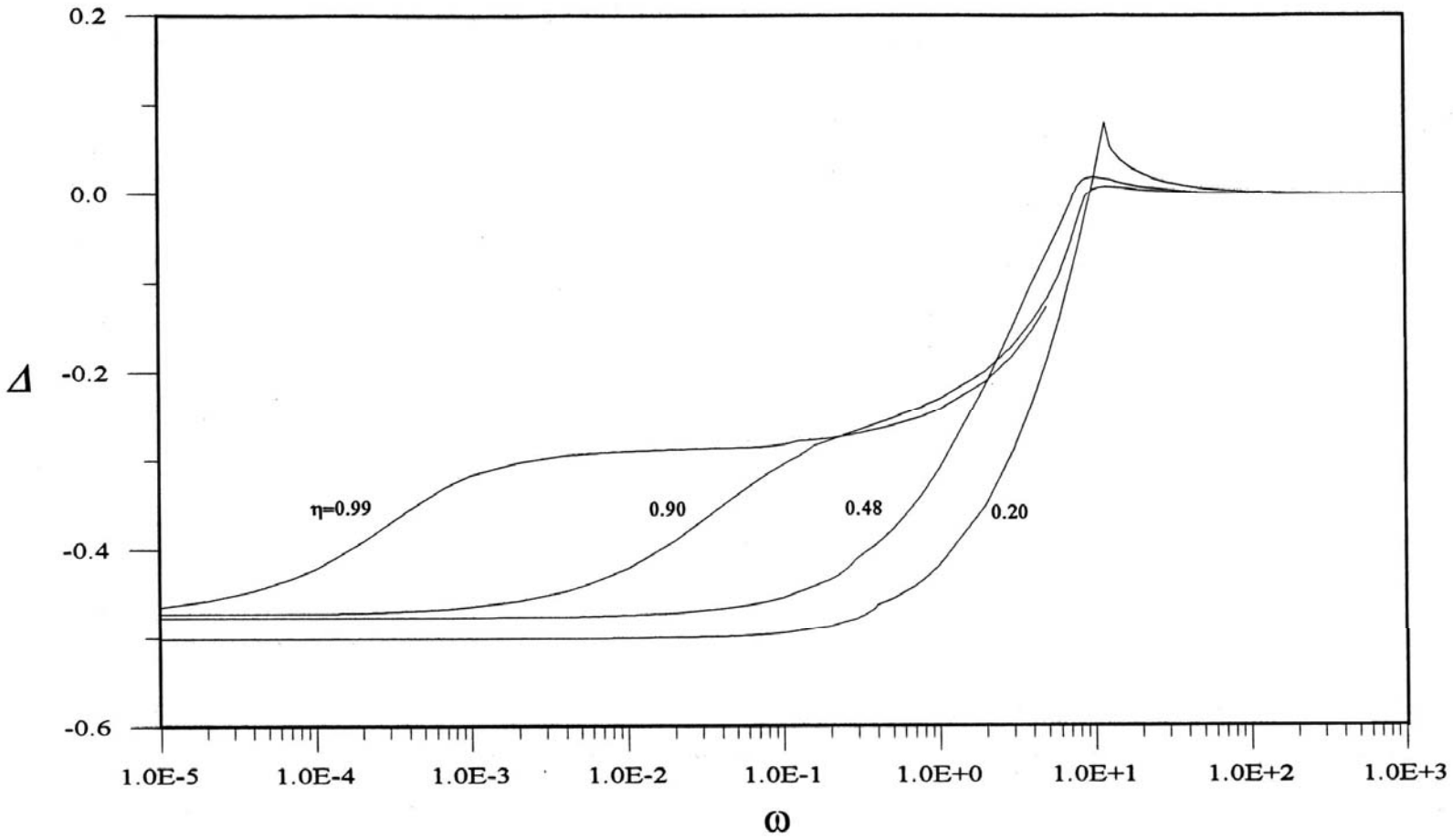

Figure 10 Relationship between the relative variable of the critical Re and frequency under different radius ratios.
(a) $\varepsilon = 1$ (b) $\varepsilon = 2$

(b) $\varepsilon = 2$

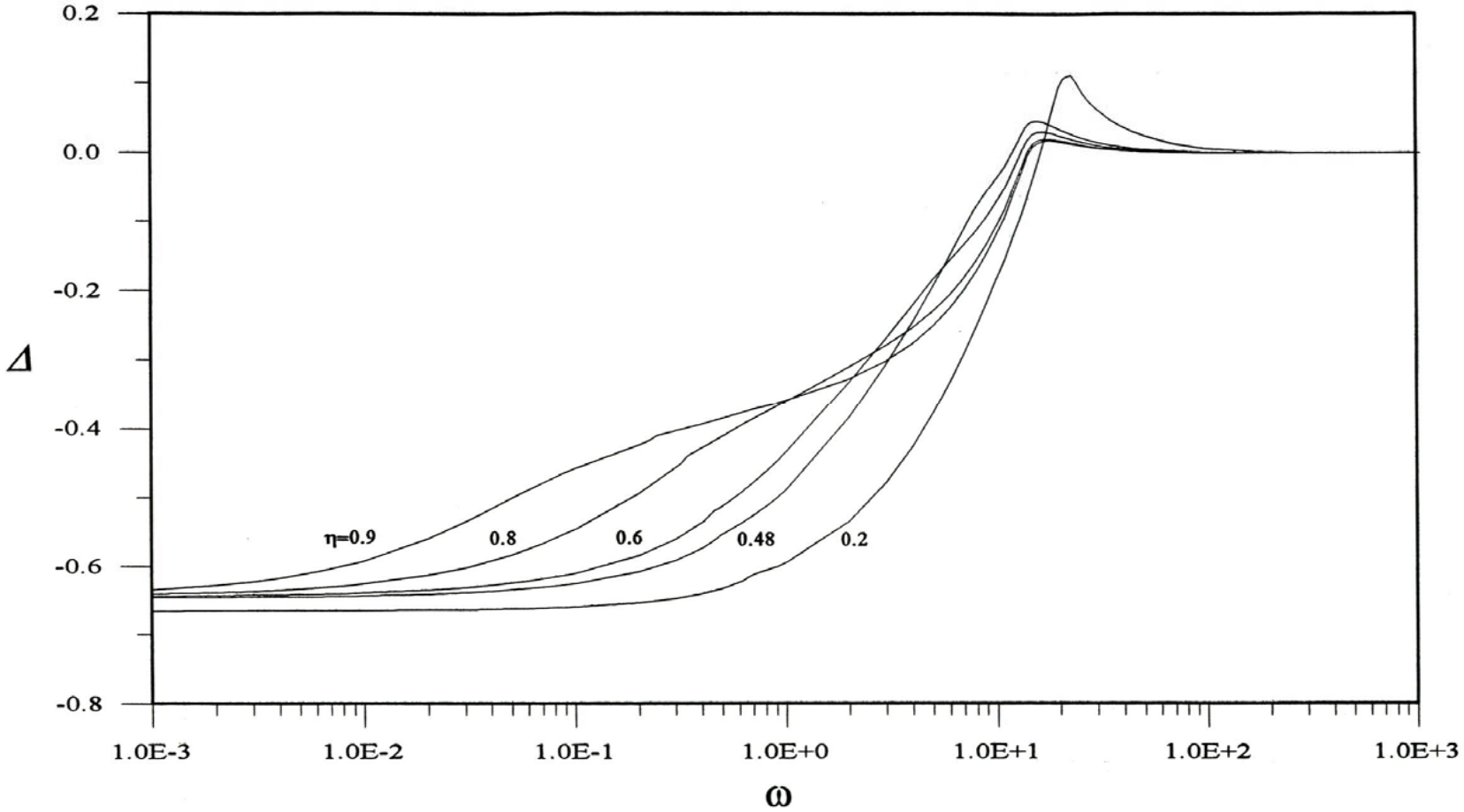

Continued.

Chapter 3 Taylor Vortex Flow

3.1 General Description of the TVF

Fluid motion between two concentric rotating cylinders is often investigated in the field of fluid dynamics. This section uses numerical methods to analyze and simulate flow patterns and relevant flow characteristics between two concentric rotating cylinders. Coles[8] was the first researcher to definitively consider Taylor vortex flow to be nonlinear, although several researchers had previously speculated that the Taylor vortex problem could be solved by considering nonlinear flow. Donnelly[47] and Hu[48] experimentally analyzed modulated flow stability. When the outer cylinder remains stationary and the inner cylinder rotates periodically, parameters such as interval, rotational frequency, and the modulated amplitude of the two cylinders can be varied to determine how the flow is affected by modulated rotation. Hall[21] utilized linear theory to determine low and high frequencies and used nonlinear theory to analyze the flow under a high frequency. Carmi and Tustaniwskyj[24] examined modulated stability under a limited gap and the influence of axial symmetry and asymmetry on modulated flow. In a former study, it was shown that the critical Reynolds number exhibits an increased unstable offset under low frequency. Marques and Lopez[49] and Lopez and Marques[50] introduced and studied more cases of time-modulated Taylor–Couette problems in which the inner cylinder moves periodically along the axial direction. Youd *et al.*[30, 51], who analyzed zero-equivalent modulated flow around concentric cylinders with a radius ratio of $\eta = 0.75$, defined as $\eta = R_1 / R_2$ where R_1 and R_2, are the inner and outer radii of cylinders, identified the formation of reversing and non-reversing modulated Taylor–Couette flow. The main objectives of the study investigate the instability of modulated Taylor vortices flow by utilizing a numerical

method. It is practical to focus attention on the transition based on varying modulated amplitudes and frequencies.

3.2 Numerical Method

3.2.1 Model description

The flow is described by the incompressible, three-dimensional Navier-Stokes equations with cylindrical coordinates (R, θ, Z) in an absolute frame of reference according to the velocity-pressure formulation. The dimensionless factors r, z are the radial and axial coordinates, τ is the time and ω is the modulated frequency with corresponding dimensional quantities are t and ω'; Re is the Reynolds number of the inner cylinder and α is the axial wave number; the velocity components and pressure are $\bar{V}_r$, $\bar{V}_\theta$, $\bar{V}_z$, and $\bar{P}$.

3.2.2 Governing Equations

The basic flow type is the one-dimensional Couette flow with the modulated amplitude and frequency of azimuthal velocity between two concentric cylinders. Then the inner cylinder rotates with the increasing Reynolds number Re, and the outer cylinder is considered to be at rest under all conditions. The dimensionless Navier-Stokes and continuity equations are as follows:

$$\frac{\partial \vec{V}}{\partial t} + \left(\vec{V}\cdot\nabla\right)\vec{V} = -\nabla \bar{P} + \frac{1}{\mathrm{Re}}\Delta\vec{V}, \quad \nabla\cdot\vec{V} = 0 \tag{3.1}$$

where $\vec{V} = \left(\bar{V}_r, \bar{V}_\theta, \bar{V}_z\right)$. The time scheme is semi-implicit and second-order accurate. It corresponds to a combination of the Crank-Nicolson scheme (for the linear term) and an explicit Adam-Bashforth scheme (for the nonlinear terms).

Cole [14] demonstrated that cylinder height does not influence the critical point for transformation from a Couette flow to a Taylor vortex flow unless the aspect ratio between cylinder height and interval is less than 8. We assume infinite cylinders and a periodic solution in the axial direction. The boundary conditions are

$$r=\frac{\eta}{1-\eta}\ :\ \bar{V}_r=\bar{V}_z=0,\ \ \bar{V}_\theta=\mathrm{Re}_1\left(1+\varepsilon\cos\omega\tau\right)$$

$$r=\frac{1}{1-\eta}\ :\ \vec{V}=0 \tag{3.2}$$

where ε and ω are the modulated amplitude and frequency, respectively.

The flow velocity and pressure profile of the Taylor vortices can be regarded as a one-dimensional flow with a perturbation and can be expressed as:

$$\bar{V}_r=0+V_r'(r,z,\tau) \tag{3.3}$$

$$\bar{V}_\theta=\bar{V}_\theta(r,\tau)+V_\theta'(r,z,\tau) \tag{3.4}$$

$$\bar{V}_z=0+V_z'(r,z,\tau) \tag{3.5}$$

$$\bar{P}=0+p'(r,z,\tau) \tag{3.6}$$

The perturbations are determined using a pseudo-spectral Fourier-Chebyshev collocation method, taking advantage of the orthogonality properties of Chebyshev polynomials and assuming exponential convergence (see Daoyi and Gerhard H.[52], Speetjens and Clercx[53]).

$$V_r'=\sum_{m=0}^{M-1}\sum_{n=2}^{N+1}A_{mn}(\tau)\phi_n(\xi)\cos m\alpha z \tag{3.7}$$

$$V_\theta'=\sum_{m=0}^{M-1}\sum_{n=2}^{N+1}B_{mn}(\tau)\phi_n(\xi)\cos m\alpha z \tag{3.8}$$

$$V_z'=\sum_{m=1}^{M}\sum_{n=2}^{N+1}C_{mn}(\tau)\phi_n(\xi)\sin m\alpha z \tag{3.9}$$

$$p' = \sum_{m=0}^{M-1}\sum_{n=0}^{N-1} D_{mn}(\tau)T_n(\xi)\cos m\alpha z \tag{3.10}$$

Here, M and N are the number of terms in the Fourier series expansion and Chebyshev polynomial expansion, respectively, and A_{mn}, B_{mn}, C_{mn}, and D_{mn} are amplitude coefficients. The definitions of T_n and ϕ_n are listed in section 2. $\bar{V}_\theta(r,\tau)$ is the velocity of one-dimensional Couette flow.

Substituting Eqs. (3.3)–(3.6) into the Eq. (3.1), the equations are transformed into an algebraic equation, which can be expressed as a matrix equation:

$$AX^{j+1} = F^{j,j-1},\quad A = \begin{bmatrix} A_{11} & 0 & 0 & A_{14} \\ 0 & A_{22} & 0 & 0 \\ 0 & 0 & A_{33} & A_{34} \\ A_{41} & 0 & A_{43} & 0 \end{bmatrix},\quad X = \begin{bmatrix} A_{mn} \\ B_{mn} \\ C_{mn} \\ D_{mn} \end{bmatrix},\quad F = \begin{bmatrix} F_1 \\ F_2 \\ F_3 \\ 0 \end{bmatrix} \tag{3.11}$$

where A is a matrix of coefficients and vector $X = (A_{mn}, B_{mn}, C_{mn}, D_{mn})^T$. The unknown values of vector F, $F = (F_1, F_2, F_3, 0)^T$, are the summation of radial, azimuthal and axial velocity components for linear term at time t_j and nonlinear term at time t_{j-1}.

$$A_{11} = \left[1 - \frac{d\tau}{2}\left(D^2 + \frac{1}{r}D - m^2\alpha^2 - \frac{1}{r^2}\right)\right]\phi_n$$

$$A_{14} = d\tau(DT_n)$$

$$A_{22} = \left[1 - \frac{d\tau}{2}\left(D^2 + \frac{1}{r}D - m^2\alpha^2 - \frac{1}{r^2}\right)\right]\phi_n$$

$$A_{33} = \left[1 - \frac{d\tau}{2}\left(D^2 + \frac{1}{r}D - m^2\alpha^2\right)\right]\phi_n$$

$$A_{34} = d\tau(-m\alpha)T_n$$

$$A_{41} = \left(\frac{1}{r} + D\right)\phi_n$$

$$A_{43} = m\alpha\phi_n$$

$$F_1 = \left[1 - \frac{d\tau}{2}\left(D^2 + \frac{1}{r}D - m^2\alpha^2 - \frac{1}{r^2}\right)\right]\phi_n A_{mn}^j - \frac{d\tau}{2}\left(3R^j V_r^{'j} - R^{j-1}V_r^{'j-1}, \cos m\alpha z\right)$$

$$-\frac{d\tau}{2r}\left(3V_\theta^{'2\,j} - V_\theta^{'2\,j-1}, \cos m\alpha z\right) - \frac{d\tau}{2r}\left(6\bar{V}_\theta^{\,j}\phi_n B_{mn}^j - 2\bar{V}_\theta^{\,j-1}\phi_n B_{mn}^{j-1}\right)$$

$$F_2 = \left[1 - \frac{d\tau}{2}\left(D^2 + \frac{1}{r}D - m^2\alpha^2 - \frac{1}{r^2}\right)\right]\phi_n B_{mn}^j$$

$$-\frac{d\tau}{2}\left(3\left(R^j + \frac{1}{r^2}V_r^{'j}\right)V_\theta^{'j} - \left(R^{j-1} + \frac{1}{r^2}V_r^{'j-1}\right)V_\theta^{'j-1}, \cos m\alpha z\right)$$

$$F_3 = \left[1 - \frac{d\tau}{2}\left(D^2 + \frac{1}{r}D - m^2\alpha^2\right)\right]\phi_n C_{mn}^j - \frac{d\tau}{2}\left(3R^j V_z^{'j} - R^{j-1}V_z^{'j-1}, \cos m\alpha z\right)$$

where $\frac{\partial}{\partial r^n} = 2^n \frac{d^n}{d\xi^n} = D^n$, $R^j = V_r^{'j}\frac{\partial}{\partial r} + V_z^{'j}\frac{\partial}{\partial z}$ and

$$(f, g) = f \circ g = \frac{\alpha}{2\pi}\int_{-\alpha/\pi}^{\alpha/\pi} f \cdot g dz$$

The coefficients A_{mn}, B_{mn}, C_{mn}, and D_{mn} are determined iteratively until the convergence condition is satisfied. When the inner cylinder rotates with a fixed rotational speed, the convergence condition is

$$\left|\frac{X^{j+1} - X^j}{X^{j+1}}\right| < 10^{-4} \tag{3.12}$$

We adopt the tolerance (10^{-4}) to avoid the computation process becomes time consuming and larger error ratio compared with those obtained by Jones [54]. When the pressure coefficient is converging to the tolerance (10^{-4}), the other coefficients in velocity components had been converging and lower to the tolerance (10^{-4}). The coefficient that satisfies the convergence condition is substituted in the appropriate equation among Eqs. (3.3)–(3.6); the speed and pressure in each time interval can then be determined. If the cylinder rotates periodically, the largest value of axial speed

attained in a particular time interval at a selected observation point in the flow is compared with the axial speed in the preceding time interval, the convergence condition is

$$\left| \frac{\bar{V}_z^{\,i+1} - \bar{V}_z^{\,i}}{\bar{V}_z^{\,i+1}} \right| < 10^{-4} \tag{3.13}$$

where i is the periodic counter. If the difference is less than 10^{-4}, then the convergence condition is considered to be satisfied.

3.2.3 Model Validation

Prior to the computation of the flow field, we analyze the degree of accuracy, which serves as the basis for the post computation. In theory, the greater the number of terms expanded, the higher is the accuracy; however, the limit to the increase of the number of terms will come from the round-off error and the computation process becomes time consuming. Therefore, the best option is to use the expansion with the least number of terms for which a certain degree of accuracy can be guaranteed. The results computed from the expanded number of terms, M and N in the computation mode of Taylor vortices, were compared with the results obtained by Jones[54] when the inner cylinder rotated at a constant velocity. Jones[54] used the Taylor number to obtain the rotating velocity of the inner cylinder, as shown in Table 2. For a low Re value (Re = 72.5), the radial velocity at the point of observation can be converged with the expanded terms 6 × 6. The difference ratio compared with the expanded terms 6 × 6 and 7 × 7 is converging to 0.19%. However, for a high Re value (Re = 259.8), the radial velocity at the point of observation can be converged with the expanded terms 10*10. The difference ratio compared with the expanded terms 10 × 10 and 11 × 11 is converging to 0.14%. These results are in agreement with those obtained by Jones[54]. For the

computation in this study, both M and N were expanded to 10 terms.

3.3 The Onset of Taylor Vortices under Modulated Effect

Fig. 11 presents the relationship between offset Δ and modulated frequency ω. At a low frequency, the modulation effect has significant and unstable effect on flow. This experimental result agrees with the experimental result obtained by Carmi and Tustaniwskyj[24]. Under the same conditions, the value acquired by numerical calculation and the experiment value are compared. At an extremely high frequency, the offset approaches 0, indicating that the critical Reynolds number Re_c approaches the critical Reynolds number Re_0 under a non-modulated effect. As the modulated frequency decreases, the calculated result becomes similar to that acquired by Riley and Laurence[22]. However, the difference between the experimental value and linear theoretical value increases.

Figure 12 shows a graph of the relationship between the rotating outer and inner cylinders. From experimental observations, when the inner and outer cylinders rotate, the critical Reynolds number Re_c of the inner cylinder increases as Re_2 increases. The derived critical Reynolds number is slightly higher than the theoretical value. However, the error is only about 5%. When the inner and outer cylinders rotate in opposite directions, the Reynolds number Re_c of the inner cylinder also increases as Re_2 increases. However, the slope is smaller than when the cylinders are rotating in the same direction. The critical Reynolds number Re_c obtained experimentally agrees with the theoretical value.

Figure 13 shows the radius ratio $\eta = 0.937$; inner cylinder $\Omega_1 = \bar{\Omega}_1$; outer cylinder rotating with a non-zero mean modulated rotation $\Omega_2 = \varepsilon \cdot \bar{\Omega}_1 \cos \omega' t$; different

amplitudes, $\varepsilon = 0.5$, 1.0 and 1.5; and the effects of experimental and theoretical values under different modulated frequencies on critical Reynolds number of the inner cylinder. The graph shows that the critical Reynolds number offset Δ of the inner cylinder approaches 0 at a low frequency. The Δ value then increases as frequency increases until $\omega \approx 0.8$, and Δ reaches the highest value. Then Δ value decreases as the frequency increases. The Δ approaches 0 again at a high frequency.

In Fig. 14 and Fig. 15, the outer cylinder is fixed and amplitude of the inner cylinder is modulated at $\varepsilon = 1$ and $\varepsilon = 2$, respectively. The axial speed changes with time at different values of Reynolds number and modulated frequency when $\xi = 0.5$. For low frequency, the dimensionless time τ becomes time consuming to obtain the iterative convergence under different Reynolds number. But for high frequency, the computation process is rapidly converged. When the inner cylinder rotates at low frequency, the flow has sufficient time to change with the velocity. Once the rotation speed of the inner cylinder exceeds the threshold value for one-dimensional flow, the flow is transformed from one-dimensional circular Couette flow to axisymmetrical Taylor vortex flow. When the instantaneous Reynolds number reaches the maximum value, the Taylor vortex flow disappears in process of time; this phenomenon is referred to as transient stability, as shown in Fig. 14(a)–(b) and Fig. 15(a)–(b). With an increase in the modulated frequency, transient stability disappears because a Stokes layer is produced near the wall. The flow beyond the Stokes layer cannot completely reflect the velocity change in the inner cylinder (Figs. 14(c), 15(c)). Meanwhile, we can employ a larger Reynolds number and ensure that Taylor vortex flow occurs at an earlier time period. The plots in Figs. 14(d), 15(d) show the flow sustain the more stable Taylor vortex flow at high frequency. It is worth noting that subharmonic flow exists at intermediate and high frequencies when $\varepsilon = 2$, as shown in Fig. 15(c). However, no such flow is

observed when $\varepsilon = 1$. The phenomenon is similar to Youd *et al.*[30, 51].

3.4 Conclusion

This study used numerical analysis to investigate the behavior of flow between two concentric cylinders. The unstable Couette flow was transformed to Taylor vortex flow by considering the flow under non-zero averaged rotation speed at different modulated amplitudes and frequencies. In general, the flow generates larger instability at low-frequency modulation. At intermediate and high frequencies, the flow instability shows a gradually decreasing trend; when the modulated amplitude is sufficiently large, the period of flow at intermediate frequency is twice that of the rotational period of cylinders, which is $4\pi/\omega$ of subharmonic flow.

In addition to the modulated effects will affect the instability of Taylor vortices flow, most of the unstable state of supercritical Taylor vortices flow between concentric cylinders are the wavy form, so-called Taylor wavy vortices, at higher Reynolds numbers of the cylinders. The transition from Taylor vortices to wavy vortices takes place via a number of intermediate flow form, and this paper will be a milestone to investigate the phenomenon of Taylor wavy vortices.

Table 2 Radial velocity at the point of observation ($\xi = 0$, z = 0) for $\eta = 0.5$ as the outer cylinder is fixed and the inner cylinder rotates at a constant velocity. The definition of T_a is represented by $T_a = 2(1-\eta)\mathrm{Re}^2/(1+\eta)$

Re (T_a) / $M \times N$	72.5 (3500)	106.1 (7500)	150 (15000)	212.1 (30000)	259.8 (45000)
4 × 4	4.6991	17.5775	-	-	-
5 × 5	3.9956	17.1988	30.5700	41.92323	-
6 × 6	4.2333	17.8566	32.8350	52.7493	67.0024
7 × 7	4.2253	17.9733	33.5851	52.8491	69.8342
8 × 8	4.2340	17.9840	33.5712	54.9975	70.7955
9 × 9	4.2376	17.9733	33.6452	55.5914	71.8347
10 × 10	4.2354	17.9840	33.6900	55.6550	72.2764
11 × 11	4.2347	17.9840	33.6754	55.6763	72.3803
12 × 12	4.2354	17.9840	33.6754	55.6975	72.4063
13 × 13	4.2354	17.9840	33.6754	55.6975	72.4063
Study of Jones[54]	4.2336	17.9733	33.6768	55.7187	72.2764

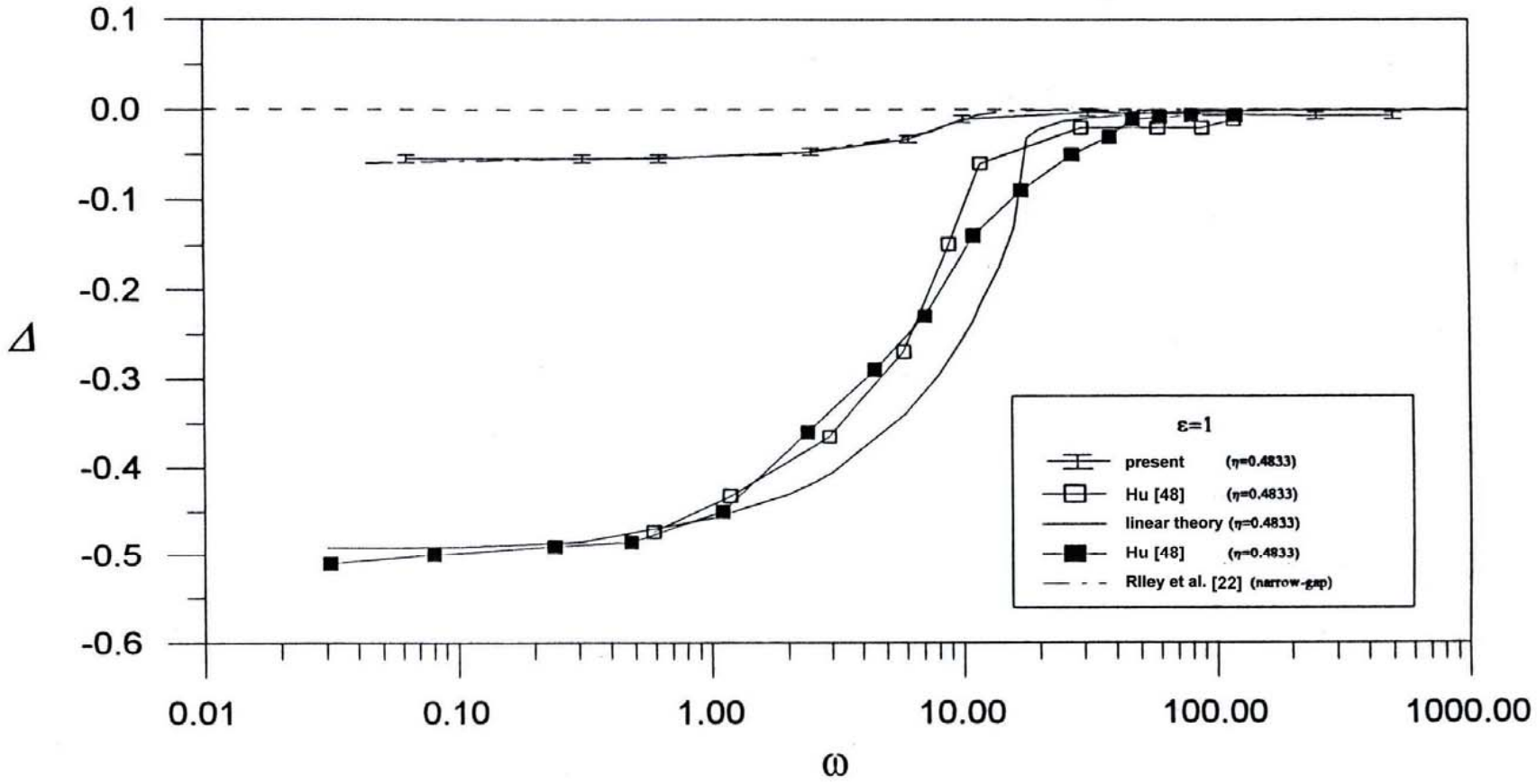

Figure 11 The relationship between offset of the critical Reynolds number Δ and modulated frequency when the outer cylinder is fixed and modulated amplitude of the inner cylinder is $\varepsilon = 1$.

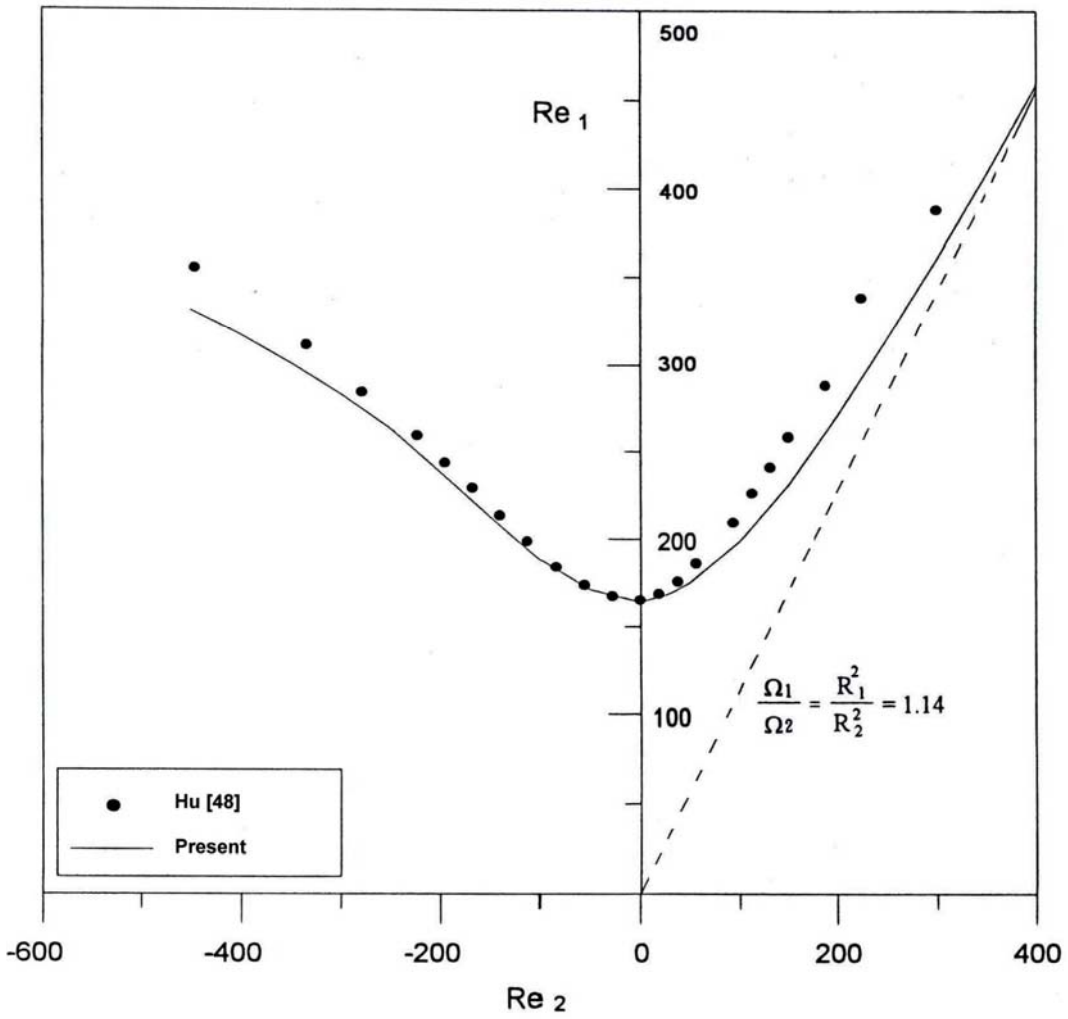

Figure 12 The flow instability of the relationship between the rotating outer and inner cylinder. ($\eta = 0.937$)

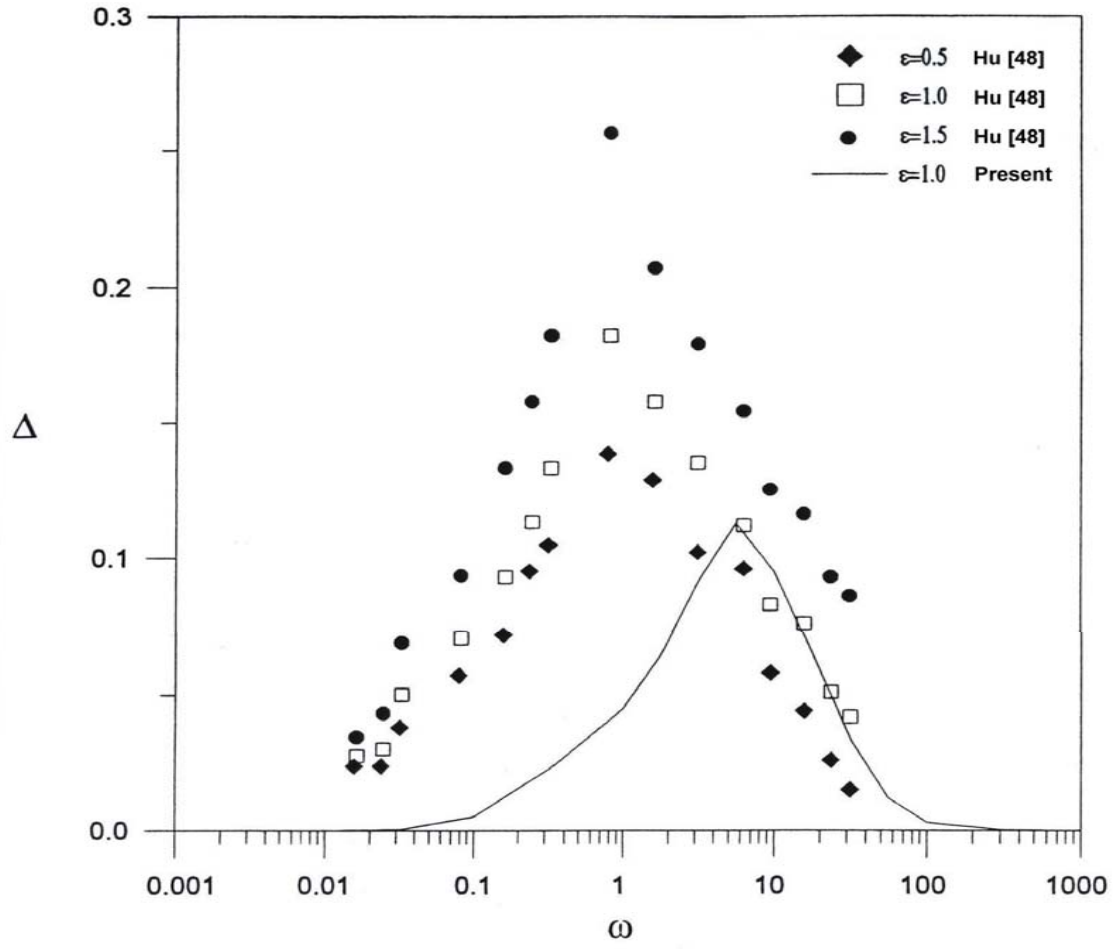

Figure 13 The inner cylinder rotates with $\Omega_1 = \bar{\Omega}_1$, the outer cylinder $\Omega_2 = \varepsilon\bar{\Omega}_1 \cos\omega' t$ rotates with a non-zero mean modulated rotation. The relationship between the Reynolds number of the inner cylinder and frequency. ($\eta = 0.937$)

(a) $\omega = 0.126$

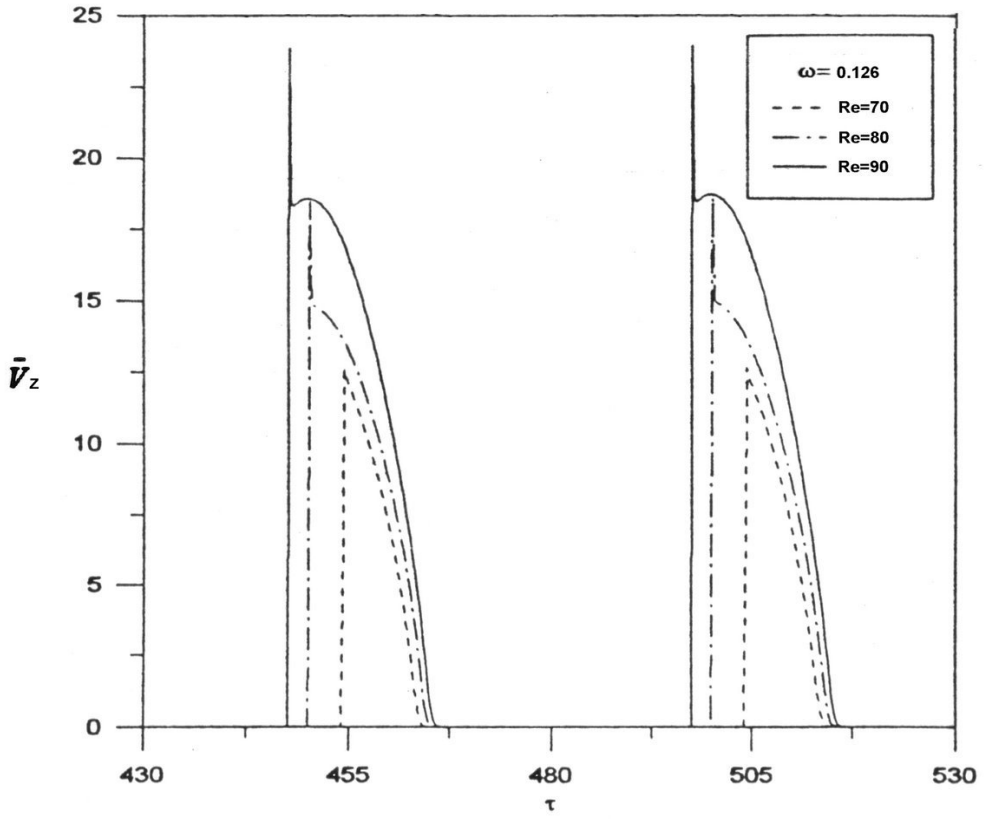

Figure 14 The outer cylinder is fixed and the inner cylinder rotates at different modulated frequencies. The axial speed $\bar{V}_z$ changes with time τ at the point of observation ($\xi = 0.5$, $Z = \lambda / 4$). ($\eta = 0.4833$, $\varepsilon = 1$)

(a) $\omega = 0.126$ (b) $\omega = 6.283$ (c) $\omega = 31.42$ (d) $\omega = 314.16$

(b) $\omega = 6.283$

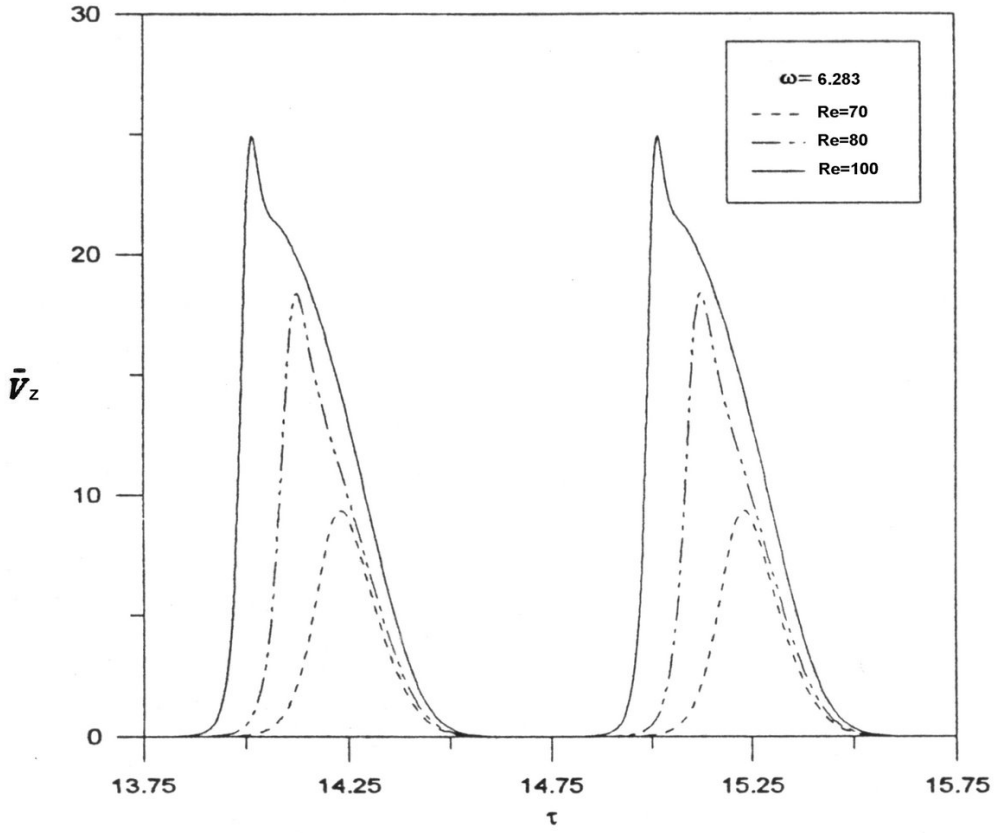

Continued.

(c) $\omega = 31.42$

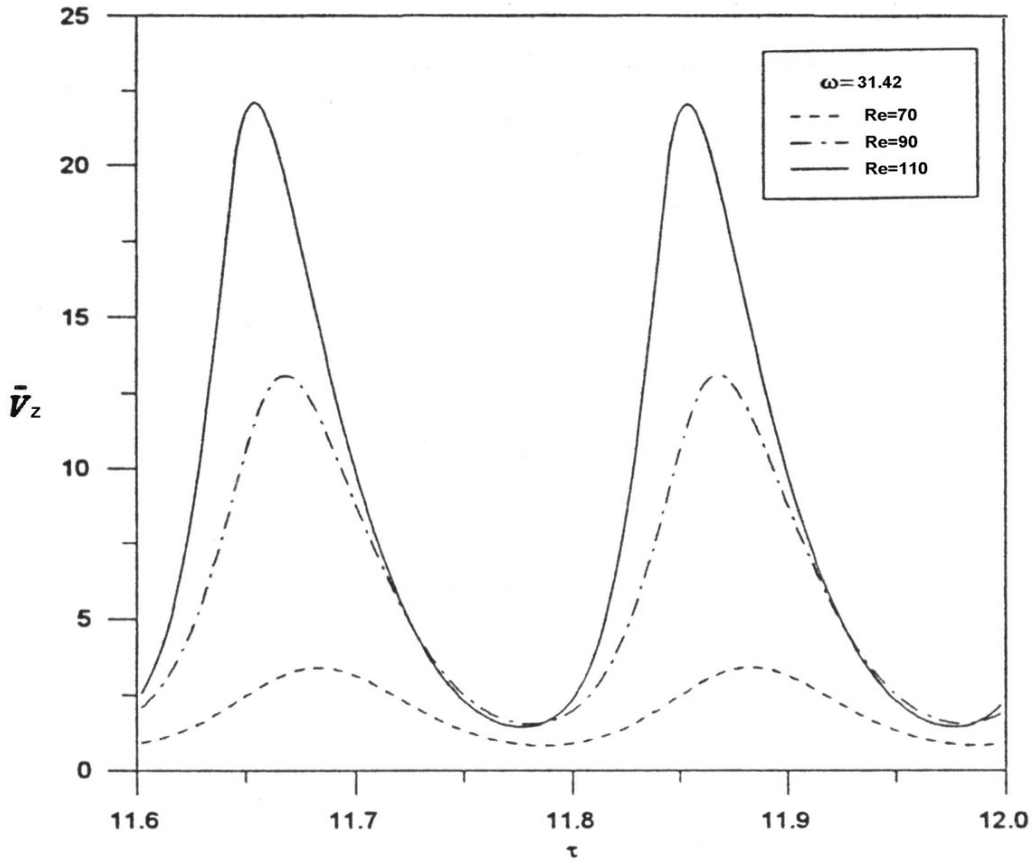

Continued.

(d) $\omega = 314.16$

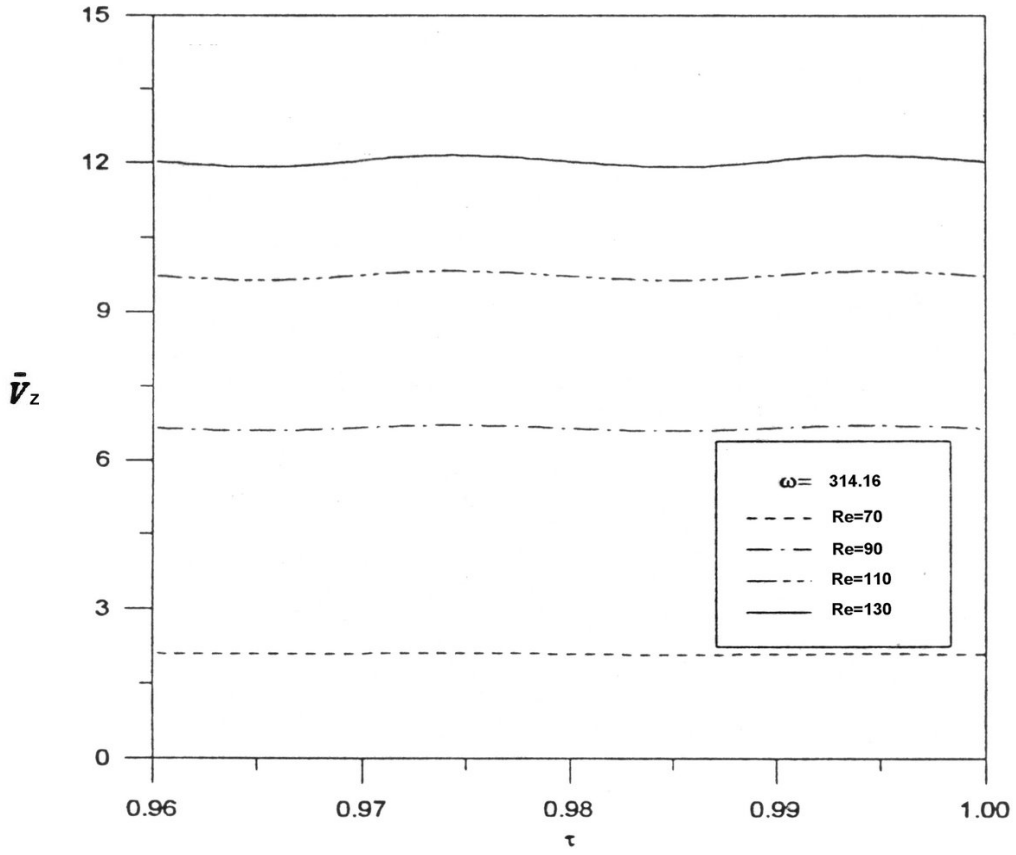

Continued.

(a) $\omega = 0.126$

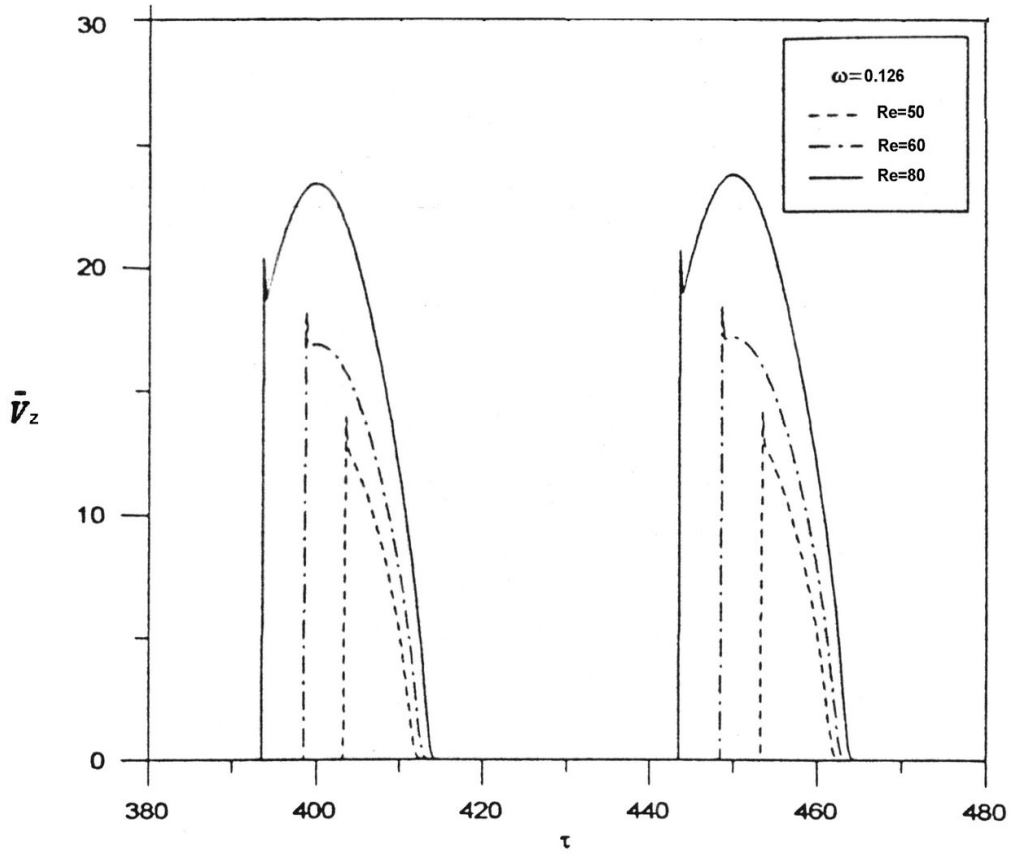

Figure 15 The outer cylinder is fixed and the inner cylinder rotates at different modulated frequencies. The axial speed $\bar{V}_z$ changes with time τ at the point of observation ($\xi = 0.5$, $Z = \lambda / 4$). ($\eta = 0.4833$, $\varepsilon = 2$)

(a) $\omega = 0.126$ (b) $\omega = 6.283$ (c) $\omega = 31.42$ (d) $\omega = 314.16$

(b) $\omega = 6.283$

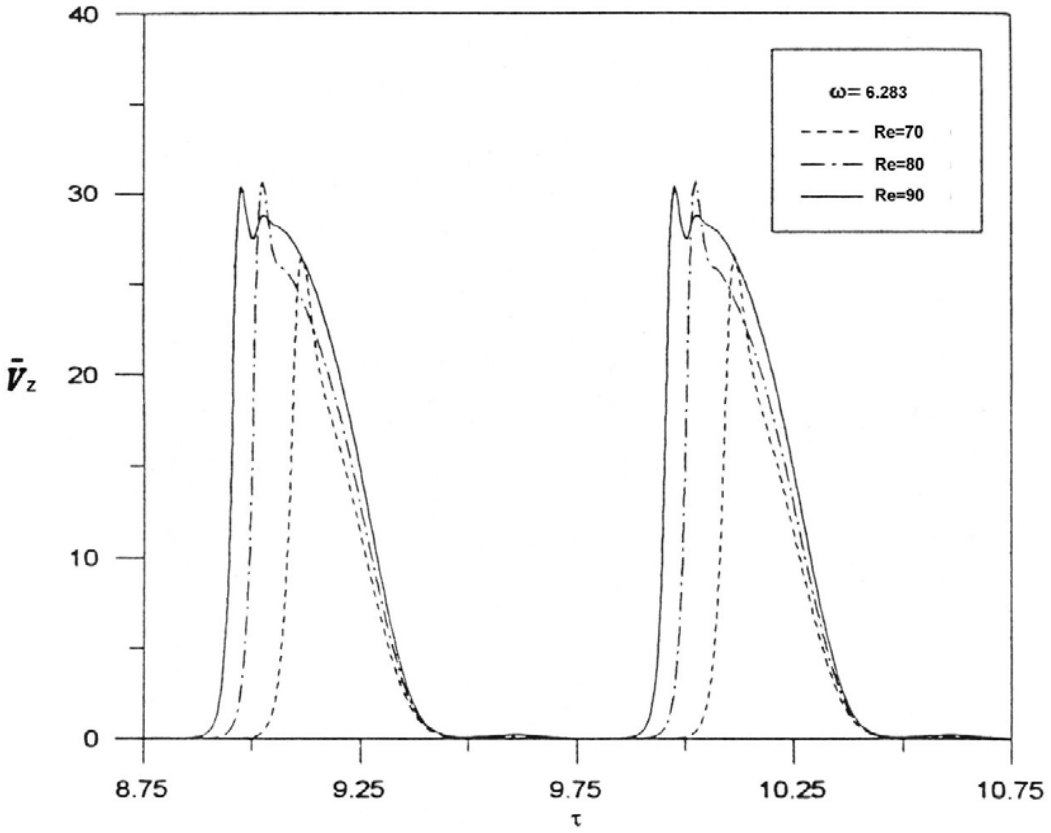

Continued.

(c) $\omega = 31.42$

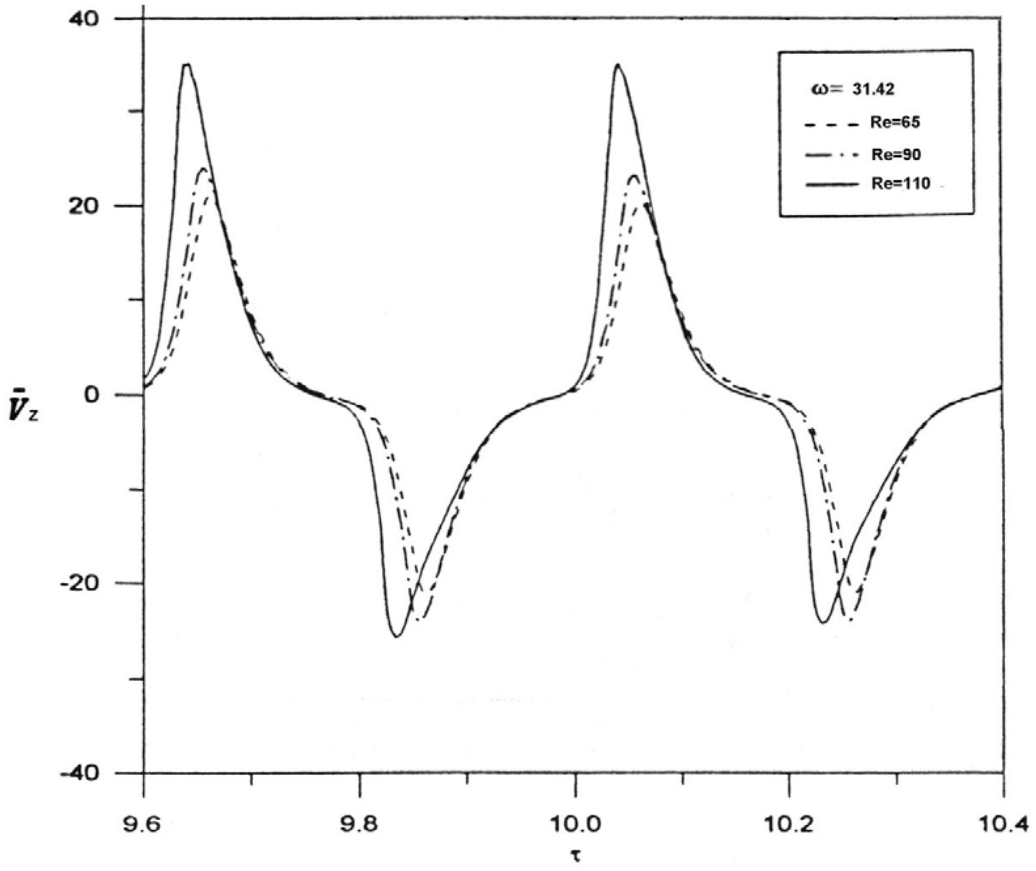

Continued.

(d) $\omega = 314.16$

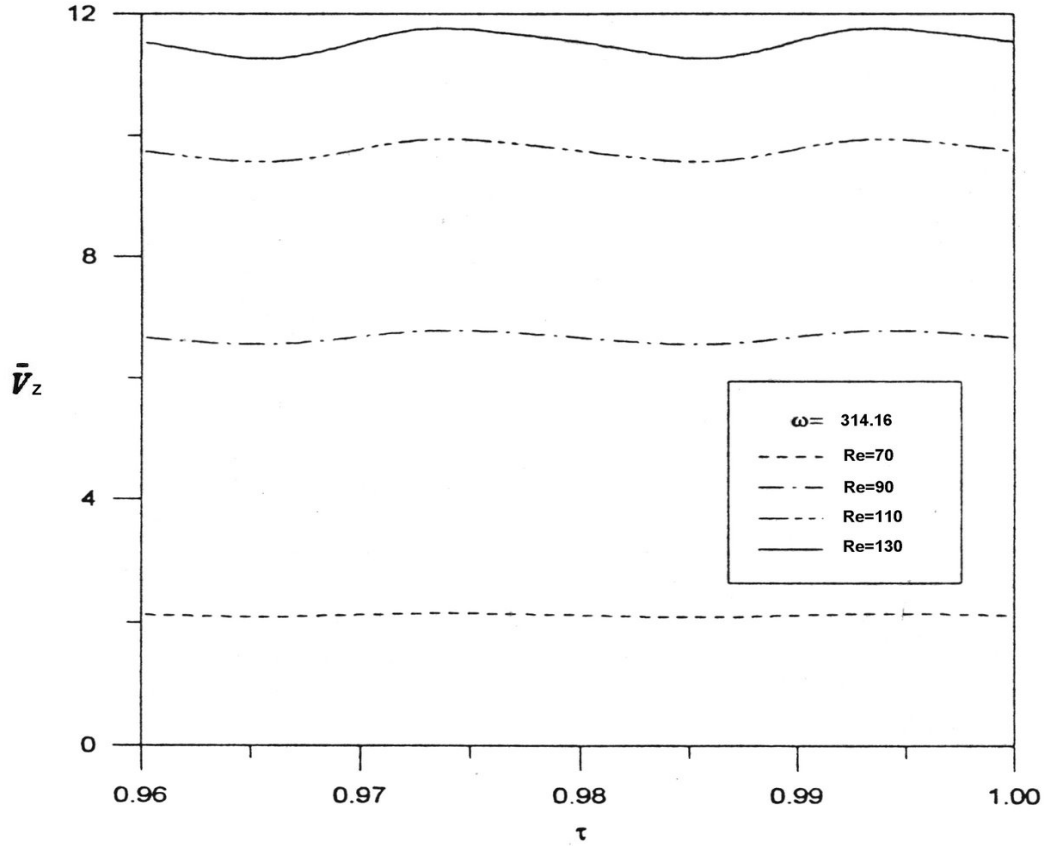

Continued.

Chapter 4 Transition to Wavy Vortex Flow

4.1 The Second Transition of Taylor-Couette Flow

After the Taylor vortex problem had teetered on the brink of being classified as a nonlinear problem for many years, Coles[8] was the first to report on the nonuniqueness of the wavy flow in the Taylor-Couette flow. The entire pattern of wavy vortices moves with a uniform velocity in the azimuthal direction. Since the term "wavy" is typically associated with motion that includes periodic vertical oscillations, this study emphasizes that wavy Taylor vortices move in the azimuthal direction as rings that have k_1 fixed sinusoidal upward and downward deformations, where k_1 is an integer number of azimuthal waves. Wavy Taylor vortices were observed by Taylor[2], Lewis[32], and Schultz-Grunow and Hein[33]; however, they were not recognized as a characteristic feature of the flow. After Coles' preliminary results were published, wavy vortices were also observed by Nissan *et al.*[10].

Burkhalter and Koschmieder[39] found that in the case of large radius ratios, the wavelength of axisymmetrical vortices is independent of the Reynolds number in fluid columns of infinite length if the Reynolds number in such fluid columns increases quasi-steadily. Jones[34] presented the stability boundary for a wavenumber of 3.13, the critical value for a quasi-static transition, for a wide range of radius ratios. Jones [34] considered the problem of calculation of nonlinear axisymmetrical Taylor vortices. A spectral method combines with Newton-Raphson iterations was used to solve the nonlinear algebraic equations. While Taylor's study analyzed such flow under supercritical conditions, Stuart[35] observed that the shape, *i.e.*, the size, of the vortices remains unchanged above the critical Reynolds number. Numerous studies (see Ahlers *et al.*[36], Andereck *et al.*[37], Park *et al.*[55]) have demonstrated the importance of

considering the acceleration/deceleration of the flow in determining the final state of the flow. These vortices have axial wavelengths that are different from those of vortices observed after a quasi-static transition. The study demonstrates that the stability boundary occurs at a critical wavelength corresponding to the quasi-static transition in addition to another wavelength. These solutions are related to the standard Taylor vortices and can be obtained quasi-statically for certain radius ratios when a mechanism is used for modifying the axial wavelength, see [36].

4.2 Numerical Method

4.2.1 Model Description

The system geometry is specified by the inner and outer radii, R_1 and R_2, of cylinders with an infinite aspect ratio and the dimensionless parameter in the problem is the radius ratio $\eta = R_1 / R_2$. The inner cylinder rotates with the Reynolds number Re_1, $\mathrm{Re}_1 = R_1\Omega_1 d / \nu$ and the outer cylinder rotates with the Reynolds number Re_2, $\mathrm{Re}_2 = R_2\Omega_2 d / \nu$ where ν is the dynamic viscosity, Ω is the angular velocity of the cylinders rotation and $d = R_2 - R_1$ is the gap of the cylinders, respectively. First, the TVF is solved numerically. The velocity components and pressure profile of TVF are solved previously in section 3.

4.2.2 Governing Equations

The stabilities of supercritical TVF are studied by introducing disturbances in the TVF. This flow type is expressed as follows:

$$f(V_r, V_\theta, V_z, p) = \bar{f}\left(\bar{V}_r, \bar{V}_\theta, \bar{V}_z, \bar{p}\right) + f'\left(V_r', V_\theta', V_z', p'\right) \tag{4.1}$$

where $\bar{f}$ denotes the flow velocity and pressure profile of the supercritical TVF

and $f^{'}$ represents the perturbations. The equations employed for the analysis, only out-of-phase wavy modes are investigated, of perturbations in normal modes are as follows:

$$V_r^{'} = \sum_{q=1}^{Q}\sum_{s=2}^{S+1} a_{qs}\phi_s(\xi)\sin q\alpha z \cdot \exp[\sigma\tau + i(k_1\theta + k_2 z)] \tag{4.2}$$

$$V_\theta^{'} = \sum_{q=1}^{Q}\sum_{s=2}^{S+1} b_{qs}\phi_s(\xi)\sin q\alpha z \cdot \exp[\sigma\tau + i(k_1\theta + k_2 z)] \tag{4.3}$$

$$V_Z^{'} = \sum_{q=0}^{Q-1}\sum_{s=2}^{S+1} c_{qs}\phi_s(\xi)\cos q\alpha z \cdot \exp[\sigma\tau + i(k_1\theta + k_2 z)] \tag{4.4}$$

$$p^{'} = \sum_{q=1}^{Q}\sum_{s=0}^{S-1} d_{qs}T_s(\xi)\sin q\alpha z \cdot \exp[\sigma\tau + i(k_1\theta + k_2 z)] \tag{4.5}$$

Here, Q and S are the number of terms in the Fourier series expansion and Chebyshev polynomial expansion, respectively. k_1 (an integer) and k_2 (a real number) are wavenumbers of the perturbations in the azimuthal and axial directions, respectively, and a_{qs}, b_{qs}, c_{qs}, and d_{qs} are amplitude coefficients.

The dimensionless Navier-Stokes and continuity equations are as follows:

$$\partial_t \vec{f} + \vec{f}\cdot\nabla\vec{f} = -\nabla p + \Delta\vec{f}, \quad \nabla\cdot\vec{f} = 0 \tag{4.6}$$

The boundary conditions are

$$f^{'} = 0 \quad \text{at} \quad r = \frac{\eta}{1-\eta} \quad \text{and} \quad r = \frac{1}{1-\eta}$$

Substituting Eq. (4.1) into Eq. (4.6) and linearizing the dimensionless Navier-Stokes equation, we can obtain the linear perturbation equations :

Continuity equation :

$$\frac{1}{r}\frac{\partial}{\partial r}\left(rV_r^{'}\right) + \frac{1}{r}\frac{\partial V_\theta^{'}}{\partial\theta} + \frac{\partial V_z^{'}}{\partial z} = 0 \tag{4.7a}$$

Momentum equations :

$$\frac{\partial V_r'}{\partial \tau}+(V_r'\frac{\partial \bar{V}_r}{\partial r}+\bar{V}_r\frac{\partial V_r'}{\partial r})+\frac{\bar{V}_\theta}{r}\frac{\partial V_r'}{\partial \theta}+(V_z'\frac{\partial \bar{V}_r}{\partial z}+\bar{V}_z\frac{\partial V_r'}{\partial z})-\frac{2\bar{V}_\theta V_\theta'}{r}=$$

$$-\frac{\partial P'}{\partial r}+\left[\left(\nabla-\frac{1}{r^2}\right)V_r'-\frac{2}{r^2}\frac{\partial V_\theta'}{\partial \theta}\right] \tag{4.7b}$$

$$\frac{\partial V_\theta'}{\partial \tau}+(V_r'\frac{\partial \bar{V}_\theta}{\partial r}+\bar{V}_r\frac{\partial V_\theta'}{\partial r})+\frac{\bar{V}_\theta}{r}\frac{\partial V_\theta'}{\partial \theta}+(V_z'\frac{\partial \bar{V}_\theta}{\partial z}+\bar{V}_z\frac{\partial V_\theta'}{\partial z})+\frac{\bar{V}_r V_\theta'+V_r'\bar{V}_\theta}{r}=$$

$$-\frac{\partial P'}{\partial \theta}+\left[\left(\nabla-\frac{1}{r^2}\right)V_\theta'-\frac{2}{r^2}\frac{\partial V_r'}{\partial \theta}\right] \tag{4.7c}$$

$$\frac{\partial V_z'}{\partial \tau}+(V_r'\frac{\partial \bar{V}_z}{\partial r}+\bar{V}_r\frac{\partial V_z'}{\partial r})+\frac{\bar{V}_\theta}{r}\frac{\partial V_z'}{\partial \theta}+(V_z'\frac{\partial \bar{V}_z}{\partial z}+\bar{V}_z\frac{\partial V_z'}{\partial z})=-\frac{\partial P'}{\partial z}+\nabla V_z' \tag{4.7d}$$

And the characteristic perturbation equations, which constitute a generalized eigenvalue problem:

$$AX=\sigma BX,\quad A=\begin{bmatrix}A_{11}&A_{12}&A_{13}&A_{14}\\A_{21}&A_{22}&A_{23}&A_{24}\\A_{31}&0&A_{33}&A_{34}\\A_{41}&A_{42}&A_{43}&0\end{bmatrix},\ B=\begin{bmatrix}B_{11}&0&0&0\\0&B_{22}&0&0\\0&0&B_{33}&0\\0&0&0&0\end{bmatrix},\ X=\begin{bmatrix}a_{rs}\\b_{rs}\\c_{rs}\\d_{rs}\end{bmatrix} \tag{4.8}$$

Here, A and B are complex matrices that depend on k_1 and k_2, and the eigenvector X contains the amplitudes of the eigenfunctions.

$$A_{11}=-\sum_{m=0}^{M-1}\sum_{n=2}^{N+1}A_{mn}D\phi_n(\xi)\cos m\alpha z*\sum_{q=1}^{Q}\sum_{s=2}^{S+1}a_{qs}\phi_s(\xi)\cdot\sin q\alpha z$$

$$-\sum_{m=0}^{M-1}\sum_{n=2}^{N+1}A_{mn}\phi_n(\xi)\cos m\alpha z*\sum_{q=1}^{Q}\sum_{s=2}^{S+1}a_{qs}D\phi_s(\xi)\cdot\sin q\alpha z$$

$$-\frac{ik_1}{r}\left(\bar{\bar{V}}(r)+\sum_{m=0}^{M-1}\sum_{n=2}^{N+1}B_{mn}\phi_n(\xi)\cos m\alpha z\right)*\sum_{q=1}^{Q}\sum_{s=2}^{S+1}a_{qs}\phi_s(\xi)\cdot\sin q\alpha z$$

$$-\sum_{m=1}^{M}\sum_{n=2}^{N+1}C_{mn}\phi_n(\xi)\sin m\alpha z*\left(q\alpha\sum_{q=1}^{Q}\sum_{s=2}^{S+1}a_{qs}\phi_s(\xi)\cdot\cos q\alpha z\right)$$

$$+\left(D^2+\frac{D}{r}-\frac{k_1^2+1}{r^2}-k_2^2\right)\sum_{q=1}^{Q}\sum_{s=2}^{S+1}a_{qs}\phi_s(\xi)\cdot\sin q\alpha z-q^2\alpha^2$$

$$\sum_{q=1}^{Q}\sum_{s=2}^{S+1}a_{qs}\phi_s(\xi)\cdot\sin q\alpha z$$

$$A_{12}=\frac{2}{r}\left(\overline{\overline{V}}(r)+\sum_{m=0}^{M-1}\sum_{n=2}^{N+1}B_{mn}\phi_n(\xi)\cos m\alpha z\right)*\sum_{r=1}^{R}\sum_{s=2}^{S+1}b_{rs}\phi_s(\xi)\cdot\sin r\alpha Z$$

$$-\frac{2ik_1}{X^2}\sum_{q=1}^{Q}\sum_{s=2}^{S+1}b_{qs}\phi_s(\xi)\cdot\sin q\alpha z$$

$$A_{13}=-\left(-m\alpha\sum_{m=0}^{M-1}\sum_{n=2}^{N+1}A_{mn}\phi_n(\xi)\sin m\alpha z\right)*\sum_{q=0}^{Q-1}\sum_{s=2}^{S+1}c_{qs}\phi_s(\xi)\cdot\cos q\alpha z$$

$$A_{14}=-\sum_{q=1}^{Q}\sum_{s=0}^{S-1}d_{qs}DT_s(\xi)\cdot\sin q\alpha z$$

$$B_{11}=\sum_{q=1}^{Q}\sum_{s=2}^{S+1}a_{qs}\phi_s(\xi)\cdot\sin q\alpha z$$

$$A_{21}=-\left(\frac{\partial\overline{\overline{V}}(r)}{\partial r}+\sum_{m=0}^{M-1}\sum_{n=2}^{N+1}B_{mn}D\phi_n(\xi)\cos m\alpha z\right)*\sum_{q=1}^{Q}\sum_{s=2}^{S+1}a_{qs}\phi_s(\xi)\cdot\sin q\alpha z$$

$$-\left(\frac{\overline{\overline{V}}(r)}{r}+\frac{1}{r}\sum_{m=0}^{M-1}\sum_{n=2}^{N+1}B_{mn}\phi_n(\xi)\cos m\alpha z\right)*\sum_{q=1}^{Q}\sum_{s=2}^{S+1}a_{qs}\phi_s(\xi)\cdot\sin q\alpha z$$

$$+\frac{2ik_1}{r^2}\sum_{q=1}^{Q}\sum_{s=2}^{S+1}a_{qs}\phi_s(\xi)\cdot\sin q\alpha z$$

$$A_{22}=-\sum_{m=0}^{M-1}\sum_{n=2}^{N+1}A_{mn}\phi_n(\xi)\cos m\alpha z*\sum_{q=1}^{Q}\sum_{s=2}^{S+1}b_{qs}D\phi_s(\xi)\cdot\sin q\alpha z$$

$$-\left(\frac{ik_1\overline{\overline{V}}(r)}{r}+\frac{ik_1}{r}\sum_{m=0}^{M-1}\sum_{n=2}^{N+1}B_{mn}\phi_n(\xi)\cos m\alpha z\right)*\sum_{q=1}^{Q}\sum_{s=2}^{S+1}b_{qs}\phi_s(\xi)\cdot\sin q\alpha z$$

$$-\sum_{m=1}^{M}\sum_{n=2}^{N+1}C_{mn}\phi_n(\xi)\sin m\alpha z*\left(q\alpha\sum_{q=1}^{Q}\sum_{s=2}^{S+1}b_{qs}\phi_s(\xi)\cdot\cos q\alpha z\right)$$

$$-\frac{1}{r}\sum_{m=0}^{M-1}\sum_{n=2}^{N+1}A_{mn}\phi_n(\xi)\cos m\alpha z * \sum_{q=1}^{Q}\sum_{s=2}^{S+1}b_{qs}\phi_s(\xi)\cdot\sin q\alpha z$$

$$+\left(D^2+\frac{D}{r}-\frac{k_1^2+1}{r^2}-k_2^2\right)\sum_{q=1}^{Q}\sum_{s=2}^{S+1}b_{qs}\phi_s(\xi)\cdot\sin q\alpha z - q^2\alpha^2$$
$$\sum_{q=1}^{Q}\sum_{s=2}^{S+1}b_{qs}\phi_s(\xi)\cdot\sin q\alpha z$$

$$A_{23}=m\alpha\sum_{m=0}^{M-1}\sum_{n=2}^{N+1}B_{mn}\phi_n(\xi)\sin m\alpha z * \sum_{q=0}^{Q-1}\sum_{s=2}^{S+1}c_{qs}\phi_s(\xi)\cdot\cos q\alpha z$$

$$A_{24}=-\frac{ik_1}{r}\sum_{q=1}^{Q}\sum_{s=0}^{S-1}d_{qs}T_s(\xi)\cdot\sin q\alpha z$$

$$B_{22}=\sum_{q=1}^{Q}\sum_{s=2}^{S+1}b_{qs}\phi_s(\xi)\cdot\sin q\alpha z$$

$$A_{31}=-\sum_{m=1}^{M}\sum_{n=2}^{N+1}C_{mn}D\phi_n(\xi)\sin m\alpha z * \sum_{q=1}^{Q}\sum_{s=2}^{S+1}a_{qs}\phi_s(\xi)\cdot\sin q\alpha z$$

$$A_{33}=-\sum_{m=0}^{M-1}\sum_{n=2}^{N+1}A_{mn}\phi_n(\xi)\cos m\alpha z * \sum_{q=0}^{Q-1}\sum_{s=2}^{S+1}c_{qs}D\phi_s(\xi)\cdot\cos q\alpha z$$

$$-\left(\frac{ik_1\bar{V}(r)}{r}+\frac{ik_1}{r}\sum_{m=0}^{M-1}\sum_{n=2}^{N+1}B_{mn}\phi_n(\xi)\cos m\alpha z\right) * \sum_{q=0}^{Q-1}\sum_{s=2}^{S+1}c_{qs}\phi_s(\xi)\cdot\cos q\alpha z$$

$$-m\alpha\sum_{m=1}^{M}\sum_{n=2}^{N+1}C_{mn}\phi_n(\xi)\cos m\alpha z * \sum_{q=0}^{Q-1}\sum_{s=2}^{S+1}c_{qs}\phi_s(\xi)\cdot\cos q\alpha z$$

$$-\sum_{m=1}^{M}\sum_{n=2}^{N+1}C_{mn}\phi_n(\xi)\sin m\alpha z * \left(-q\alpha\sum_{q=0}^{Q-1}\sum_{s=2}^{S+1}c_{qs}\phi_s(\xi)\cdot\sin q\alpha z\right)$$

$$+\left(D^2+\frac{D}{r}-\frac{k_1^2}{r^2}-k_2^2\right)\sum_{q=0}^{Q-1}\sum_{s=2}^{S+1}c_{qs}\phi_s(\xi)\cdot\cos q\alpha z - q^2\alpha^2$$
$$\sum_{q=0}^{Q-1}\sum_{s=2}^{S+1}c_{qs}\phi_s(\xi)\cdot\cos q\alpha z$$

$$A_{34}=-q\alpha\sum_{q=1}^{Q}\sum_{s=0}^{S-1}d_{qs}T_s(\xi)\cdot\cos q\alpha z$$

$$B_{33} = \sum_{q=0}^{Q-1}\sum_{s=2}^{S+1} c_{qs}\phi_s(\xi)\cdot\cos q\alpha z$$

$$A_{41} = \frac{1}{r}\sum_{q=1}^{Q}\sum_{s=2}^{S+1} a_{qs}\phi_s(\xi)\cdot\sin q\alpha z + \sum_{q=1}^{Q}\sum_{s=2}^{S+1} a_{qs}D\phi_s(\xi)\cdot\sin q\alpha z$$

$$A_{42} = \frac{ik_1}{r}\sum_{q=1}^{Q}\sum_{s=2}^{S+1} b_{qs}\phi_s(\xi)\cdot\sin q\alpha z$$

$$A_{43} = -q\alpha\sum_{q=0}^{Q-1}\sum_{s=2}^{S+1} c_{qs}\phi_s(\xi)\cdot\sin q\alpha z$$

where $\frac{\partial}{\partial r} = 2\frac{d}{d\xi} = D$ and $\frac{\partial^2}{\partial r^2} = 2^2\frac{d^2}{d\xi^2} = D^2$.

4.2.3 Solution Method and Definition of Instability

The stability of the flow can be determined by the real part of the growth rate of a complex disturbance. When $\sigma_r < 0$, the entire flow is stable. The disturbance decreases with an increase in time. When $\sigma_r > 0$, the disturbance increases with time and the flow becomes unstable. When $\sigma_r = 0$, the flow has neutral stability.

The eigenvalue of the generalized eigensystem is obtained by using the subroutine DGVLCG in the IMSL library, which determines all eigenvalues with a high level of accuracy. Re is searched on the neutral stable curve, i.e., the curve on which the real part of the most unstable eigenvalue vanishes, using the secant method; this method requires two initial guesses. The iteration is not terminated until the real part of the most unstable eigenvalue is less than 10^{-6}. The Re values for different wavenumbers can be obtained for neutral stable states. The minimum Reynolds number is called the critical Reynolds number and corresponds to the critical wavenumber.

4.3 Lowest Instability of the Wavy Vortices under Inner Cylinder Rotation which is Re_1

Fig. 16 shows the numerical result (with $k_2 = 0$) together with the experimental data obtained by Ahlers *et al*.[36]. Each symbol (solid circle) corresponds to a solution in their study (onset of the WVF at $k_1 = 3$). The range of wavenumbers considered is 2.6–4.0 and the range of $\mathrm{Re}/\mathrm{Re}_c$ is 0.8–2.0. Re_c is the critical value of Re, i.e., the value at which the TVF occurs. The model used in the present study assumes that the wavy Taylor vortices are perfectly periodic in the axial direction and thus ignores the end effects. This model is similar to that developed by Ahlers *et al*.[36].

A comparison of the model used in the present study with the models developed by Park[38] and Jones[56] indicates that the agreement between experimental and theoretical values for $k_1 = 2$ is good (see Table 3).

The plots in Figs. 17(a)–(i) show the stability boundaries at the onset of wavy Taylor vortices with k_1 in the range 1–3 in the parameter plane $(\alpha, \mathrm{Re}/\mathrm{Re}_c)$. Every plot has been compared with the plots obtained by Jones[34], and good agreement has been observed.

For η in the range 0.7–0.74605, the lowest stability of the transition from TVF to WVF depends strongly on α, which is less than 3.13. For $\eta = 0.76$ and $\eta = 0.78415$, the dominant transition occurs at $k_1 = 3$, which is below a certain α. When η is increased above 0.78415, a new transition curve with $k_1 = 1$, for which α is equal to approximately 3.13, represents the lowest stability boundary.

Fig. 18 presents the wavenumbers of the lowest stability boundary for various η values. For the transition from TVF to WVF, α is less than 3.13 for three sections: the first section is $0.76 \le \eta \le 0.7842$ with an upper branch of $k_1 = 1$, the second section

is $0.7 \le \eta \le 0.7248$ with $k_1 = 2$, and the third section is $0.7248 \le \eta \le 0.7842$ with $k_1 = 3$ (see Figs. 19). The critical Reynolds number shifts to values of α that are substantially less than 3.13, *i.e.*, waves are easily generated. Fig. 20 also shows the new stability boundary curves for the transition from TVF to WVF and presents different stability boundary curves for axisymmetrical TVF when η is lower than approximately 0.7842.

4.4 The Lowest Instability Curve of the Transition from TVF to WVF under the Condition of Concerntric Rotating Cylinders

The regime diagram of the onset of WVF was determined by Coles[8] (see Fig. 21). The Coles' result is a remarkable confirmation of Taylor's[2] stability diagram for the onset of axisymmetric TVF as a function of the rotation rate of both cylinders. The axisymmetric TVF will be transformed to WVF when the rotational speed of the cylinders exceeds the critical value Re_c, the instability boundary will be changed with different axial wavelength, rotational direction and speed of the cylinders. In this study, we consider the case wherein $\eta = 0.88$, $\alpha = 2.7$–3.5, and $k_1 = 1$–3, and we solve the lowest instability boundary of TVF for two concentric rotating cylinders. Fig. 22(a) shows that the TVF is more stable during corotation rather than counterrotation of the cylinders. In the case of flow in corotational cylinders, the lowest instability occurs when $\mathrm{Re}/\mathrm{Re}_c = 2$–$4$ for $0 < R_2 < 400$; however, $\mathrm{Re}/\mathrm{Re}_c = 1.31$ for $R_2 = 0$. The numerical result is in good agreement with that obtained by Coles[8]. However, with regard to the flow in the case of counterrotating cylinders, the instability boundary, with various azimuthal wavenumbers $k_1 = 1$–3 and axial wave numbers $\alpha = 2.7$–3.5, is different from that of axisymmetric TVF. Fig. 22(b) shows that the lowest TVF

instability boundary occurs when the rotational speed of the outer cylinder is (1) $-290 \le R_2 \le 0$ for k_1 = 1 or 2, (2) $-1000 \le R_2 \le -290$ for k_1 = 3, and (3) $-1300 \le R_2 \le -1000$ for k_1 = 2 or 3. When R_2 ($-4000 \le R_2 \le -1300$) increase gradually for any value of k_1, the instability of TVF is occurred immediately by $\mathrm{Re}/\mathrm{Re}_c$ = 1.006-1.06.

4.4 Results Summary

The effect of a variation in the wavenumber of a TVF on the stability of the flow can be studied by the infinite cylinder approximation. The wavenumber is considered as an external parameter and is not determined theoretically, but is measured experimentally. In some apparatuses such as those used by King and Swinney[57], fluid can be added or removed even when the cylinders are rotating, thereby allowing direct control of the wavelength. The present study determines a new lowest stability boundary curve for the transition from a supercritical TVF to a WVF. This curve differs from that obtained by Jones[34], who assumed that the Reynolds number of the inner cylinder increases quasi-statically. This study also investigates the lowest stability boundary for different wavenumbers and various radius ratios ranging from the ratio corresponding to a supercritical TVF to that corresponding to a WVF. The variation in the wavenumber is found to affect the stability of the flow for radius ratios less than 0.7842 (at Re_1 of the inner cylinder).

We also investigated the lowest stability boundary in the case of different azimuthal wavenumbers k_1 corresponding to a axisymmetric TVF that is transformed to a WVF. The axial wavenumber is considered as an external parameter and is not determined theoretically, but is measured experimentally. In the present study, we determined a new lowest stability boundary curve for the transition from a supercritical TVF to a WVF at

the rotating cylinders. This curve differs from that obtained by Coles [8], who assumed that the Reynolds number of the cylinders increased quasi-statically.

Table 3 Comparison of experimental and theoretical data of Re values for $\eta = 0.782$

	Experiment	Theory	
	Park[38]	Jones[56]	Present
Onset of k_1=1	Not seen	110	109.5
Onset of k_1=2	137.3	120	119.5
k_1=2 gone	161.3	163	167.5
k_1=1 gone	Not seen	169	167.8
Onset of k_1=3	322	None	None

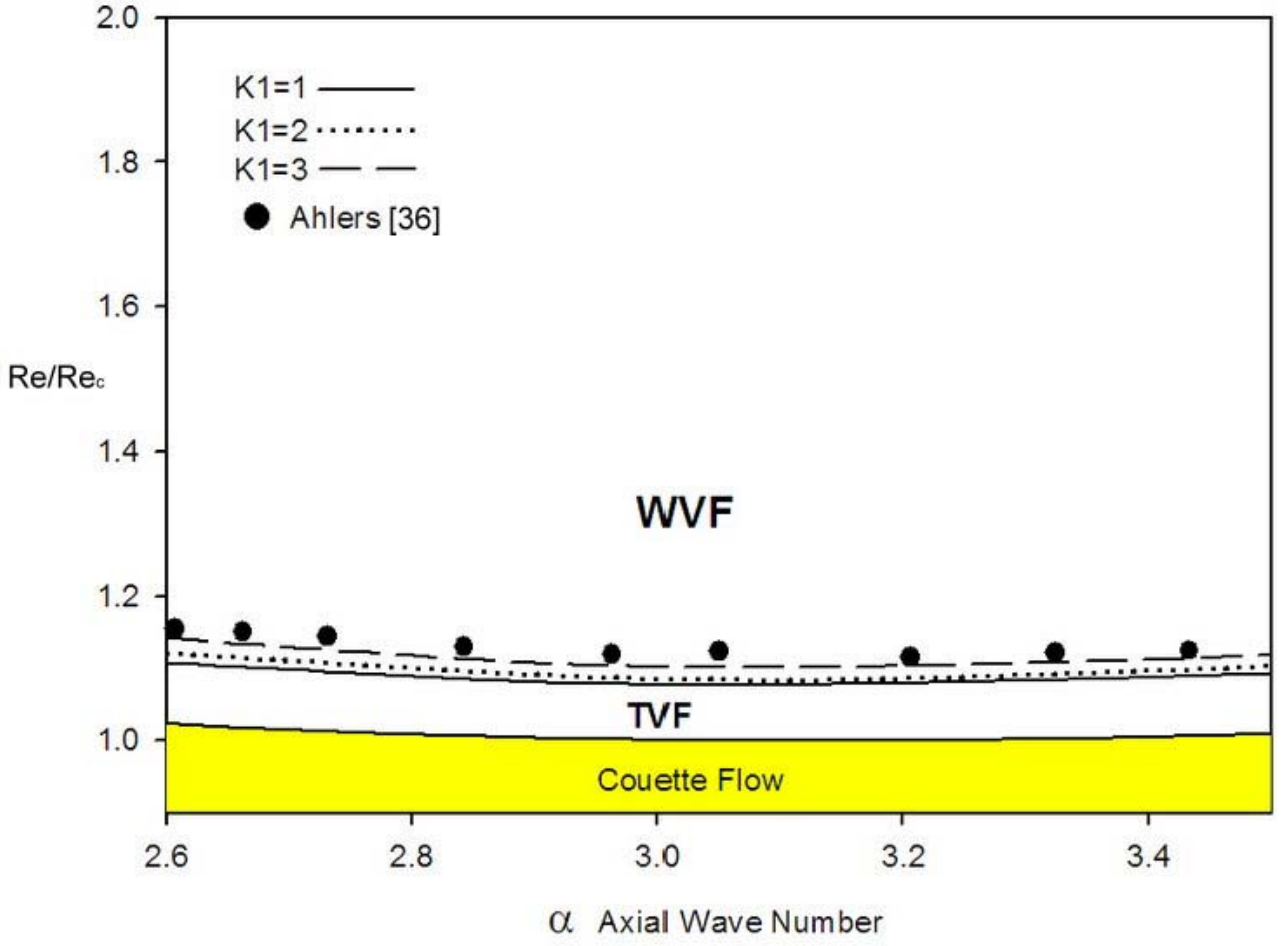

Figure 16 Combines both numerical and experimental results for the onset of WVF for $\eta = 0.893$.

(a) $\eta = 0.7$

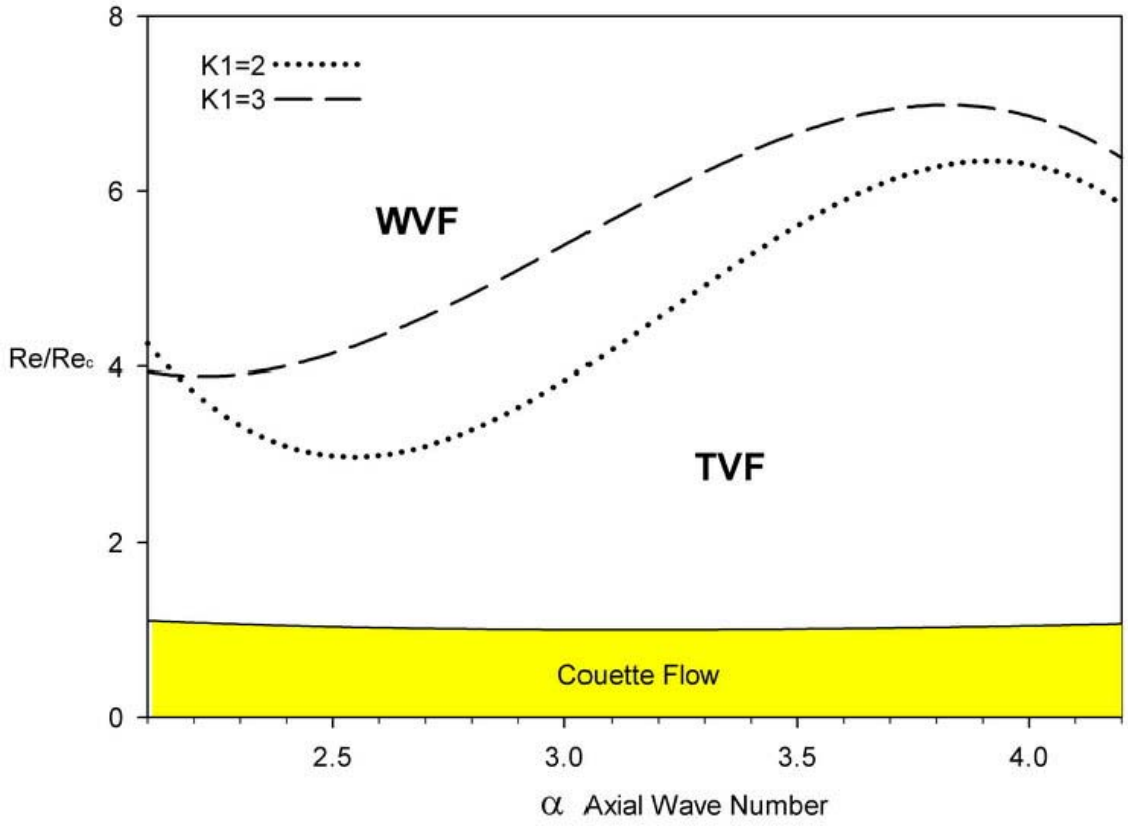

Figure 17 Neutral stability curves of the transition of Taylor vortex flow to wavy vortex flow for various η.
(a) $\eta = 0.7$ (b) $\eta = 0.727$ (c) $\eta = 0.74605$ (d) $\eta = 0.76$ (e) $\eta = 0.78415$ (f) $\eta = 0.8032$
(g) $\eta = 0.82$ (h) $\eta = 0.88$ (i) $\eta = 0.93$

(b) $\eta = 0.727$

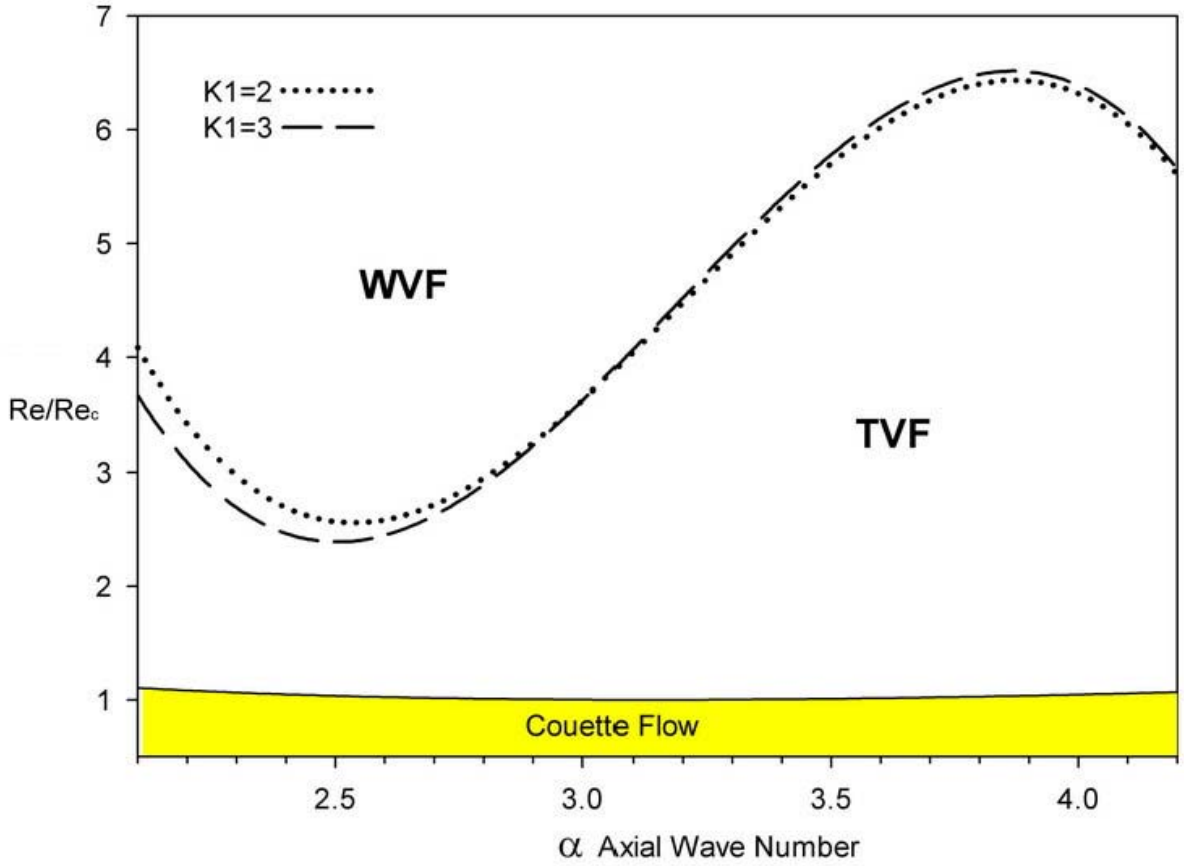

Continued.

(c) $\eta = 0.74605$

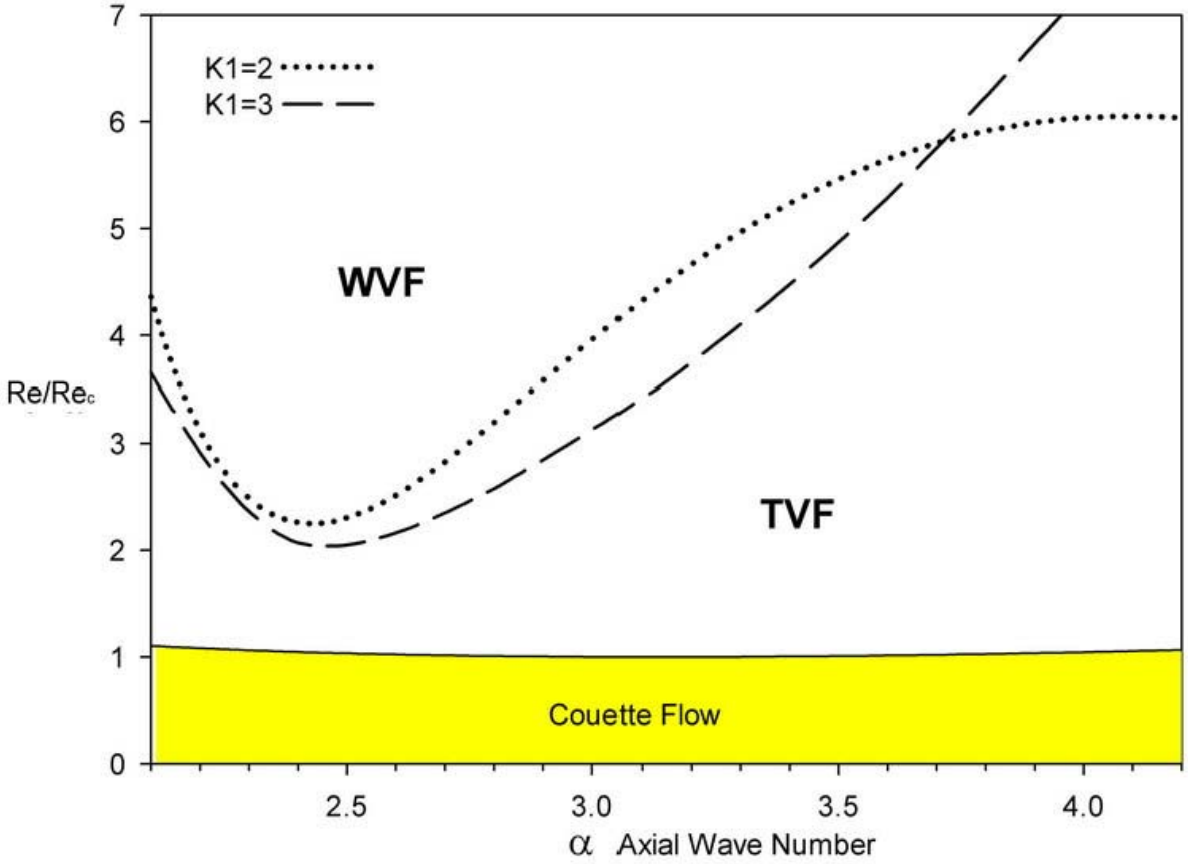

Continued.

(d) $\eta = 0.76$

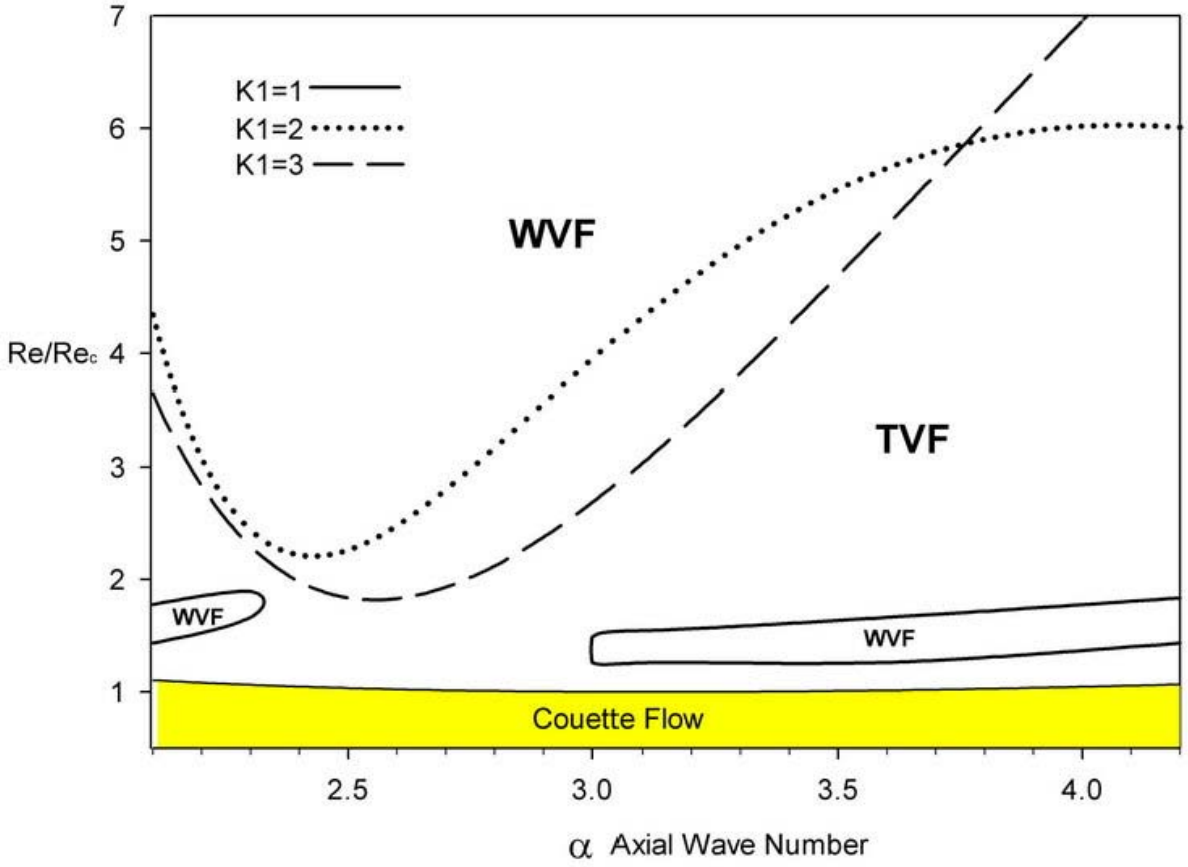

Continued.

(e) $\eta = 0.78415$

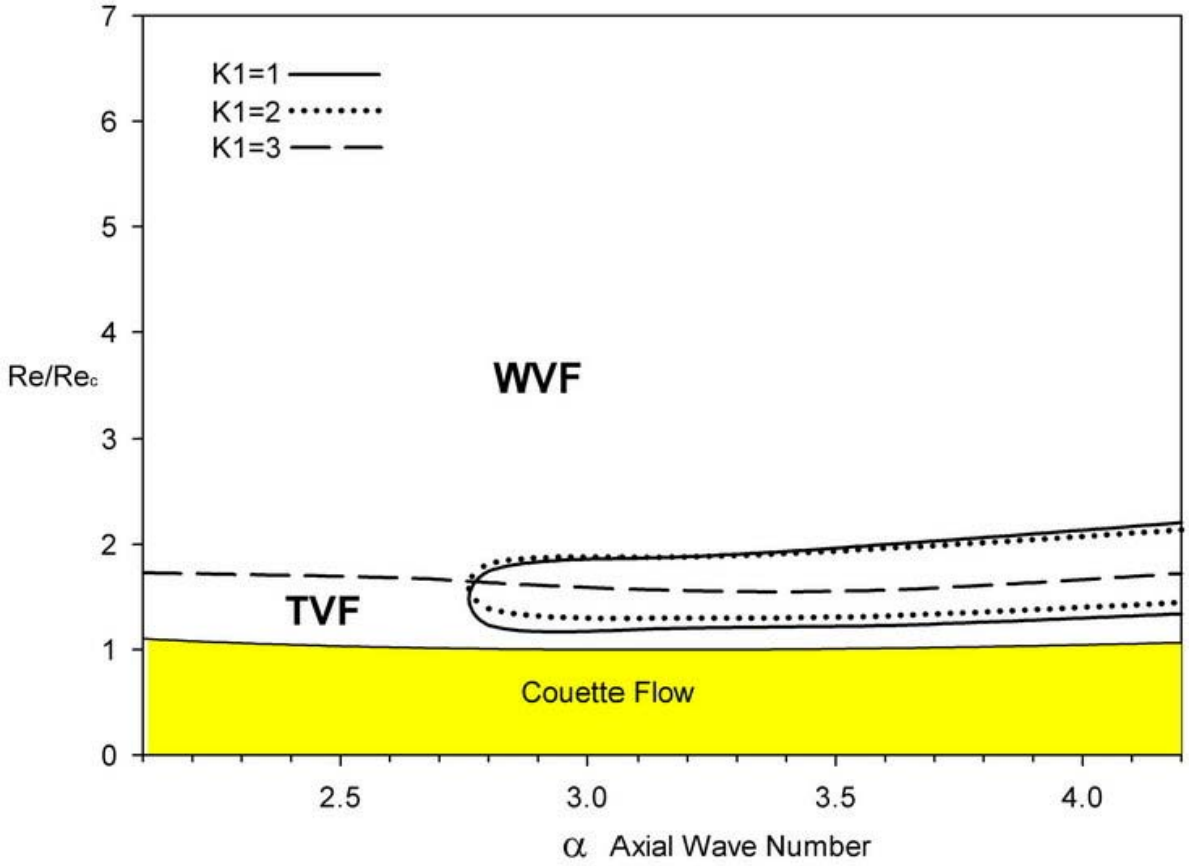

Continued.

(f) $\eta = 0.8032$

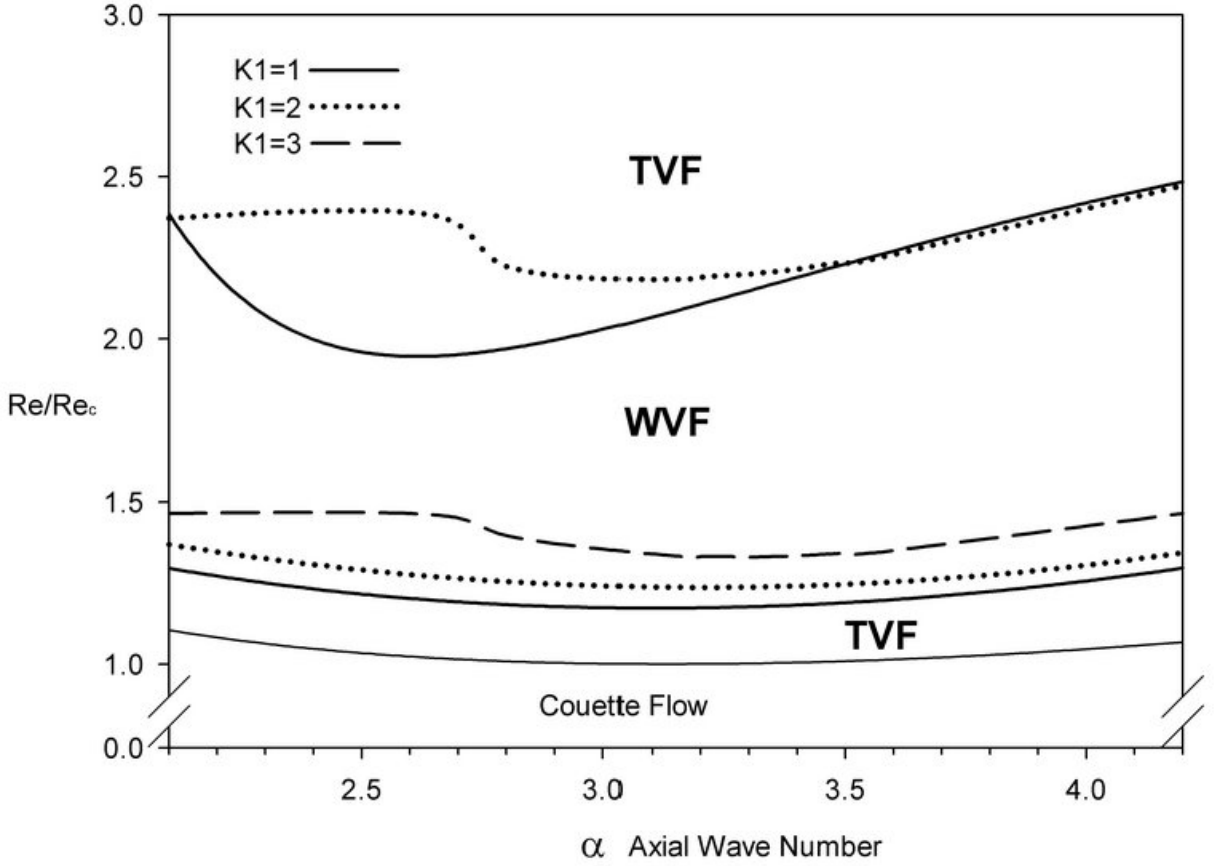

Continued.

(g) $\eta = 0.82$

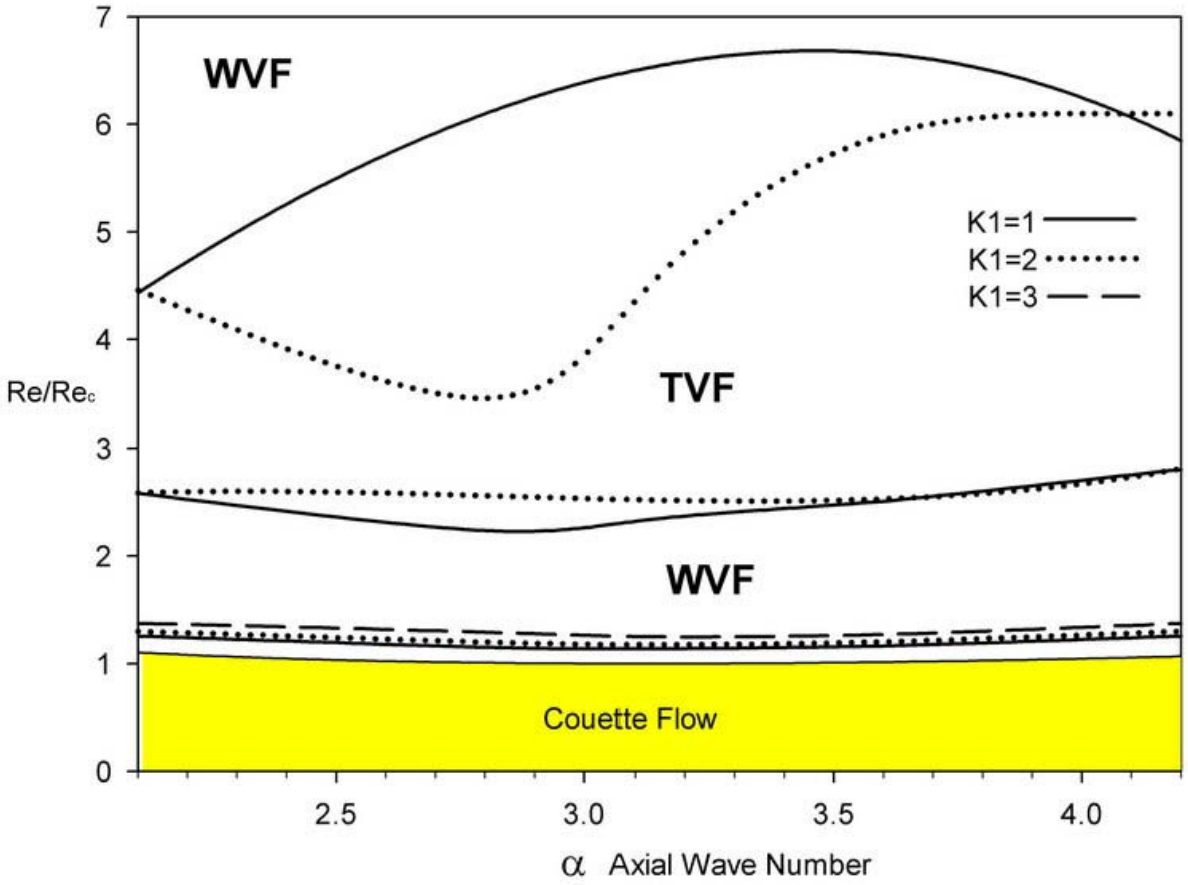

Continued.

(h) $\eta = 0.88$

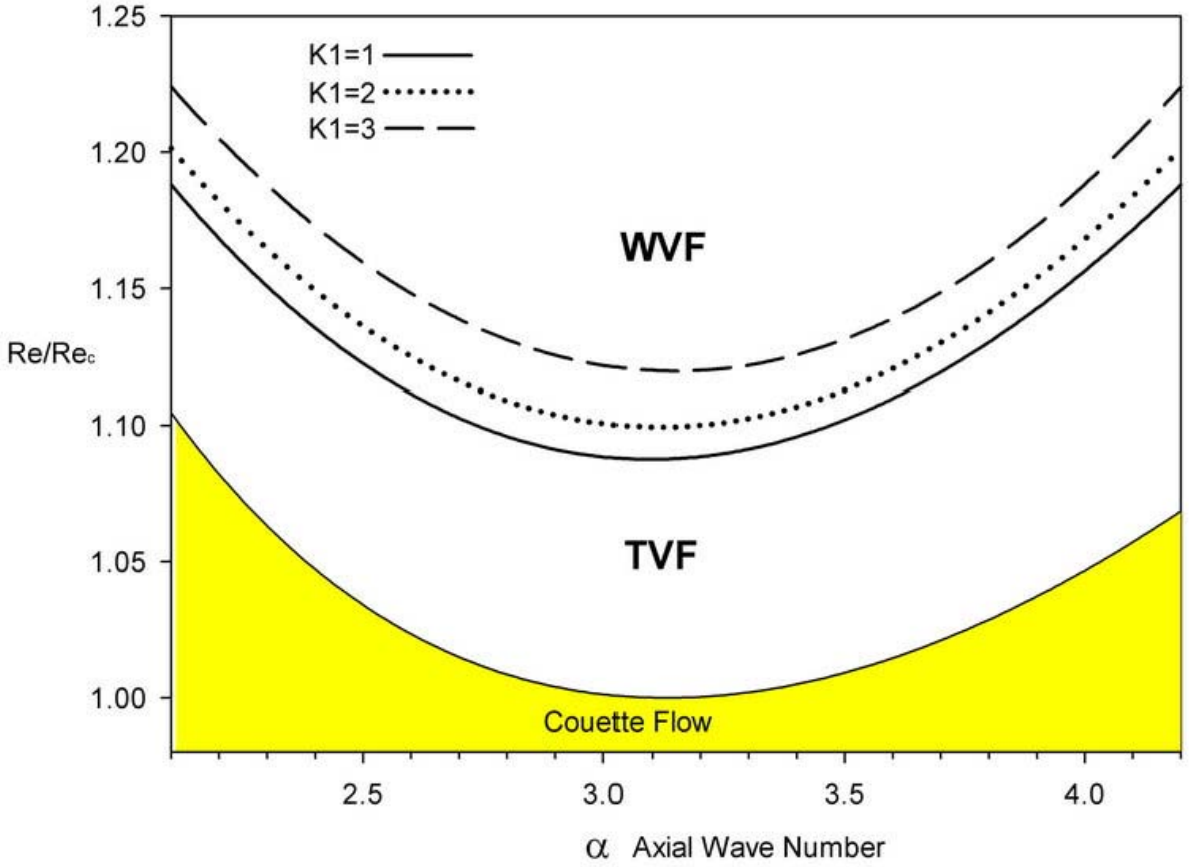

Continued.

(i) $\eta = 0.93$

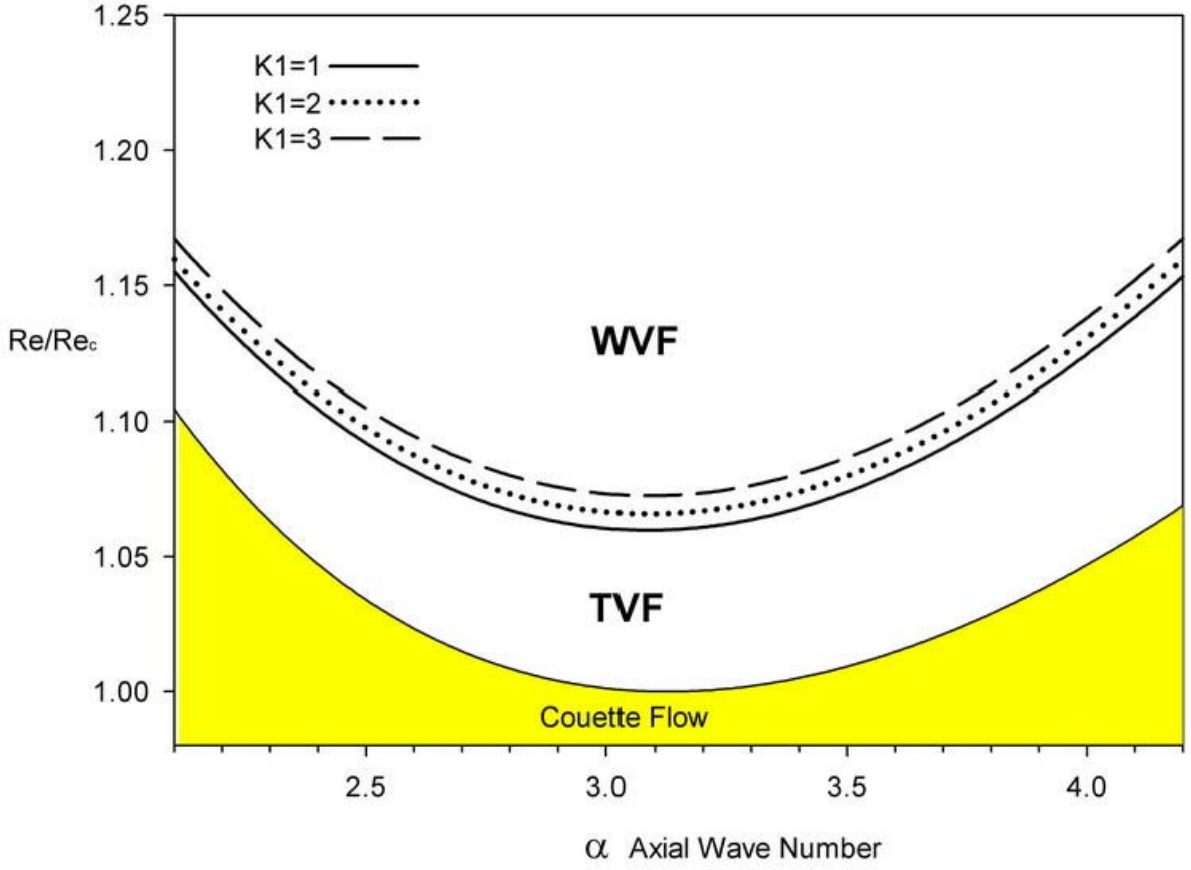

Continued.

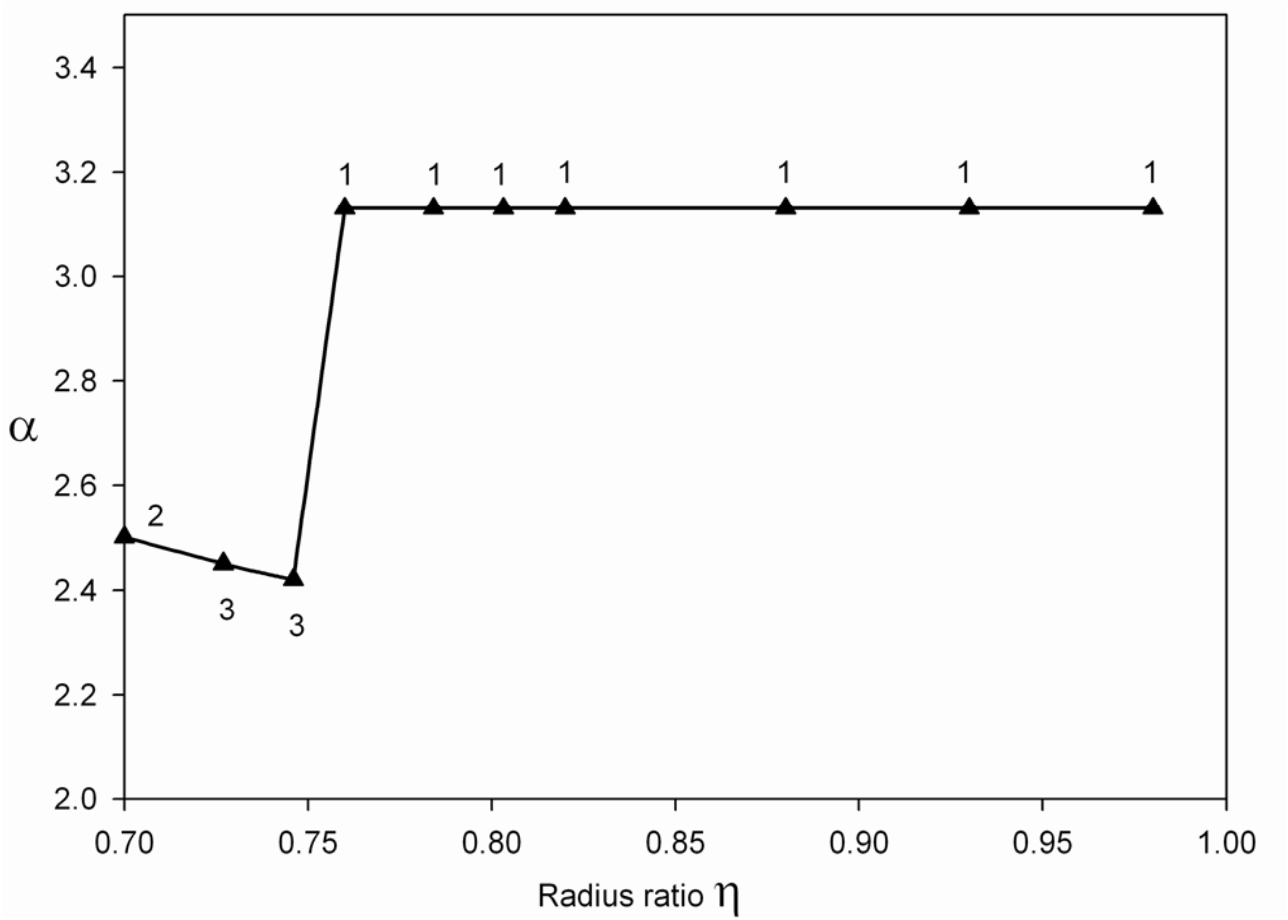

Figure 18 The wave number of the lowest stability boundary for various η. The numbers denote k_1.

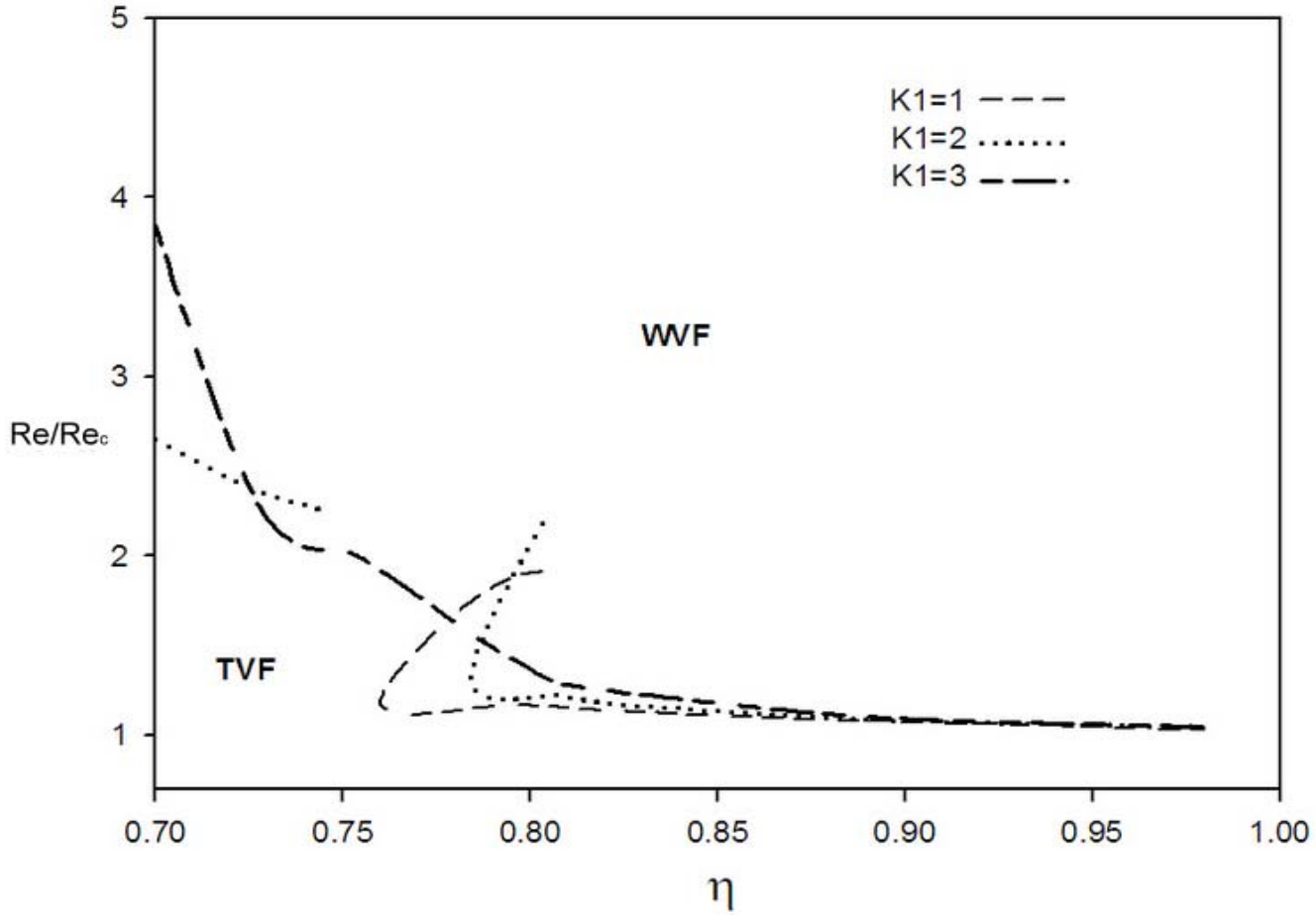

Figure 19 The lowest stability boundary for the bifurcation from Taylor vortices.

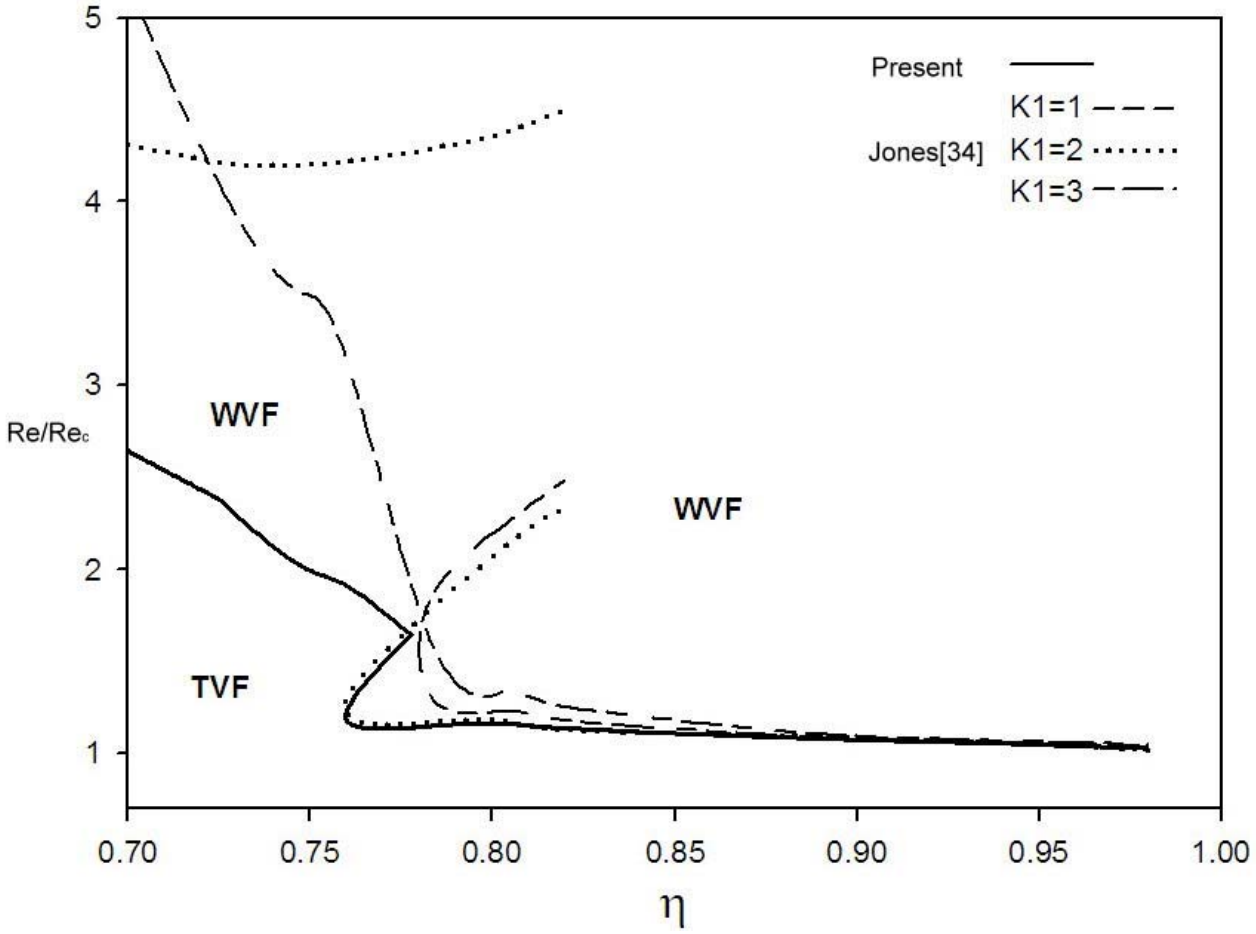

Figure 20 The lowest stability boundary for the bifurcation from Taylor vortices (with the simulated result obtained by Jones[34]).

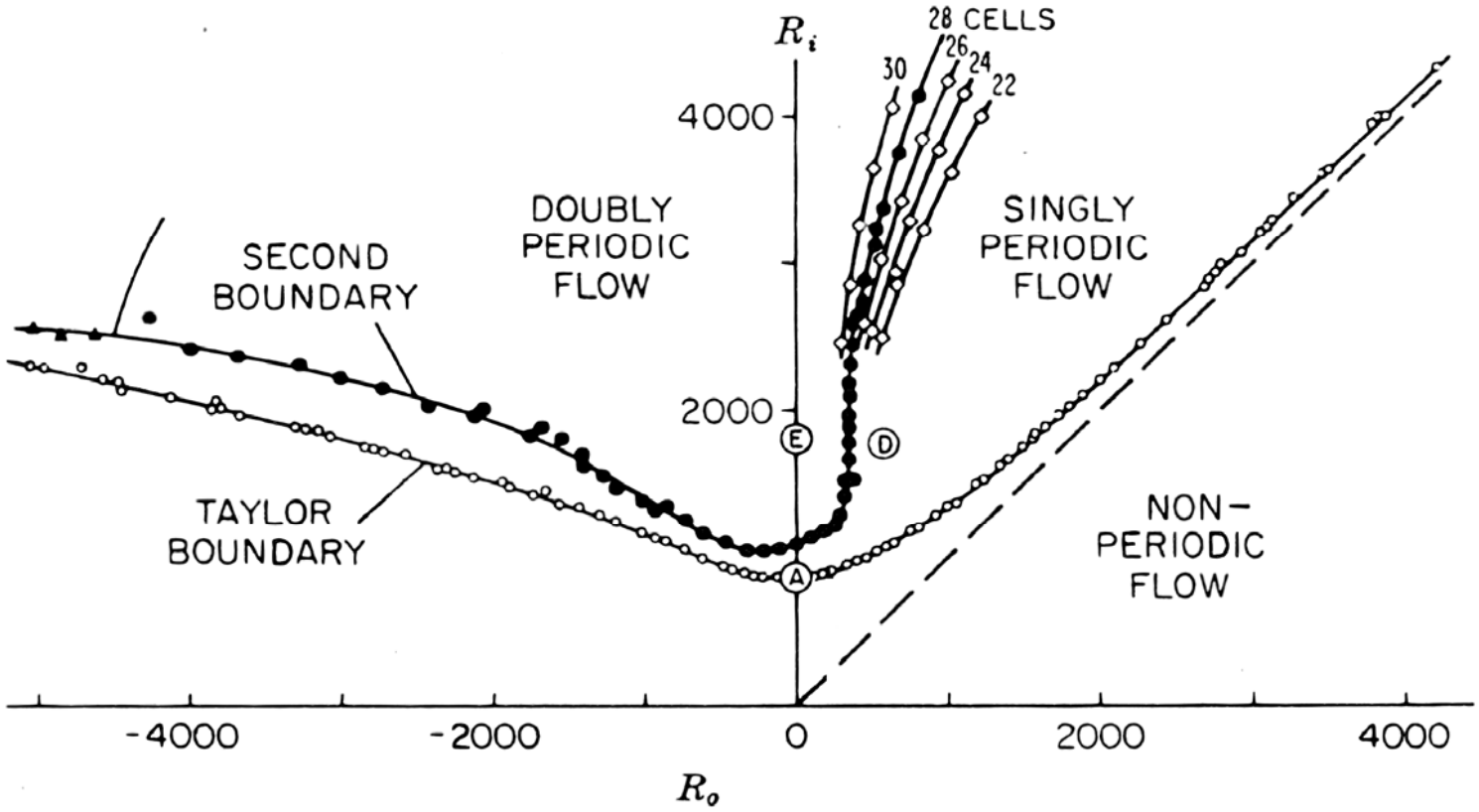

Figure 21 Different regimes in the flow between two rotating cylinders. $\eta = 0.88$, $\Gamma = 14.4$. The fluid is silicone oil of 0.11 cm^2/sec viscosity. Below the Taylor boundary there is circular Couette flow. Above the Taylor boundary there is axisymmetric Taylor vortex flow. Above the second boundary marked by the full circles there is wavy (doubly periodic) Taylor vortex flow. After Coles [8]

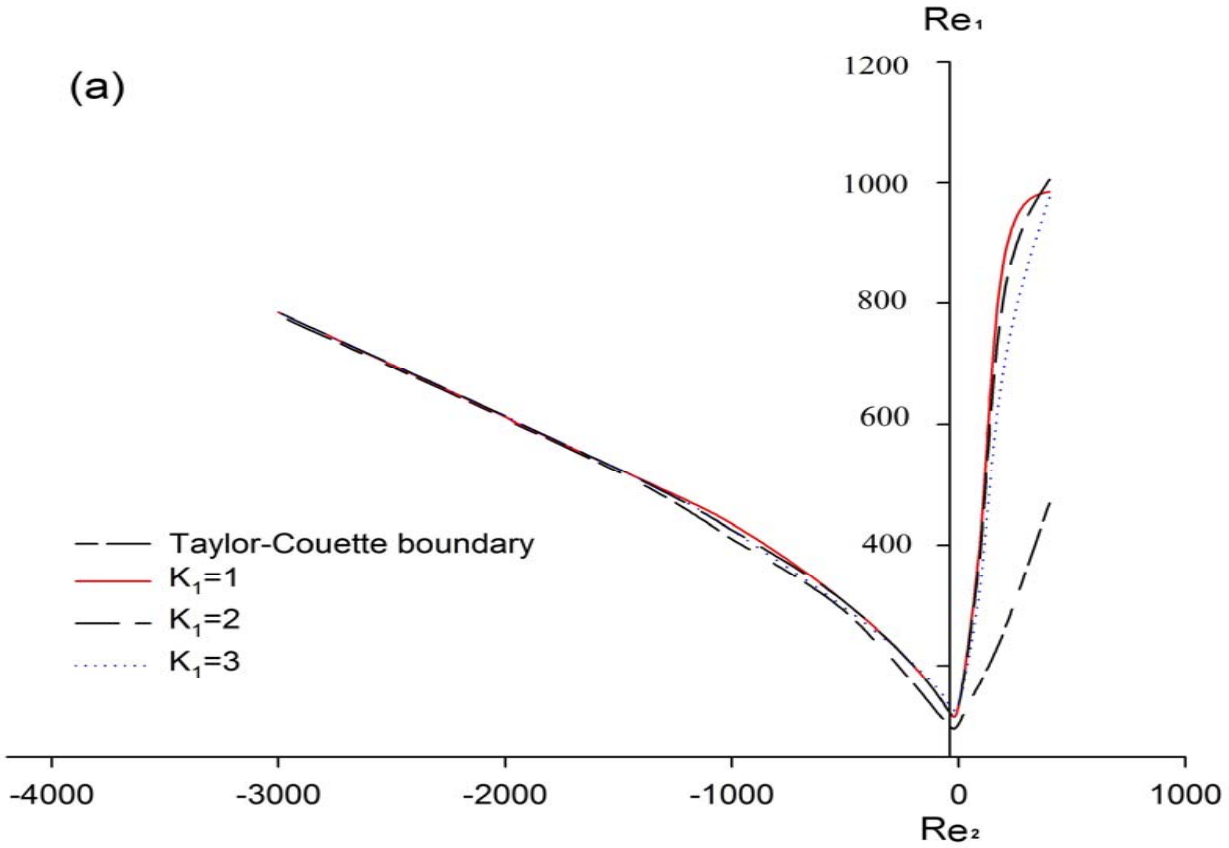

Figure 22 Lowest stability boundary for different azimuthal wavenumbers k_1 corresponding to nonaxisymmetric TVF that is transformed to a WVF.

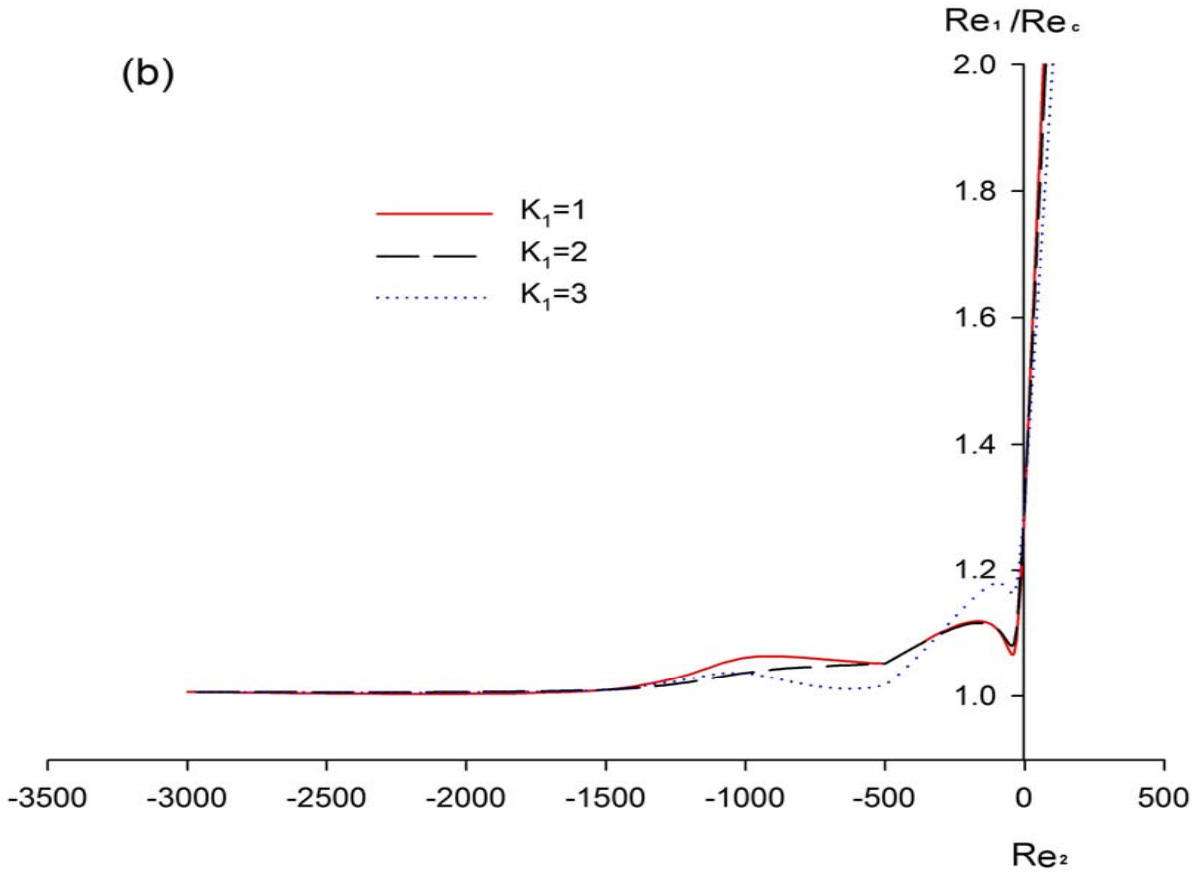

Figure 22 Lowest stability boundary for different azimuthal wavenumbers k_1 corresponding to nonaxisymmetric TVF that is transformed to a WVF.

Chapter 5 Concluding Remarks

Looking back on what we have learned about TVF since Taylor's[2] original paper, what seems to be most impressive is the tremendous progress that has been made in the experimental field. Foremost among the modern experimental discoveries is the observation of the WVF by Coles[31].

This study analyzes both the fluid flow of rotating cylinders and the stability of the modulated Couette flow by numerical methods; under different modulated amplitudes and frequencies, the unstable behavior caused by fluid flow influences the Couette flow to become TVF.

Then this study investigates the instability analysis of modulated TVF by utilizing a numerical method. Based on the consideration that the outer cylinder is fixed and the inner cylinder rotates at a non-zero averaged speed under varying modulated amplitudes and frequencies, the flow is converted from one-dimension Couette flow to TVF. When the modulated amplitude is greater than one and the rotation speed of the inner cylinder exceeds the threshold value for one-dimensional flow, the flow will be more stable at intermediate and high frequencies. When the modulated amplitude is sufficiently large and the inner cylinder rotates at medium frequency, subharmonic flow arises.

When the rotational speed of cylinders exceeds the threshold value of stable TVF, the flow will be transformed from TVF to WVF. First, we numerically investigate the lowest stability boundary of TVF for flows with different wavenumbers and for various radius ratios under the inner cylinder rotates at a fixed speed and outer cylinder is stationary. The variation in the wavenumber of a supercritical TVF will cause the various stability of the flow and the wavenumber of Taylor vortices is constant only as long as the flow is quasi-static. The variation in the wavenumber is examined and found to be important when the radius ratio is less than 0.7842. And then we consider the case

wherein η = 0.88, α = 2.7–3.5, and k_1 = 1–3, and we solve the lowest instability boundary of TVF for two concentric rotating cylinders.

One may ask whether it is worth the effort to pursue these obviously very difficult nonlinear aspects of the Taylor vortex problem. The answer to this question seems to be yes, because in the case of TVF we can pursue the formation of turbulence from laminar flow to full turbulent with great precision in all detail through a number of very characteristic stages. In other words, basic theoretical work can be done on this problem, which, in the end, rank as high as the pioneering studies that we have examined in this study.

References

1. Couette, M., *Etudes sur le frottement des liquides.* Ann. Chim. Phys., 1890. **6**: p. 433-510.

2. Taylor, G. I., *Stability of a viscous liquid contained between two rotating cylinders.* Philos Trans. R. Sec. London, 1923. **A223**: p. 289-343.

3. Donnelly, R. J., *Experiment on the stability of viscous flow between rotating cylinders I. Torque measurement.* Proc. Roy. Soc. London, 1958. **A246**: p. 312-325.

4. Simon, N. J. and Donnelly R. J., *An empirical torque relation for supercritical flow between rotating cylinders.* J. Fluid Mech., 1960. **7**: p. 401-418.

5. Koschmieder, E. L., *Turbulent Taylor vortex flow.* J. Fluid Mech., 1979. **93**: p. 515-527.

6. Burkhalter, J. E. and E. L. Koschmieder, *Steady supercritical Taylor vortex flow.* J. Fluid Mech., 1973. **58**: p. 547-560.

7. Swinney, H. L. and J. P. Gollub, *The transition to Turbulence.* Phy. Today August, 1978. **August**: p. 41-49.

8. Coles, D., *Transition in circular Couette flow.* J. Fluid Mech., 1965. **21**: p. 385-425.

9. Schwarz, K. W., B. E. Springett, and R. J. Donnelly, *Modes of instability in spiral flow between rotating cylinders.* J. Fluid Mech., 1964. **20**: p. 281-289.

10. Nissan, A. H., J. L. Nardacci, and C. Y. Ho, *The onset of different modes of instability for flow between rotating cylinders.* A. I. Ch. E. J., 1963. **9**: p. 620-624.

11. Walsh, T. J. and R. J. Donnelly, *Couette flow with periodically corotated and counterrotated cylinders.* Phys. Rev. Lett., 1988. **60**: p. 700-703.

12. Gollub, J. P. and H. L. Swinney, *Onset of turbulent in a rotating fluid.* Phys. Rev. Lett., 1975. **35**: p. 927-930.

13. Walden, R. W. and R. J. Donnelly, *Reemergent order of chaotic circular Couette flow.* Phy. Rev. Lett., 1979. **42**: p. 301-304.

14. Cole, J. A., *Taylor-vortex instability and annulus-length effects.* J. Fluid Mech., 1976. **75**: p. 1-15.

15. Hall, P. and P. J. Blennerhasset, *Centrifugal instability of circumferential flow in finit cylinders.* Proc. Roy. Soc. London, 1979. **A365**: p. 191-207.

16. Barenghi, C. F. and C. F. Jones, *Modulated Taylor-Couette flow.* J. Fluid Mech.,

1989. **208**: p. 127-170.

17. Murray, B. T., G. B. McFadden, and S. R. Coriell, *Stabilization of Taylor-Couette flow due to time-periodic outer cylinder oscillation.* Phys. Fluids, 1990. **A2**: p. 2147-2156.

18. Walowit, J., S. Tsao, and R. C. Diprima, *Stability of flow between arbitrarily speed concentrical surfaces including the effect of a radial temperature gradient.* J. Appl. Mech., 1964. **31**: p. 585-593.

19. Snyder, H. A. and S. K. F. Karlsson, *Experiments on the stability of Couette motion with a radial thermal gradient.* Phys. Fluids, 1964. **7**: p. 1696-1706.

20. Donnelly, R. J., F. Reif, and H. Suhl, *Enhancement of hydrodynamic stability by modulation.* Phys. Rev. Lett., 1962. **9**: p. 363-365.

21. Hall, P., *The stability of unsteady cylinder flows.* J. Fluid Mech., 1975. **67**: p. 29-63.

22. Riley, P. J. and R. L. Laurence, *Linear stability of modulated circular Couette flow.* J. Fluid Mech., 1976. **75**: p. 625-646.

23. Davis, S. H., *The stability of time-periodic flows.* Ann. Rev. Fluid Mech., 1976. **8**: p. 57-74.

24. Carmi, S. and J. I. Tustaniwskyj, *Stability of modulated finite-gap cylindrical Couette flow:linear theory.* J. Fluid Mech., 1981. **108**: p. 19-42.

25. Walsh, T. J., W. T. Wagner, and R.J. Donnelly, *Stability of modulated Couette flow.* Phys. Rev. Lett., 1987. **58**: p. 2543-2546.

26. Kuhlmann, H., D. Roth, and M. Lucke, *Taylor vortex flow under harmonic modulation of the driving force.* Phys. Rev. , 1989. **A39**: p. 745-762.

27. Ganske, A., T. Gebhardt, and S. Grossmann, *Taylor-Couette flow with time modulated inner cylinder velocity.* Phys. Lett., 1994. **A192**: p. 74-78.

28. Meksyn, D., *New methods in laminar boumdary-layer theory.* 1961, London: Pergamon press.

29. Sparrow, E. M., W. D. Munro, and V. K. Jonsson, *Instability of the flow between rotating cylinders:the wide gap problem.* J. Fluid Mech., 1974. **20**: p. 35-46.

30. Youd, A. J., A. P. Willis, and C. F. Barenghi, *Reversing and non-reversing modulated Taylor--Couette flow.* J. Fluid Mech., 2003. **487**: p. 367-376.

31. Coles, D., *On the instability of Taylor vortices.* J. Fluid Mech., 1965. **31**: p. 17-62.

32. Lewis, J. W., *An experimental study of the motion of a viscous liquid contained between two coaxial cylinder.* Proc. Roy. Soc. London, 1928. **A117**: p. 388-407.

33. Schultz-Grunow, F. and H. Hein, *Beitrag zur Couettestromung.* Z. Flugwiss, 1956. **4**: p. 28-30.

34. Jones, C. A., *The transition to wavy Taylor vortices.* J. Fluid Mech., 1985. **157**: p. 135-162.

35. Stuart, J. T., *On the nonlinear mechanics of hydrodynamic stability.* J. Fluid Mech., 1958. **4**: p. 1-21.

36. Ahlers, G., D. S. Cannell, and M. A. D. Lerma, *Possible mechanism for transitions in wavy Taylor-vortex flow.* Phys. Rev. A, 1983. **27**: p. 1225-1227.

37. Andereck, C., S. S. Liu, and H. L. Swinney, *Flow regimes in a circular Couette system with independently rotating cylinders.* J. Fluid Mech., 1986. **164**: p. 155-183.

38. Park, K., *Unusual transition sequence in Taylor wavy vortex flow.* Phys. Rev. A, 1984. **29**: p. 3458-3460.

39. Burkhalter, J. E. and E. L. Koschmieder, *Steady supercritical Taylor vortices after sudden starts.* Physics of Fluids, 1974. **17**: p. 1929-1935.

40. Antonijoan, J. and J. Sanchez, *On stable Taylor vortices above the transition to wavy vortices.* Physics of Fluids, 2002. **14**: p. 1661-1665.

41. Snyder, H. A., *Wave-number selection at finite amplitude in rotating Couette flow.* J. Fluid Mech., 1969. **35**: p. 273-298.

42. Coddington, E. A. and N. Levinson, *Theory of ordinary differential equations.* 1955: McGraw-Hill.

43. Canuto, C., et al., *Spectral Methods in Fluid Dynamics.* 1988.

44. Fox, L. and I. B. Parker, *Chebyshev polynomials in numerical analysis.* 1968, London: Oxford University Press.

45. Hung, Y. M., *Experiments on the instability of modulated circular Couette flow.* NCTU, Master thesis, 1995.

46. Donnelly, R. J., *Experiments on the stability of viscous flow between rotating cylinders. II. Visual observation.* Proc. Roy. Soc. London, 1960. **A258**: p. 101-123.

47. Donnelly, R. J., *Experiments on the stability of viscous flow between rotating cylinders III. Enhancement of stability by modulation.* Proc. Roy. Soc. London, 1964. **A281**: p. 130-139.

48. Hu, S. J., *Experimental measurement of modulated Taylor vortex flow.* NCTU, Master thesis, 1996.

49. Marques, F. and J. M. Lopez, *Taylor-Couette flow with axial oscillations of the inner cylinder: Floquet analysis of the basic flow.* J. Fluid Mech., 1997. **384**: p.

153-175.

50. Lopez, J. M. and F. Marques, *Dynamics of three-tori in a periodically forced Navier-Stokes flow.* Phys. Rev. Lett., 2001. **85**: p. 972-975.

51. Youd, A. J., A. P. Willis, and C.F. Barenghi, *Non-Reversing Modulated Taylor-Couette Flows.* Fluid Dynamics Research, 2005. **36**: p. 61-73.

52. Daoyi, C. and G. H. Jirka, *Linear instability of the annual Hagen-Poiseuille flow with small inner radius by a Chebyshev pseudospectral method.* Internatioal Journal of Computation Fluid Dynamics, 1994. **3**: p. 265-280.

53. Speetjens M. F. M. , C. H. J. H., *A spectral solver for the Navier-Stokes equations in the velocity-vorticity formulation.* Internatioal Journal of Computation Fluid Dynamics, 2005. **19**: p. 191-209.

54. Jones, C. A., *Numerical methods for the transition to wavy Taylor vortices.* J. Comp. Phys., 1985. **61**: p. 321-344.

55. Park, K., L. Gerald, and R. J. Donnelly, *Determination of transition in Couette flow in finite geometries.* Phy. Rev. Lett., 1981. **47**: p. 1448-1450.

56. Jones, C. A., *Nonlinear Taylor vortices and their stability.* J. Fluid Mech., 1981. **102**: p. 249-261.

57. King, G. P. and H. L. Swinney, *Limits of stability and irregular flow patterns in wavy vortex flow.* Phys. Rev. A, 1983. **27**: p. 1240-1243.

E S A 1896

自傳

姓　　名：林豪傑

性　　別：男

出生年月：民國 58 年 05 月 19 日

出 生 地：高雄市

聯絡電話：(O)0919650519　(H)03-5358549

住　　址：台中縣潭子鄉勝利路 249 巷 3 號 5 樓

E-mail　:herojake.lin@gmail.com

學　　歷：

1. 漢翔航空公司「生產管理工程師培訓」
2. 中正理工學院兵器系統工程研究所畢業
3. 中正理工學院航空工程學系畢業
4. 台灣省立鳳山高級中學畢業

專　　長：

1. 程式設計。
2. 流體穩定論、流體力學、熱力(傳)學、黏性流體力學、邊界層理論、系統工程與管理。
3. 氣渦輪機理論與實務。
4. 系統模擬與整合及模擬軟體開發。
5. 風險管理計畫撰擬與實務。